Ship collision on inflatable weirs

Case study: weirs in the Meuse

B.C.N. Stikvoort

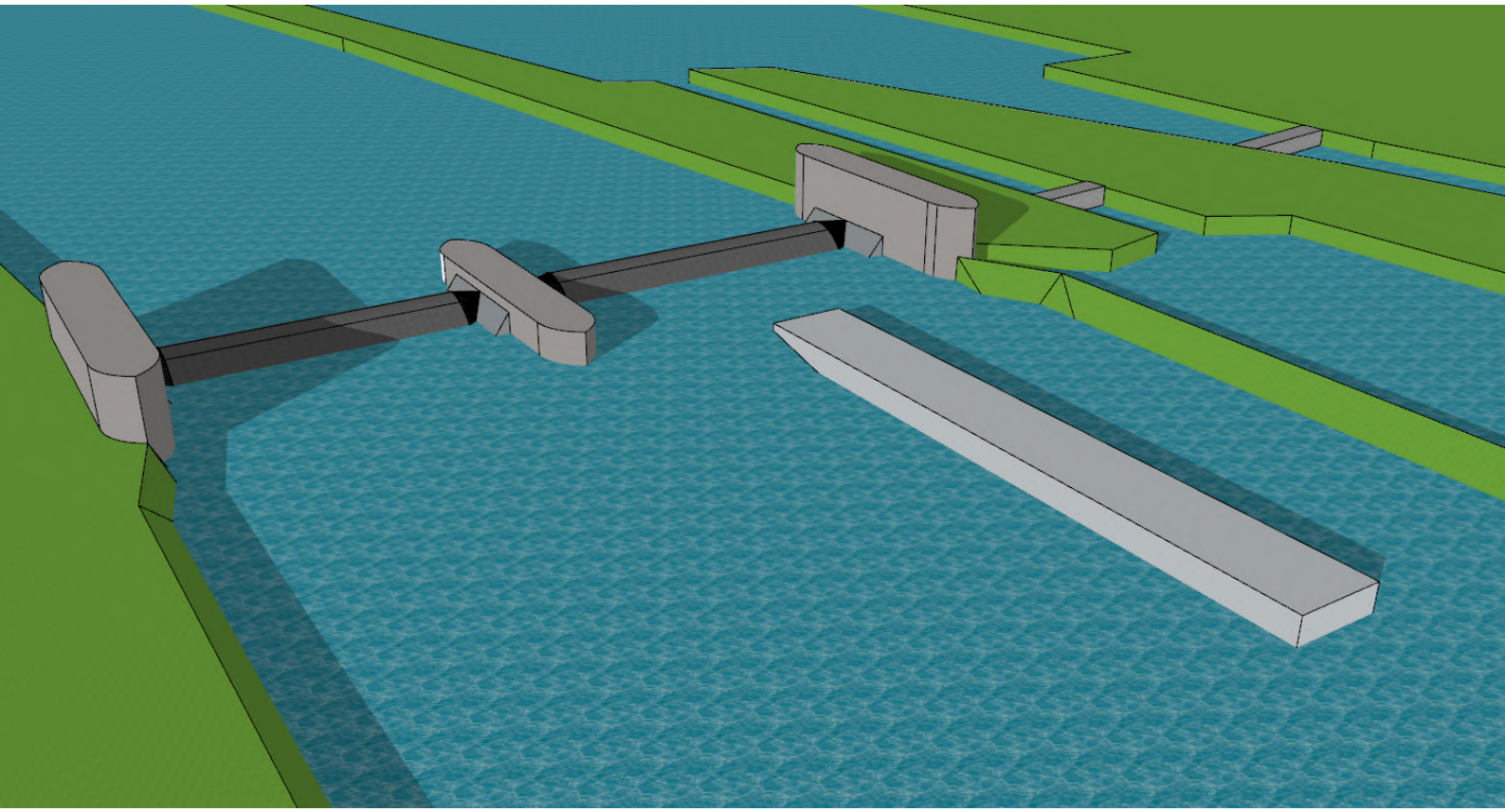

TU Delft Delft University of Technology

bam

Ship collision on inflatable weirs

Case study: weirs in the Meuse

by

B.C.N. Stikvoort

to obtain the degree of Master of Science in Civil Engineering

at the Delft University of Technology,

to be defended publicly on November 2, 2020 at 3:00 PM.

Student number:	4293347	
Project duration:	November 11, 2019 – November 2, 2020	
Thesis committee:	Prof. dr. ir. S. N. Jonkman,	TU Delft, chairman
	Ir. W. F. Molenaar,	TU Delft, daily supervisor
	Dr. ir. P. C. J. Hoogenboom,	TU Delft
	Ir. J. S. Reedijk,	BAM

An electronic version of this thesis is available at `http://repository.tudelft.nl/`.

TU Delft Delft University of Technology

bam

Preface

In front of you is presented the study 'Ship collision on inflatable weirs'. The study is made to complete the master Hydraulic Engineering at the TU Delft and is done in collaboration with BAM Infraconsult.

I would like to thank my supervisors for their advise and feedback during the meetings. Prof.dr.ir S.N. Jonkman for reviewing my draft reports. Ir. W.F. Molenaar for his guidance and availability for my questions. Dr.ir. P.C.J. Hoogenboom for giving detailed feedback. My satisfaction to ir. J.S. Reedijk, with emphasis to giving the opportunity using the new BAM waterlab research facility, to do my experiments. Here with the presence of ir. M. Muilwijk. His helping hand was much appreciated to me.

Thank you Luc for reviewing my report. I would like to thank my family supporting me during the time doing this research. My mom for always supporting me even in harder times. In special my girlfriend Bo motivating me to the finish.

Bram Stikvoort
Delft, November 2020

Abstract

In the Meuse seven weirs are located in the Dutch reaches, controlling the water level to enable inland navigation through the river. The weirs are being scheduled for replacement, where weir Grave is the first one in 2028. They are reaching their end-of-life time and are not in compliance with the working conditions anymore.

One of the main issues that became of more importance in the recent years is ship collision. In the past 20 years two major ship collisions happened on two different existing weirs in the Meuse, one at Grave and one at Linne. The place of impact at the weirs was significantly damaged after those collisions. The weirs, made of steel plates and girders, were not stiff enough to resist those impacts. As a consequence, the water level dropped and inland navigation was not possible for one month.

The inflatable rubber weir is being developed since 1955. One of the aspects that has not yet been considered for those inflatable weirs is ship collision. Where ship collision has been often researched for steel gates. The theory and formulas found for the existing collision analysis are not fully applicable to the inflatable weir, mainly due to large elastic deformation of the inflatable weir. For insight into ship collision on inflatable weirs two main questions are derived:

1. How can the inflatable weir-ship interaction by ship collision at Grave be modelled to predict the motions of the ship and the inflatable weir?
2. What happens when a push convoy ship collides with an inflatable weir at Grave?

To answer those questions, first a conceptual inflatable weir design is proposed for location Grave, that can replace the existing weir. The design is based on existing literature, such as the inflatable storm surge barrier Ramspol. The design for Grave is considered to be scalable to the overflow (Poirée) parts of the Meuse weirs. Three methods are used to analyse ship collision on the designed inflatable weir. First, an analytical model is made to study the behaviour of the inflatable weir and ship during ship collision. Second, an effort was made to develop a numerical model in Ansys. Lastly, physical model tests were performed to see what happens during ship collision on the inflatable weir and calibrate the analytical model, see figure 1. The full video experiments are uploaded to the 4TU-datacentrum (`https://data.4tu.nl/portal`)

In literature a standard expression has been found to quantify the ship force on the colliding structure. This expression forms the basis of the analytical model. The inflatable weir in the analytical model is schematized by a two-dimensional plate sheet. With the analytical model, the strain in the sheet is quantified by ship collision for different push convoy CEMT-classes (ship classes). The side effects of water during impact were taken into account separately. It was showed that ship waves did not have significant influences on the stresses and strain of the inflatable weir. However, the water overflow showed a flow velocity of 4.4 m/s, which can lead to damage of the bottom protection behind the weir. An effort was made to validate the strain found in the analytical model by a numerical model in Ansys. However numerical instabilities were found that lead in considerable modification of the desired model and so the results indicated no representative outcomes.

To see what happens during the ship collision a physical scale model was made, with scale 1:25 for accurate representation of the physical phenomena. Sixteen experiments were done with four different draughts and four different velocities of the ship. For the experiment with the scaled maximum draught (0.14m) and velocity (1.1m/s), the interaction in time is shown in figure 1. In six steps the ship collision interaction experiment is elaborated:

1. The ship is heading towards the weir, with the measured velocity.
2. The bow of the ship is almost colliding on the weir and the bow wave is already topping over it.
3. The bow of the ship collides on the weir and is uplifted by the air pressure inside the membrane.
4. The ship is gliding over the weir, losing its energy and is further uplifted.
5. The ship is glided the maximum distance over the weir and is accelerating downwards.
6. The ship and weir are bouncing back by the elongated sheet of the weir.

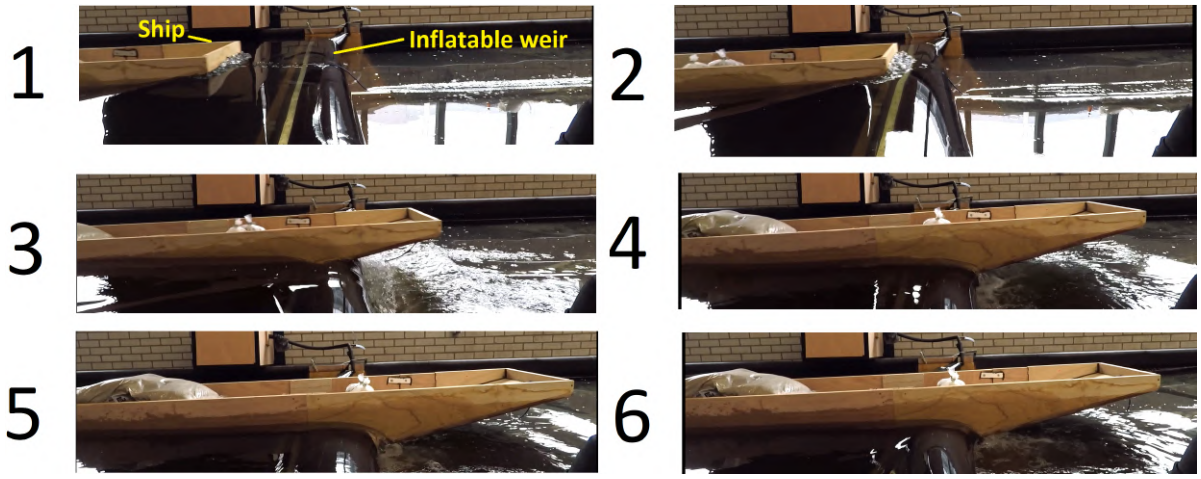

Figure 1: snapshots ship collision experiments in time

The two aspects uplift of the ship and gliding over the weir are not yet included in the analytical model, therefore the analytical model is extended. In equation 1, the potential energy (E_{pot}) is added to account for the uplift and the gliding coefficient ($C_{glide,mean}$) to account for the gliding of the ship.

$$F = C_{glide,mean}\sqrt{2(k_{circ} + k_{long})(E_{kin} - E_{pot})} \tag{1}$$

The extended analytical model showed a 25% deviation with the uplift of the ship and a 15% deviation with the displacement of the weir from the experiments. With the extended model it was calculated that the limit strain is not exceeded and that the strain is maximum 5% on top of the static strain of 1.9%.

Conclusion: The first steps have been taken into research of ship collision on inflatable weirs. An analytical model is developed to indicate quantitatively what happens during collision. The physical model test helps to get insight what happens during collision and is useful for calibrating. Further investigation on the ship with V-bow, the propeller of the ship and a more extensive numerical model is recommended for ship collision on inflatable weirs.

Contents

1 Introduction

In this chapter an introduction is given about ship collision on inflatable weirs. First background information will be given on which this research is based. Next the research questions will be defined based on the problem statement. The methodology used in the research will then be described to answer the research questions.

1.1. Background information

The weirs in the Meuse have been built between 1920 and 1940 [8]. Each weir spans in total more than 100 meter, covering the width of the river Meuse to regulate the water level. The weirs are reaching the 100-year lifetime, most are not in compliance with the working conditions anymore and are scheduled for replacement. In 2017 a program has been setup by Rijkswaterstaat for the replacement of the weirs called 'Grip op de Maas' [53]. The replacement of the weirs, based on their building year, is scheduled to be executed between 2020 and 2040. The program suggests having an 1:1 replacement of the weirs to keep the characteristics of the river Meuse the same. Three reasons for replacement of the weirs can be given. First the old weirs may fail due to decreased resistance of the materials over the years. Second, the maintained increased water head in the Meuse causes an increased load on the weirs [1]. At last the weirs have an old design and may missed out on applicable innovations. In total there are seven weirs located in the Dutch reaches of the Meuse, see figure 1.1. They span a reach from Maastricht until 's Hertogenbosch.

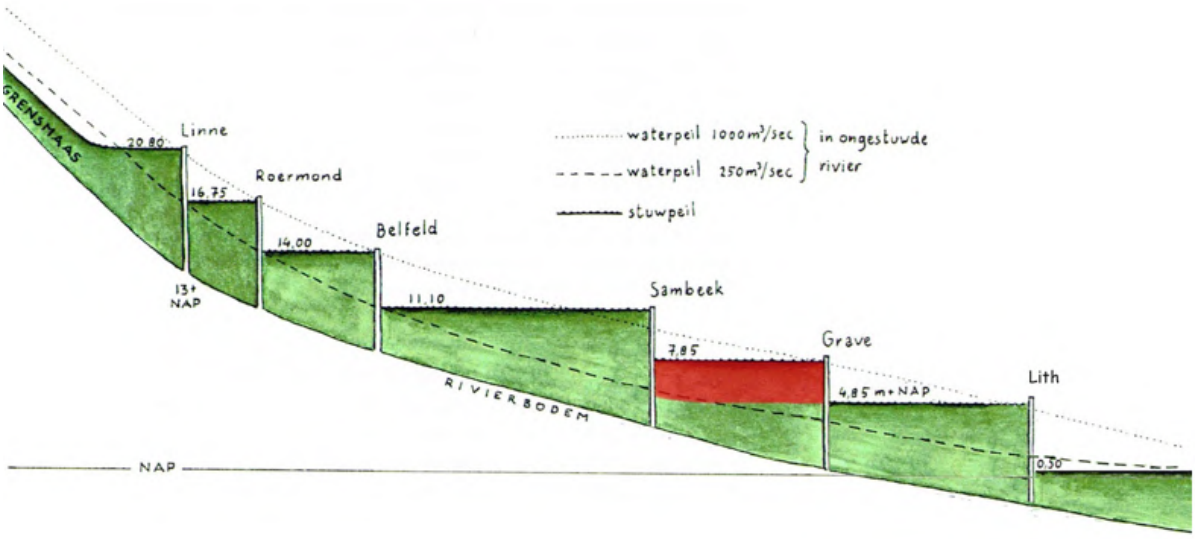

Figure 1.1: side view weirs in the Meuse [46]

[1] The water load is proportional to the square of the water head

Looking back in history of weirs, there is a relevant event for designing the replacement of the weirs. This event is ship collision on one of the weirs. In 2016 a 2000-ton benzene tanker collided on the weir at Grave in the Meuse [46], see figure 1.2. The weir at Grave is made of baffles, enough to retain the water and was clearly not prepared for a ship collision of such size. The whole upstream water level dropped and no shipping was possible for a month. Also, this had impact on the houseboats in the nearby region, see figure 1.3. Information about the ship and why this could have happened is found in chapter 2.

Recently another accident happened with ships hitting the weir Linne in the Meuse. During storm Ciara in 2020 two push convoys got loose of the quay and drifted downstream towards weir Linne. Those two ships were unloaded and did not have a self-propelled velocity, which reduces the size of impact. The reparation of the weir is found in chapter 2.

Back in the time the weirs were made for the Meuse, they were possibly not designed for ship collision. The shipping industry was much smaller by then. The amount of trade going by ship increased since 1980 with an average rate of 3% over a global scale [40]. With the increased shipment over the year it is more plausible to have a collision accident.

Figure 1.2: weir Grave after ship collision [46]

Figure 1.3: houseboat with water level drop[46]

For the replacement program a new type of weir concept is being proposed, to investigate its behaviour due to similar ship collision events. This is an inflatable weir made of a rubber sheet filled with air (and/or water). The invention of the inflatable dam comes from the prof. Mesnager, from France, in 1955 and is patented later in 1965 by Norman Imbertson from the USA [42, p. 9]. The development is later improved in Japan. More than 2000 rubber dams exists around the world [45], an overview is given in appendix B.

In the Netherlands this concept is used once as a barrier at Ramspol and is the biggest in its kind [51]. At the Ramspol storm surge barrier the design storm conditions has an occurrence of around 1/700 years, whereas ship collision is accounted for a probability of 1/1250 years [38]. Although the collision probability is less, it is still considered in the design process. One of the purposes for this type of barrier is that this barrier is considered a safe and cheaper option comparing to the traditional vertical lifting gate barrier [31, p. 91].

In line with the 1:1 replacement of the seven weirs of the Meuse, the inflatable concept is assumed a conceivable design. It is assumed the design of the inflatable weir can be uniform and deployable for all the weirs in the Meuse in the Dutch reaches. Due to increased number of shipping, ship collision on the proposed inflatable weir design is considered increasingly important.

1.2. Problem statement

Most weirs in the Netherlands are made of steel, therefore a lot of knowledge is existing on these type of weirs. The inflatable weir concept, made of rubber, is relatively new and behaviour on loads is different from the commonly used steel and concrete structures. A structure that can be thought of that uses rubber is a fender for mooring ships at quays. On both steel/concrete hydraulic structures and fenders, ship collision analysis is performed. For example, a simplified model for ship collision on lock gates is created by Buldgen, to calculate among other things the displacement of the gates [32]. Another model description on how to simulate scraping collisions on guide works is done by Dommelen [69]. For ship collision analysis on fenders a general approach is given by PIANC [43], see appendix F. For the ship collision on the inflatable weir no ship collision analysis is performed yet.

In practice the inflatable weir is designed for types of loading that have a common occurrence in a river. The inflatable weir is designed for static loading such as the hydrostatic water pressure and dynamic loading such as the wave-impact and wind. A high safety factor is included to account for the uncertainties in the behaviour of the rubber membrane during loading. The mechanics of the inflatable weir during ship collision are different than for steel weirs. Fender systems are getting closer to the mechanical behaviour of an inflatable weir, nonetheless those structures are specially designed for ship collision.

The problem stands in not knowing what happens when a ship collides with an inflatable weir. There is currently no model describing this phenomenon and ship collision never happened on an existing inflatable weir yet. The consequences of the potential event are uncertain, therefore it cannot be included in an integrated design process.

1.3. Research questions

From the problem statement emerged that a method for the behaviour of ship collision on an inflatable weir is not readily available. A model is desired to get insight into the consequences of the ship-inflatable weir interaction. A simplified and clear model is sought, where the inflatable weir and the hull of the ship is modelled, to gain insight of the potential event. The question derived to make such an understandable and clear model is described as:

1. How can the inflatable weir-ship interaction by ship collision at Grave be modelled to predict the motions of the ship and the inflatable weir?

To answer the main question, four sub questions are defined in order to allow a better answer for the main question:

- Can numerical modelling help to verify the analytical model?
- Can a physical model test help to verify the analytical model?
- How much strain in the sheet will develop during the ship structure interaction?
- What side effects of the water do need to be taken into account for the consequences of the ship collision?
- Can the analytical model examine the resistance of the conceptual design to ship collision?

The above main question will quantitatively describe the ship collision scenario. For better insight of what happens during ship collision, it is of interest to know what happen qualitatively (visually). So, within the scope of this research a second main question is defined:

2. What happens when a push convoy ship collides with an inflatable weir at Grave?

The following sub questions are formulated to allow a better answer for the main research question:

- Will the ship bounce back from, glide over or glide fully over the inflatable weir?
- Will the ship rupture the sheet of the inflatable weir during collision?
- How will the push convoy collide into the inflatable weir?

1.4. Research methodology

First the characteristics, weirs and ship collision events of the river Meuse will be investigated. Then a location in the Meuse will be chosen for the design of an inflatable weir and the ship collision event. The inflatable weir is designed up to the conceptual design phase, which gives enough details for the ship collision analysis. Most of the design is based on what is found from experience in literature.

The analytical model is built based on the parameters of the ship and the inflatable weir design. The ship parameters are determined from general guidelines used in the Netherlands. Any side effects of the water were also investigated. Based on the found results more understanding of ship-inflatable weir was desired. Numerical software Ansys was consulted to perform more extensive calculations about the collision event. Results from the numerical calculations, were tried to compare with what was found in the analytical study.

Physical model tests were done, to extract the significant process during the ship collision event. These tests could be performed at the cooperating company BAM Infra bv. The availability of space made it possible to do large scale model tests, what is preferred based on literature. The ship collision tests were visually analysed with cameras on top and side of the scale model. The data was visually analysed and put into graphs.

Finally, the results of the physical model tests were compared with the analytical model, to develop a more extensive analytical model that is calibrated on the physical model tests. With what is found during the research the main questions are answered.

1.5. Thesis outline

The thesis is outlined in seven chapters and a last chapter consisting of conclusions and recommendations, see flowchart in figure 1.4. The thesis starts with an introduction in chapter 1, which gives background information on the subject. The problem statement for this research is then described along with the research questions. In chapter 2 more information about water supply and management of river Meuse is elaborated. Then the weirs in the Dutch reaches belonging to the Meuse are categorized and the recent ship collisions are described. Chapter 3 presents the design for the inflatable weir as replacement for the existing weir at Grave. First the process of the design is explained and then different features of the design are described.

Following up, chapter 4 starts with the analysis of ship collision on the inflatable weir design. It gives results about the deformation and possible failure. Some calculations are done for the importance side effects of the water. Further, numerical modelling is performed in chapter 5 for ship collision on the rubber sheet of the inflatable weir. Software program Ansys is consulted to carry out the numerical calculations. Next, chapter 6 is committed to describe the scale model tests done, to gain understanding of the ship collision mechanism. The results were of the experiments are used in an improved analytical model in chapter 7.

Lastly, chapter 8 is a distillate of what is found in the previous. Conclusions and recommendations are given based on the research done.

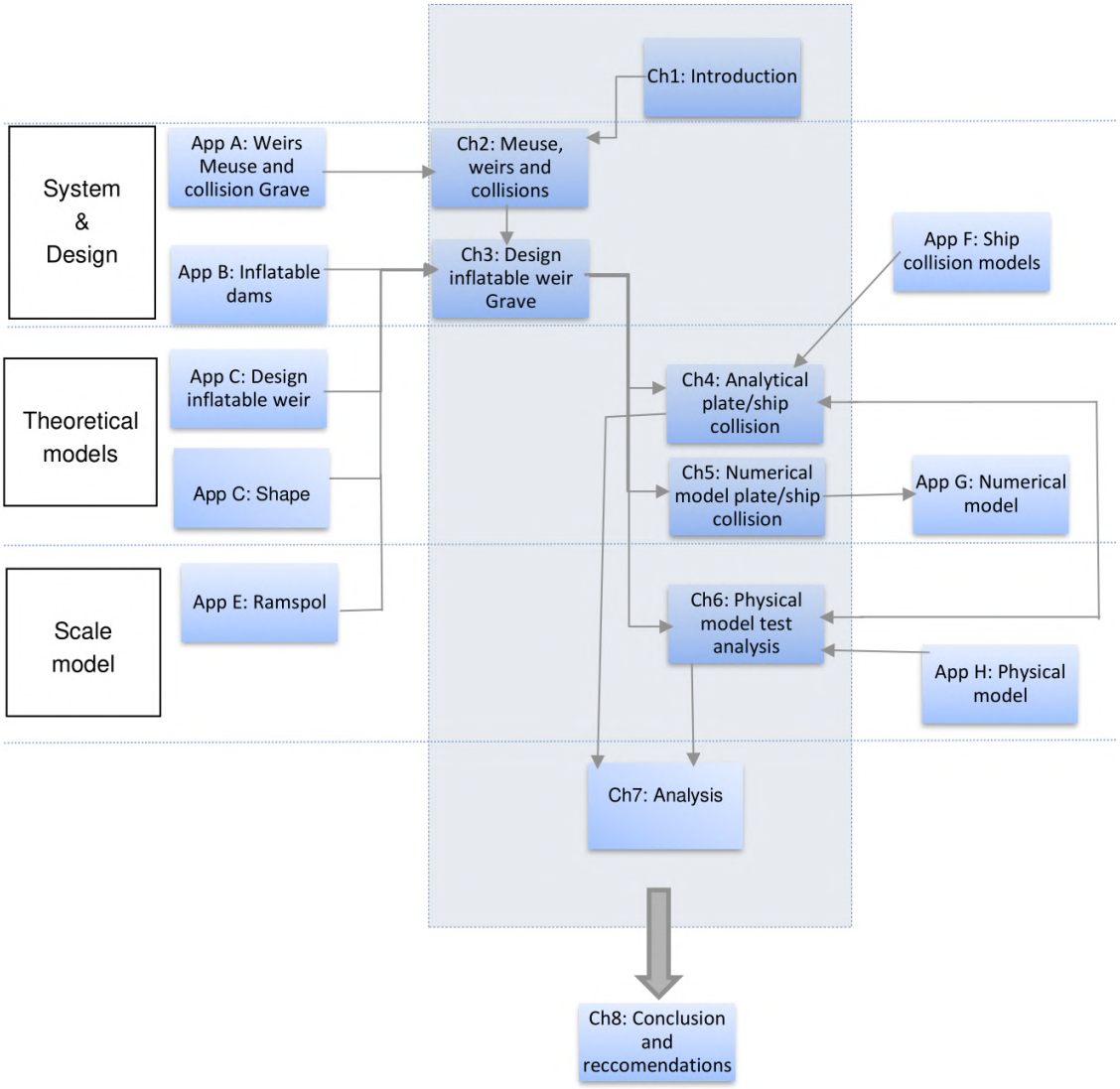

Figure 1.4: flowchart

2

River Meuse and the seven weirs

This chapter gives an overview of river the Meuse. The first paragraph 2.1 sets out how the river itself works and how it is characterized. Then an overview is given of the Meuse weirs in the Dutch reaches, in paragraph 2.2. The weirs are described by their type and functionality. Lastly the shipping in the Meuse is highlighted and relevant collision accidents in paragraph 2.3.

2.1. River Meuse

The Meuse is a free-flowing river which ends up in the Netherlands. The Meuse starts in France and then crosses Belgium and finally the Netherlands, see figure 2.1. The whole path of the river stretches over a length of 925 km and is for most part through mountains.

Figure 2.1: Meuse overview

The river gets most of its water from rain and melting snow from the Ardennes, see figure 2.2. The water follows the path with least resistance, which is to the direction of the lower laying areas. As can be seen from figure 2.2, the river is at a higher elevation in France. So, the river flows through the mountains in Belgium and finally enters the Netherlands where it ends up in sea.

2.1.1. Catchment area Meuse

The Meuse itself gains most of its water supply through connected side branches of the river in the mountains. In those side branches rainwater assembles that has been falling down on the mountains. The side branches coming all together to river the Meuse. At the location of Ardennes in Belgium there are a lot of side branches with high gradient, see figure 2.2. In combination with the low gradient downstream of those side branches, more water volume is available per unit length downstream of the river.

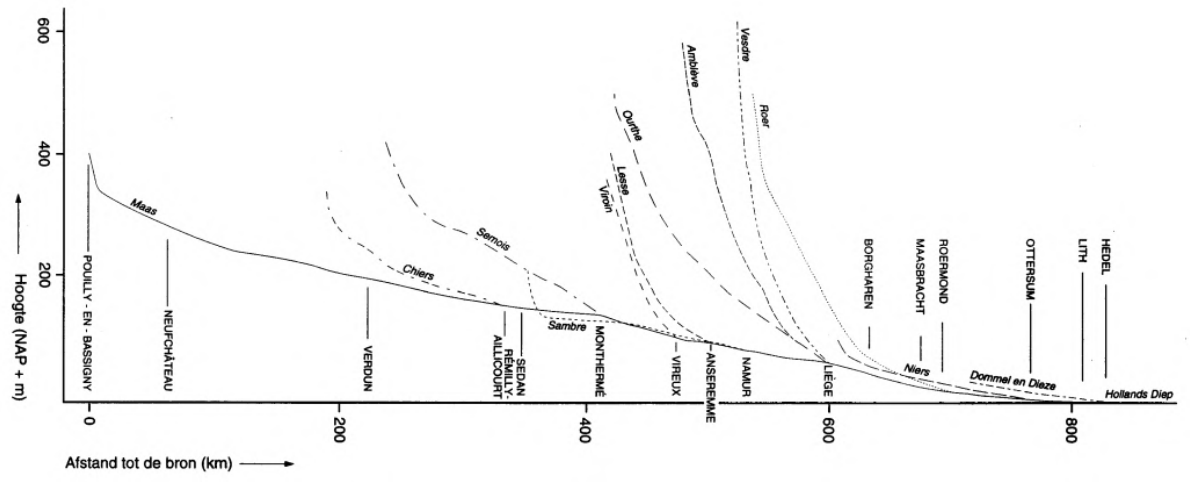

Figure 2.2: Meuse side branches [20]

2.1.2. Discharge characteristics

The water in the Meuse is automatically controlled, this is done by operation of the weir gates. In general, there are two options for the weir:

- A free-flowing river when the weirs are open
- A dammed river when the weirs are operational

For a free-flowing river, the water can move without disturbance through the river, this the case on average 5 days a year in the Meuse. If the discharge is large enough and so the water depth, the free-flowing situation is maintained. When the discharge drops below a threshold value, the weirs are activated. The weirs dam up the water level, to regulate a sufficient water depth for navigation. Every 10 minutes the weirs are adjusted based on the expected discharge and measured water level. The threshold value of the discharge is dependent on the Chézy value, which is an indication of the roughness of the bed. The Chézy value comes from the formula for averaged flow velocity in the river. The formula is defined as follows:

$$\overline{v} = C\sqrt{Ri} \tag{2.1}$$

where: $\overline{v}$ = average flow velocity [m/s]
C = Chézy value [$m^{1/2}/s$]
R = hydraulic radius [m] (equal to depth river)
i = slope [i]

If there is a (almost) flat bed, the Chézy value can be calculated as follows:

$$C = 18log_{10}\frac{12R}{2d} \tag{2.2}$$

Where d is the grain size diameter [m].

The water level is controlled by a negative feedback control system. The change in river discharge triggers to heighten or lower the weir. a higher discharge means a lower weir level and vice versa. The operation of the weir aims to achieve a steady state situation. The water level at the set points remains the same, but the surrounding water level can changes due to backwater curves. A water depth of 3 meters will be maintained for navigation [50].

In figure 1.1 the weirs are fully closed, hence retaining the maximum water level [46]. In this figure there is a zero discharge, because the water levels are flat. When the discharge increases water will flow over the weir. A second effect is that a back-water curve will develop, where the water level increases upstream. When the critical discharge value is reached, the weir will be lowered or lifted to increase the discharge capacity and maintain the same water level. The weirs have a certain target point where the maintained water level is based on. When the discharge increases the target point can change its value. An increase in discharge means a higher water level upstream. To maintain the minimum water depth over the whole river for navigation, the target point value will be changed [16].

Generally speaking, the Meuse is a calm flowing river. The discharge in the Meuse is on average 230 m^3/s ranging from 132 m^3/s in the summer to 320 m^3/s in the winter [23]. The discharge varies also a lot within the years. The minimum discharge can be 30 m^3/s and the largest flood wave in 1926 had a discharge of 3000 m^3/s [20] [55, p. 8]. For this high variability in discharge it is essential that the weirs can be adjusted for the required discharge. If the discharge is still too high another measure is taken that is the use of flood plains. These are areas which stay normally in dry and no vulnerable objects are placed in it such as houses. The flood plains will be flooded with water during very high discharge events also called flood waves.
Essentially the discharge is formulated with help also of equations 2.1 and 2.2 as:

$$Q = \overline{v} A_r \tag{2.3}$$

where: Q = discharge [m^3/s]
$\overline{v}$ = average water flow velocity [m/s]
A_r = latitude cross sectional area river [m^2]

From the equation of the water velocity it can be seen that the discharge is dependent on the inclination and the water depth. The inclination is more or less constant over the river stretch and changes over long periods of time. The water depth is dependent on the rainfall and melting snow from the Mountains, which differ daily. An overview of the variability in discharges in the river Meuse are shown in figure 2.3. The measurement data is the discharge of the Meuse including the Albertcanal, which is not of interest for the weir design in chapter 3. The Albertcanal starts at Liége and so takes water from the Meuse before it enters the Netherlands.

In figure 2.3 the months of the year are shown on the horizontal axis and the discharge on the vertical axis. The general trend shows that the discharge in the summer is lower than in the winter. The graph can be read as follows:

- Red line: the maximum discharge over the year 1911 to 2019 by the corresponding day of the year
- Green line: the average discharge over the year 1911 to 2019 by the corresponding day of the year
- Black line: the minimum discharge over the year 1911 to 2019 by the corresponding day of the year
- Blue line: the discharge for year 2019 per day

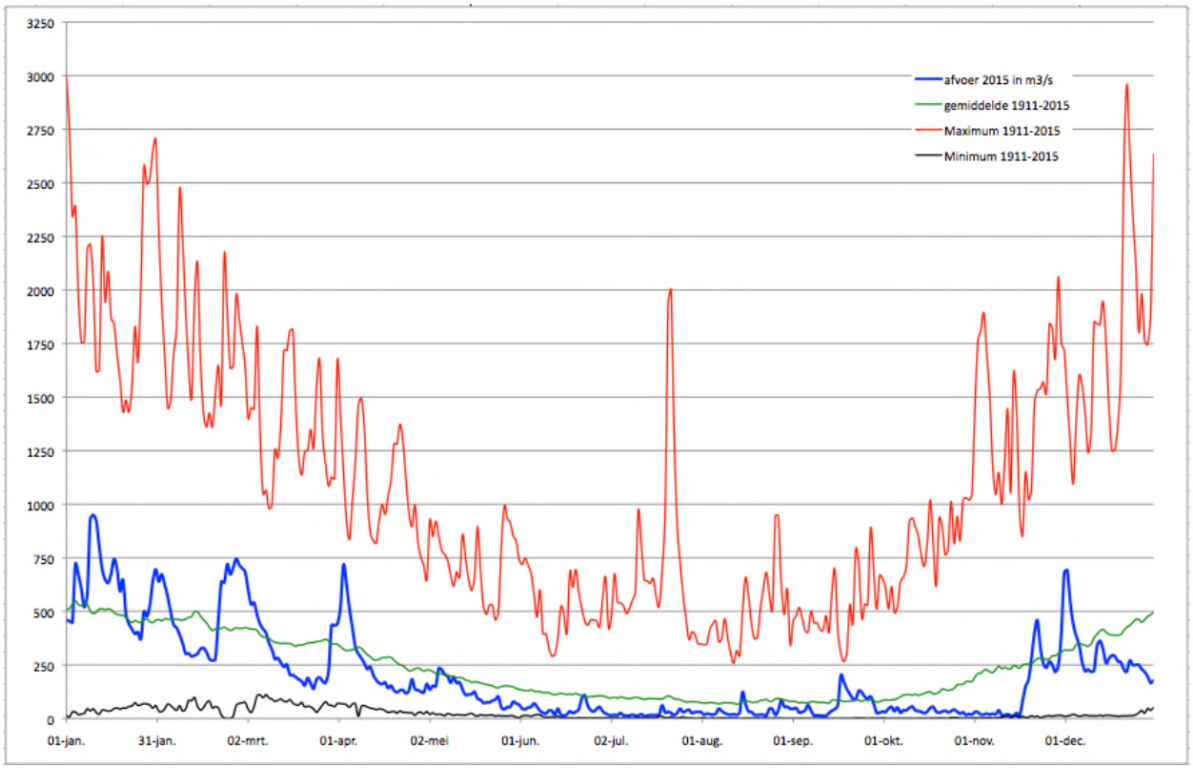

Figure 2.3: Meuse discharge from 1991 to 2015 [2]

To use the data of figure 2.3 an exceedance probability function is needed. For the Meuse discharge the exceedance probability is calculated for various discharges and shown in figure 2.4. The dots represent calculation points. Research is done about the changes in river the Meuse that alter the discharge regime. In the future the discharge exceedance curve is likely to be different due to the mentioned cases as building of dams and global warming. This research is done in the master thesis of Rooij [34].

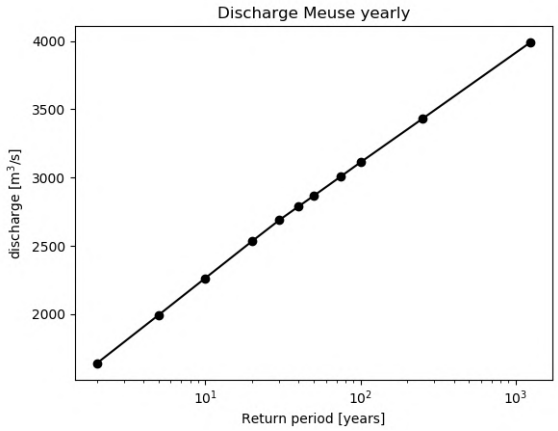

Figure 2.4: exceedance probability vs discharge Meuse [34]

2.1.3. Water levels in the Meuse

The water levels in the Meuse are based on stage relation curves (Dutch: bettrekkingslijnen). The discharge is measured at a certain point and with that information the corresponding water level is calculated. The measurement location point for the Meuse is taken at St. Pieter Noord, this is just south of Maastricht. For a given discharge at location St. Pieter Noord the water level downstream can be calculated. The stage relation curve gives the maximum expected water level based on the discharge, which is shown in figure 2.5. The lines, that indicate the water level in the Meuse, are based on yearly measurements and are interpolated with a WAQUA model. These water levels are used to argue the different collision scenarios, starting from chapter 4.

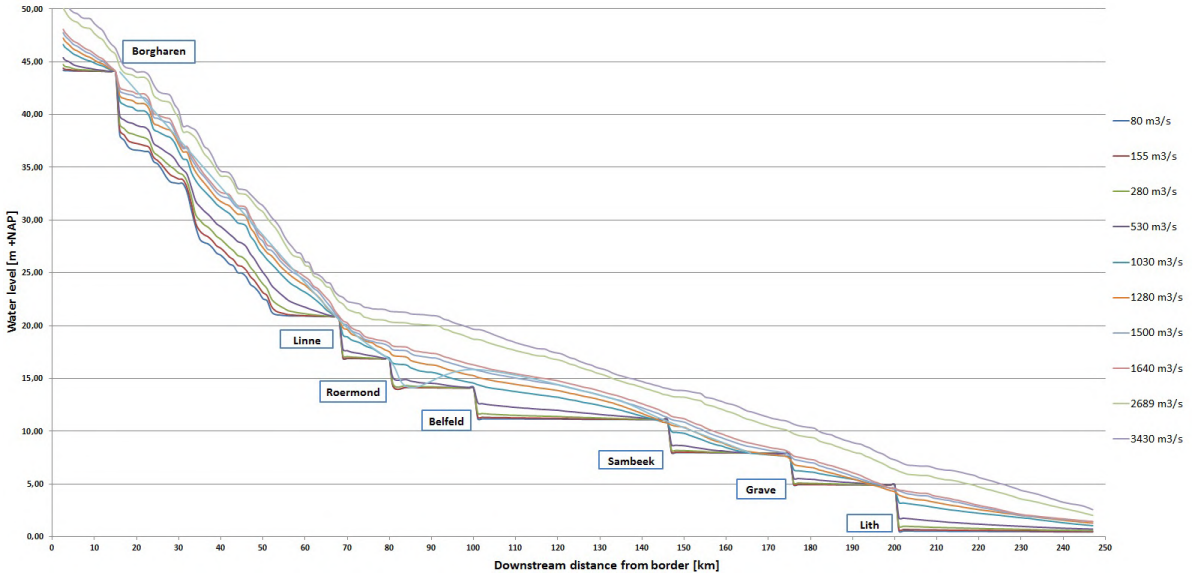

Figure 2.5: water levels Meuse for various discharges [49]

2.2. Seven weirs in the Dutch reaches

The Meuse is a large river, where its natural flow is disturbed by weirs constructed on the way downstream. In the Netherlands seven weirs are constructed in the Meuse, see figure 2.6. The weirs are constructed to achieve a controlled water depth for ship navigation. Multiple weirs needed to be constructed in order to achieve the desired minimal controlled water depth along the river. The ships that navigate through the river Meuse, need a minimal water depth, otherwise they will be stuck somewhere along the river.

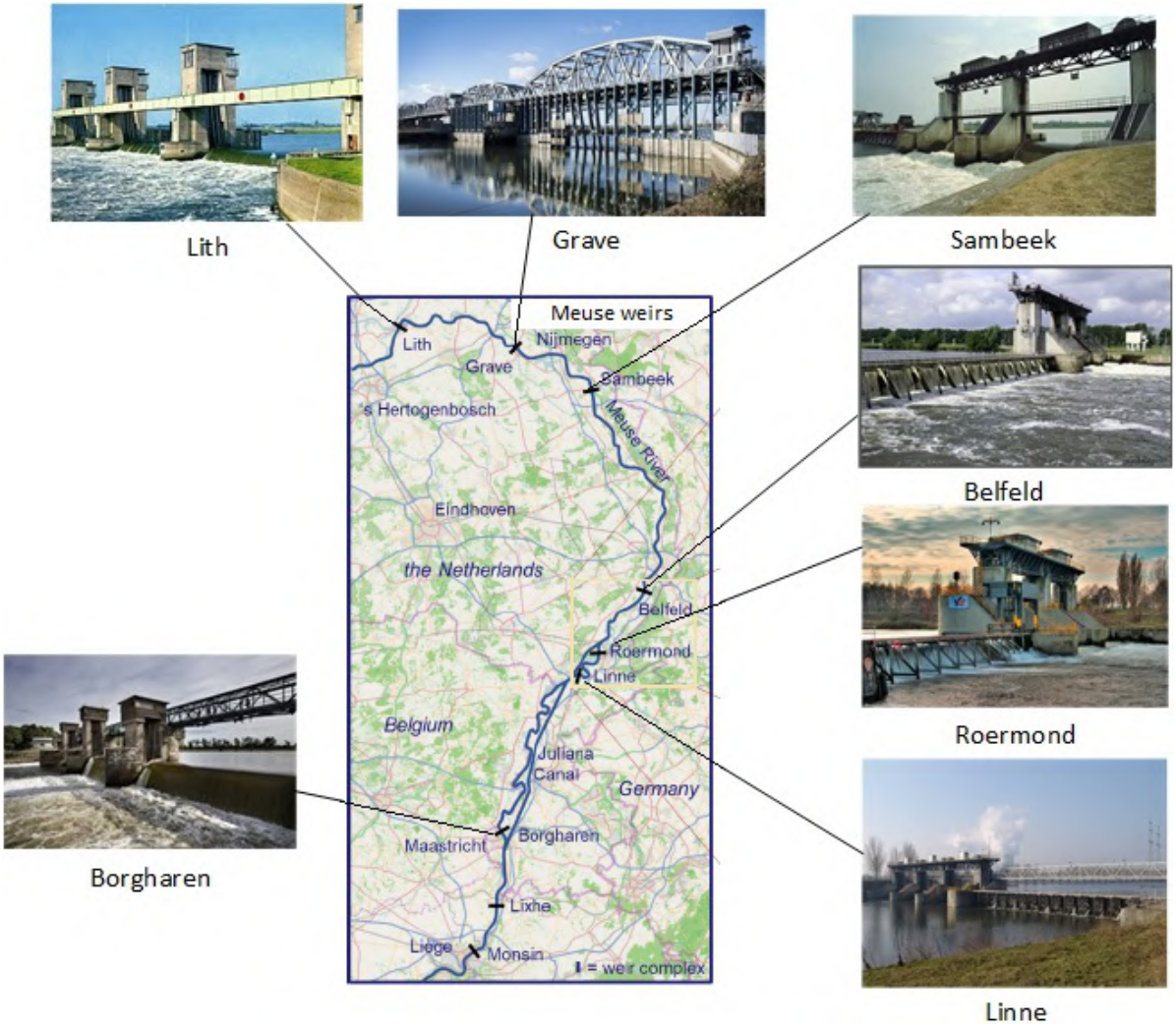

Figure 2.6: weirs in the Meuse (OpenStreetMap Nederland, n.d.)

2.2.1. Construction and replacement

The weirs are scheduled for replacement, one of the reasons is due to their oldness. Placing new weirs on a new location is seems infeasible, because the agreement of water distribution over the Netherlands and Belgium is fixed. When 2030 is reached one-to-one weir replacement will be done, if in the meantime no other design alternative is presented which preventing changes in the groundwater table and the water distribution over the length of the river [55, p. iii]. The seven weirs and their age are shown in table 2.1. The replacement of the weirs is scheduled in the years between 2025 and 2040 [8].

	Construction year	Scheduled replacement
Borgharen	1928	2025-2030
Linne	1921	2035-2040
Roermond	1921	2030-2035
Belfeld	1924	2030-2035
Sambeek	1925	2030-2035
Grave	1926	2030-2035
Lith	1936	2035-2040

Table 2.1: weirs Meuse construction year and replacement [8]

2.2.2. Weir complex decomposition

In this paragraph an elaboration is given how the weirs look like and how they function. The weir is a structure in a river or a canal, that is constructed to change the flow conditions. In case of the Meuse it is used to regulate the water level in the river. To regulate the flow there are two possibilities dependent on the weir structure: [39, p. 70].

- Overflow weir: The upstream water level can be well controlled
- Underflow weir: The discharge trough the structure is well-controlled

In case of the Meuse most weirs exists of an over- and underflow part excepts weir Grave, which is explained further in this paragraph. For the overflow weir there are two types: broad crested and sharp crested weir. In the Netherlands most weir are sharp crested weirs. [39, p. 72].

Stoney-poirée

The weirs Sambeek, Belfeld, Roermond and Linne exist of a Stoney and Poirée part, which act as under- and overflow respectively. The Stoney part consists of a frame with steel plates in front of it. On the frame round wheels are attached, that guides the steel plates to a lower or higher position. The suspension is regulated such that by lowering or heighten the steel plates, the trolley can move with half the velocity for smooth movement. The Stoney part has two steel plates between the columns. Those two plates roll past each other to regulate the water level. In first instance the plates are put on top of each other. To increase the discharge, the upper panel is lowered. When the two panels hit the sill, the discharge can be further increased by raising both panels above the water. The Stoney part can take about half the capacity discharges of the weirs. Each Stoney opening consists of a 17-meter-long opening with columns on each side. The Stoney steel plates are lowered or raised every 10 minutes based on measurements of water level and expected discharges. It fine tunes the water level and is automatically controlled.

The Poirée Part consists of two individual slides, which are placed on top of each other. The weir is closed by using both slides on top of each other. The weir can be opened by removing the steel panel and laying down the beams on the bottom of the river. In this case ships can freely navigate through the river without use of the shipping locks. For the four weirs the Stoney part is located next to the Poirée part. The Poirée part consist of 13 to 17 meter beams horizontally (Dutch: Jukken), with a total of 3 steel panels which can placed on top of each other. At Sambeek these panels are 4.85m wide and 1.90m high. The Poirée part is used for coarse regulation of the water level.

When the discharge increases, first the Stoney part is used to let the water through, by lifting the steel panels. If the discharges increases too much, then the steel panels are removed at the Poirée part, usually 3 panels in a row at a time. These panels are removed manually what makes the weir times consuming. The steel panels are removed by the top row, the middle row and finally the lowest row. Then the beams can be put down on the bottom, when also the steel panels at the Stoney part are lifted a free-flowing river appears.

Grave is characterized by an inversed Poirée weir. At Grave the weir consists in total of 20 beam columns with also three rows of steel panels. The beams are distributed over two openings and the panels are removed partly manually. The top and the middle panel can be removed automatically based on the configurations determined by the stewards (In Dutch: stuwmeester). The beams can also be lifted above the water level to provide ship passing.

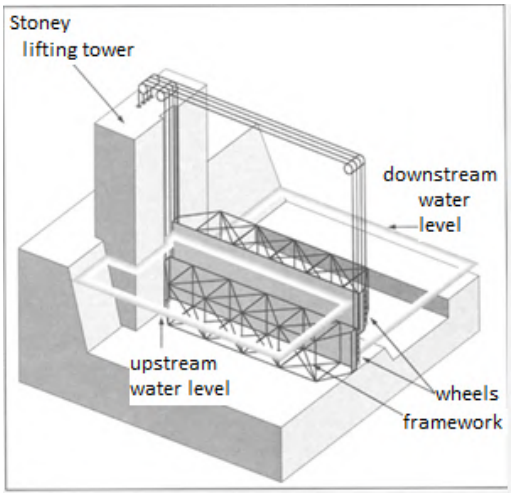

Figure 2.7: Stoney part [29]

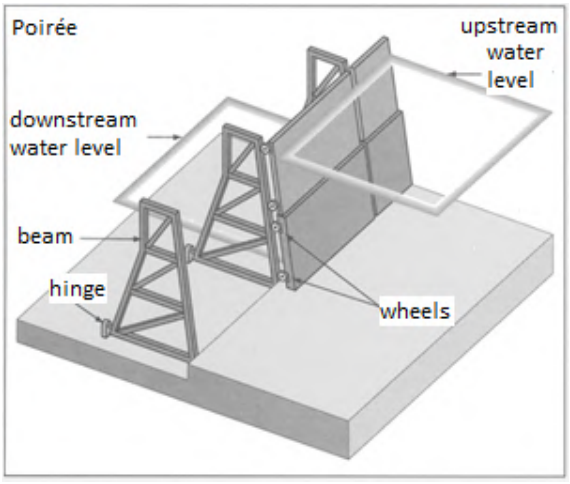

Figure 2.8: Poirée part [29]

Slides and valves

The weirs of Lith and Borgharen consists of different openings than the rest. Lith has 3 openings and Borgharen 4. The closure consists of a steel framework (slide) with a flap on top of it. By raising or lowering the flap, the discharge can be regulated. When the flap is laying horizontal and additional discharge capacity is needed, then the steel framework is lifted above the water to increase the discharge. Every 10 minutes the system is adjusted depending on the measured water level and expected discharge. The flap can so regulate the overflow of the weir and the lifting will create an underflow. For high discharges the underflow is used, since it can create a free-flowing river by totally rising the slide plus valve. See figure 2.9 for an illustration how the slides with valves look like.

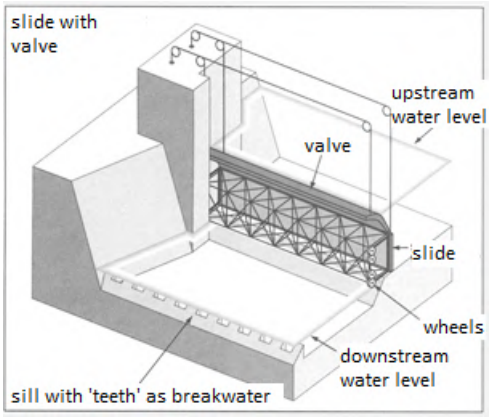

Figure 2.9: wheel valve [29]

Limit discharge

For all weirs there is a limit capacity of water discharge they can handle. The Stoney part can discharge their limit capacity when the steel panels are lifted. The Poirée part can discharge their limit capacity when the steel panels are removed and the beams laying on the bottom. For the weirs with slides and valves this is when all the slides (with valves) are lifted. The limit discharges per weir is given in table 2.2. The table shows a variation of the limit discharge. This is due to the difference in opening width of the weirs and the maintained water depth.

Weir	Lith	Grave	Sambeek	Belfeld	Roermond	Linne	Borgharen
Limit discharge [m^3/s]	1097	1070	1205	800	984	1278	1250

Table 2.2: limit discharges for the various weirs

2.2.3. Dimensions

The different weir types have all their own dimensions. Some parts in the Meuse are wider than other parts, that is why the total width of the weirs differ. Further the weirs have their own weir type configuration depending on the needs of the flow characteristics. The dimensions for each weir is given in table A.2 in the appendix.

2.2.4. Bed protection

Bed protection at the weirs is necessary to prevent erosion downstream of the weir. Erosion can eventually lead to instability of the weir and in the limit case will collapse. The bed protection of the weirs have been reported in RINK reports and is summarized in table A.1 of the appendix. The bed protection at Roermond is the shortest and least robust. It is plausible that the protection at Roermond has been reinforced based on the conclusions of the RINK reports. Further only at weir Linne the bed protection is different behind the Stoney and Poirée part. The other three weirs have the same bed protection for the Stoney and Poirée part. Ship collision on inflatable weirs can cause rupture of the sheet or overflow over the weir and as consequence the waterflow can damage the bottom protection.

2.3. Shipping

The size of ships that navigate through the Meuse, are elaborated in this section. The ships passing the Meuse are transporting cargo to or from the port of Rotterdam. To indicate the size of a ship, an international system is setup that is called the CEMT (=Conférence Europeenne des Ministres des Transports). With this system the size of a ship is indicated ranging from class I to VII (small to big).

In general, the waterway defines the maximum CEMT class that can navigate through the waterway. For the Meuse this is CEMT class Va at the time of writing. The waterway class and ship classes that navigate through the Meuse, are shown in figure 2.10.

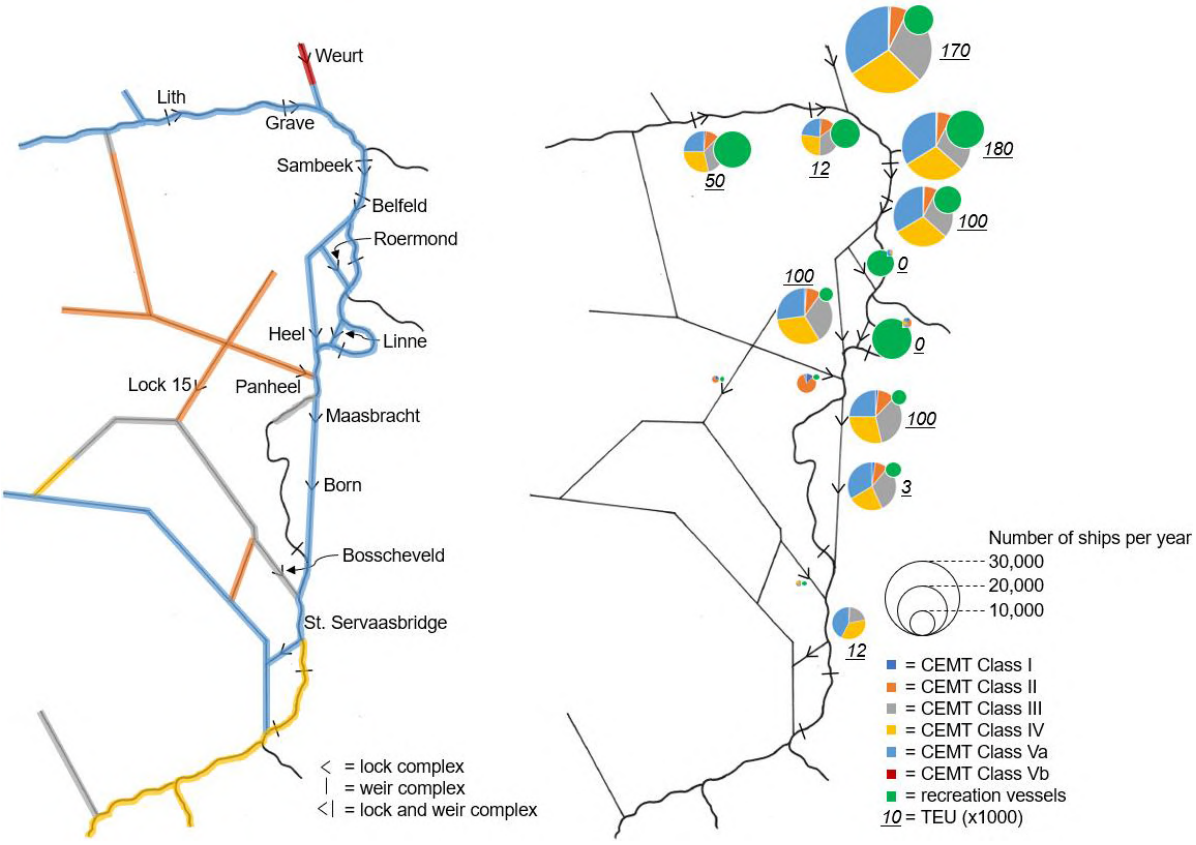

Figure 2.10: waterway- and ship classes Meuse [55]

There are some uncertainties with the given data in the figure. This figure is created by a previous Master thesis, doing research for design of an adaptive weir at Belfeld [55].

- The average is taken from 2005 until 2008
- In Maastricht data is missing
- Recreational ship have not been counted, but is considered insignificant for ship collision
- The total number of commercial ships is taken as two-third of the number counted at lock Born

The data from figure 2.10 is based on the load capacity of the ship. So, for a certain loading capacity the ship is placed in a certain CEMT class, but by dimensions the ship can be one CEMT class higher or lower.

Since the ship trade in the Meuse is increasing and so the amount of ships and their size, an upgrade of the Meuse is expected. With this upgrade a ship class of Vb is possible, which applies to push convoys. Currently, the canal is upgraded with wider sections where ships can pass each other. Widening of the Bend of Elsloo, to accommodate Class Vb ships is just feasible [10]. The maximum ship length is now 110 m in the Juliana canal. Also deepening of the river is scheduled to accommodate a draught of 3.5 meters. The maximum draught is now 3.0 m.

2.3.1. Ship collision events

Ship collision on a weir is not a regular event in the Meuse. Sometimes it happens, but depending on the mass of the ship and its velocity a significant impact can follow. All registered ship collisions in the Netherlands of a few selected years are found in appendix A, to give an indication. Two significant ship collision on weirs that have happened in the Meuse, are described below. The size and mass of those ships in the events are also used in this research. The first collision was in 2016 at Grave and the second happened at in 2020 at weir Linne. Both damaged the weirs such that they were out of operation for a while.

Grave

The ship started at Klein Ternaaien in Belgium a day before the collision. In around 30 hours the ship navigated to Grave where it collided with the weir on 29 December 2016. That day a thick fog was present. Fog can create a circumstance for a higher probability of ship collision. In appendix A a fault tree is represented how fog and other factors affect the ship collision probability.

By the force of the collision five baffles got loose, see figure 1.2, where a powerful current of water developed. The ship glided through the opening and landed 3 meters behind the weir. Normally the ship would make a fall motion, but the strong current and resistance of the baffles above the ship made it happened that the ship could glide with the movement of the water. The engine was stopped shortly after the collision, but would not let the ship come to a standstill. Thereafter the anchors were dropped and the ship stopped 600 meters behind the weir.

To navigate through fog with a ship it is obligated to have good radar equipment on board. On the ship a radar system was available that got his information through a circular panel. The circular panel registers objects with pulses that are displayed as dots on the panel. Although it was available it could not be derived if there was a closed weir upfront [64].

The ship that collided into the weir Grave, is called the Maria Valentine. It is a tanker ship that sails under the German flag. Some of the characteristics of the ship are given below:

	Symbol	Dimension	Unit
Length	L_s	110	m
Width	B_s	11.4	m
Draught	D_s	3.64	m
Loading capacity	m_s	3015	tonnage
Max ship velocity	v_s	6.1	m/s
Ship class	-	Va (RWS class M8)	-

Table 2.3: ship Maria Valentine characteristics

The velocity of the ship during collision is investigated by the Dutch Safety Board. They investigated a velocity of 4.05 m/s just 150 meters in front of the gate. This was the last velocity that could being distracted, before the ship hit the weir. At the day of collision, the ship was loaded with benzene and had a total load of 2000 ton, deriving from this a draught can be estimated of 3.64*2000/3015=2.41 m. According to the starting course, velocity, load of the ship and the observed damage of the weir, the Maria Valentine had to navigate straight to the weir without much velocity reduction. The baffles in the middle were hit by the ship and damaged. In figure 2.11 is shown where the ship hits the weir. After collision a temporary structure was placed around the damaged weir, so it was shielded and could be repaired.

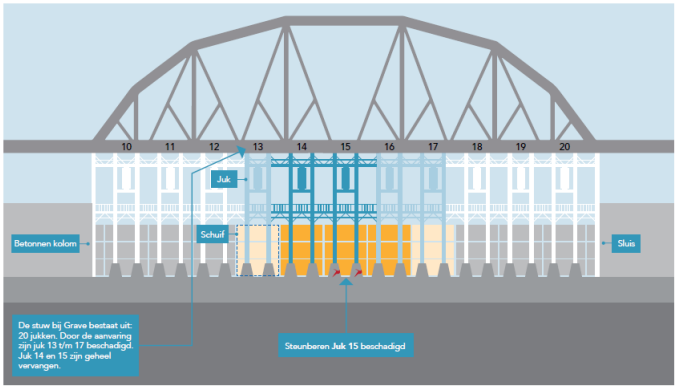

Figure 2.11: collision Grave front view [64]

Linne

On 10 February 2020 two empty push convoys got loose the quay. They were torn loose by storm Ciara that was ravaging the Netherlands, that day. Both push convoys were driven downstream by the current and hit the weir of Linne. With the impact five baffles were damaged. A temporary fracture stone dam is place in the Meuse to stabilise the situation. The dam takes over the water retaining function of weir Linne. It is noted that the breach of the weir induced a limited increase on the water level in Linne and Roermond, less than the actual high-water level during the storm Ciara. In Linne an increase of 60 cm can be expected and in Roermond 30 cm.

Figure 2.12: loose push convoy heading to weir Linne during storm Ciara [56]

Figure 2.13: reparation of weir Linne [52]

2.4. Discussion

The river Meuse is a free flowing river as described in this chapter. With the building of the weirs for inland navigation, the free flowing conditions are altered to a controlled flow of the river. These weirs are located at specific points in the Meuse. It is a study how the flow conditions and so the water depths will change, by replacing the weirs upstream or downstream of the existing location. The graph in figure 2.5 will then change. Another possibility to change the flow condition is with a different configuration of the under- or overflow part of each weir or Poirée and Stoney part respectively, described in paragraph 2.2.2. In this research no study will be conducted on the possibilities of doing a replacement different than 1:1. In the next chapter the design for a inflatable weir is presented, using 1:1 replacement as boundary condition.

In the past 20 years of the existing weirs in the Meuse, ship collisions with significant consequences only happened twice in the past 5 years. A reason for this can be the growing inland navigation, but two times in this short period is quite remarkable. Also, the ships become bigger and bigger, but the limit eventually is what the Meuse can take. All together it can be reasoned that ship collision is of increasing importance for hydraulic structures. Research is done into ship collision on an designed inflatable weir at Grave from chapter 4.

3

Design of an inflatable weir Grave

In this chapter the design is presented for the inflatable weir at Grave. The design is tested on ship collision in later chapters. First an overview of Grave is given in the first paragraph 3.1. The process of the design and the design itself is explored in paragraph 3.2. Building further on the design the next paragraph 3.3 describes the components needed for the design itself, such as the sheet length and the clamping structure. The last paragraph 3.4 deals with an overview of the design.

3.1. Overview Grave

In the previous chapter 2, already some key aspects of weir Grave are given. Weir Grave is here elaborated deeper. In principle, the weir in connected to a spanning bridge, where the weir is used to manage the water level in the river for navigation. When the weir is closed or partly opened it is not suitable for ships to pass through this route. A lock is situated next to the weir to let ships pass the river section. In figure 3.1 the place of the weir and its two locks are shown.

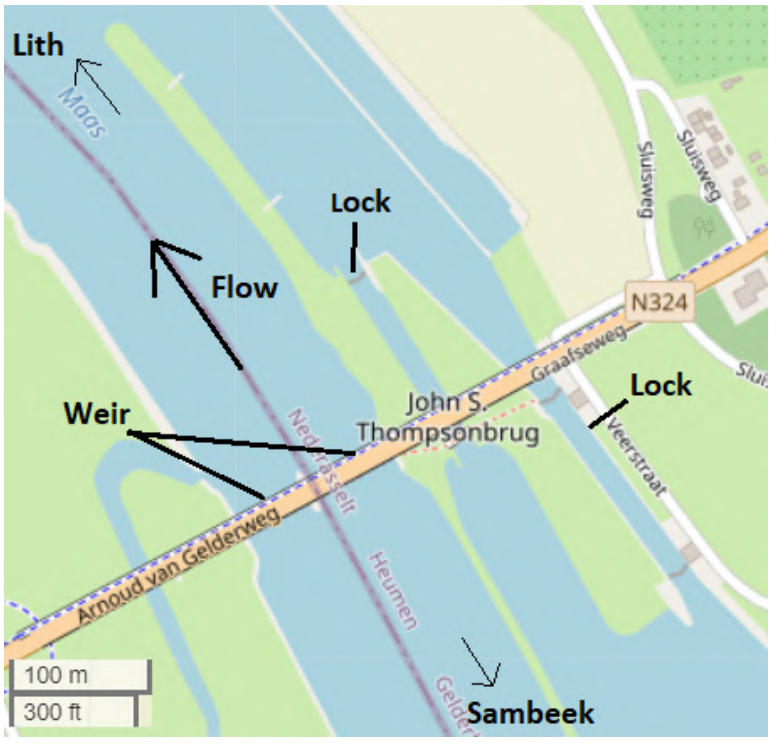

Figure 3.1: overview weir Grave (OpenStreetMap Nederland, n.d.)

The weir Grave is against the trend of using bigger parts to regulate the water discharge. The weir has to retain 3.5 m water drop height. Bigger parts that are used for Poirée parts, would be too weak for the high-water drop height. Vertical pillars are used which are hinge supported to the bridge above. Between the pillars, steel plates can glide on top of each other from the top of the bridge to dam up the water level upstream. The bottom of the pillars are resting on a threshold at the river bottom. The dimensions of weir Grave are shown for the front view in figure 3.2 and a cross section from the side in figure 3.3. As is shown from the cross section figure, the maintained water level was lower (-30 cm) 100 years ago. The increase in maintained water level can be explained by the larger ships navigating through the Meuse.

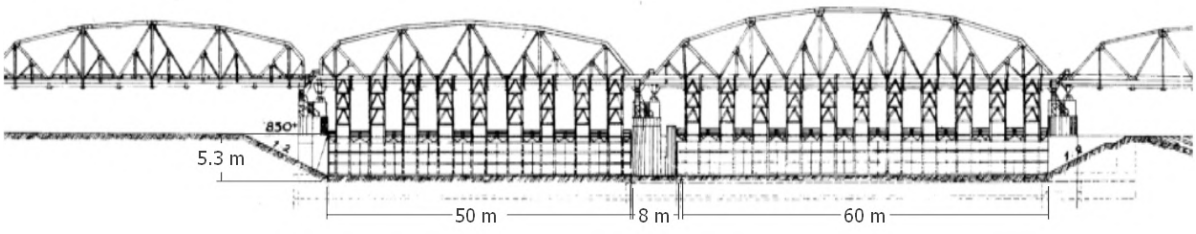

Figure 3.2: Weir Grave cross section front view [8]

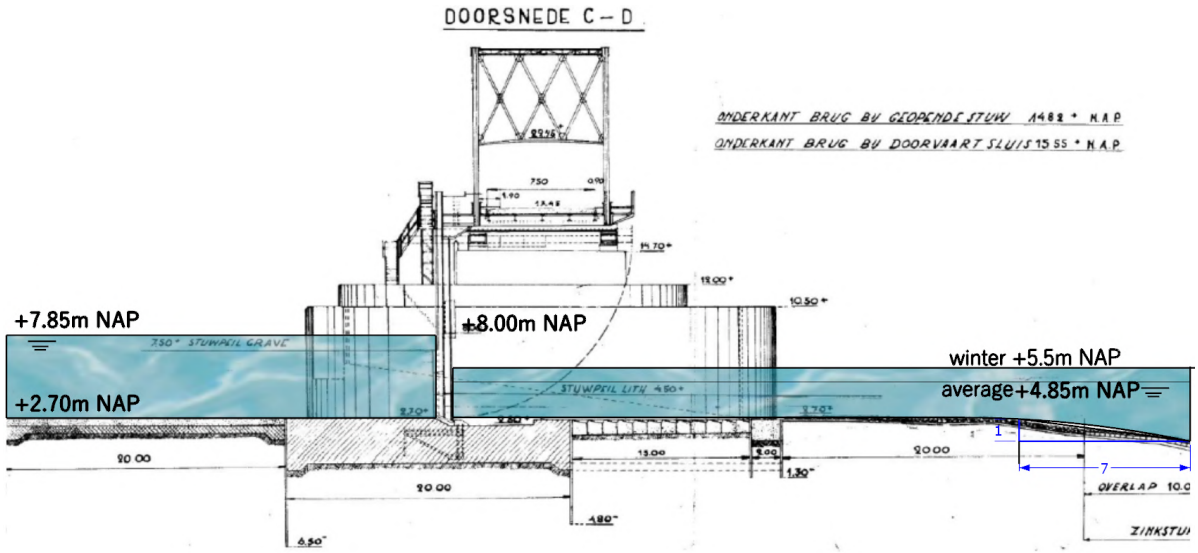

Figure 3.3: Cross section weir Grave side view [33]

3.2. Design process inflatable weir

As described in paragraph 2.4, the design made in this chapter is narrowed to 1:1 replacement of the existing weirs in the Meuse. This design process only focuses on the inflatable weir, which is an overflow weir. The design of the inflatable weir is made to research ship collision on this structure. According to Rijkswaterstaat the inflatable weir shows enough potential for further investigation [68]. In a normal design process also other kind of weirs would be considered, but are not in the scope of this research. Other type of overflow weirs are included in appendix C, to give an impression what kind of weirs exist.

The inflatable weir is an option for the replacement of existing Poirée parts at the Meuse weirs. Both are overflow weirs, where the water flows over the top of the weir. The Stoney parts are all underflow weirs, hence for 1:1 replacement the inflatable weir is not applicable. It will be time consuming to design for all suitable locations an inflatable weir and will be of less interest for this research. A solution is sought for in a general design of the inflatable weir, where its dimensions are sizeable to the desired location. For the replacement of the existing weirs it needs to be considered how the river Meuse will be and be used in the future.

For the location of the initial design, Grave is chosen. The existing weir of Grave has two inversed Poirée parts and Grave is scheduled as first weir for replacement in 2028, making it a suitable design location. It has to be noted that the current weir at Grave is attached to the bridge above. During the second world war (WWII), this bridge gained attention of its transportation function. Now the bridge is turned into a monumental object, which is likely to be maintained.

First the design process of making a design is given. Then the conceptual design phase for this research is described. Within the design process more design phase are usually needed, which consists mainly of five steps. The analysis step consists of the criteria, where the design step is built on. Within these criteria possible design solutions are developed, which is called the synthesis step. The possible design solutions are tested and elaborated on the cons and pros, this is the simulation step. Then the evaluation is started, based on the grouped pros and cons of each design the ranking is determined. A decision will be made, which designs are further developed in the next phase. One whole design cycle (phase) is given in figure 3.4. In general, the design phases are as follows: orientation, preliminary design, final design and detailed design. In scope of the research only the preliminary (conceptual) design cycle will be made. Assumptions are therefore needed that narrows the design process prematurely.

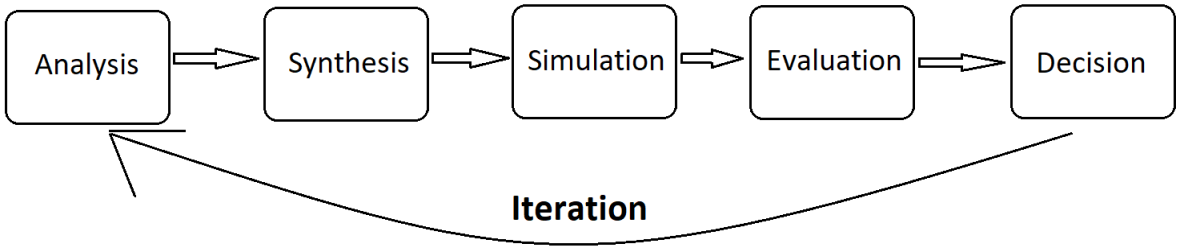

Figure 3.4: design process

The first phase in the design phases is the orientation phase. This phase is assumed to be already done in 'Vervangingsopgave stuwen in de Maas', where the weirs are scheduled for replacement. The next phase is the preliminary (or conceptual) design phase. In this phase a first design is presented that can be suited as replacement of the Poirée parts in the Meuse. This research is limited to ship collision on an inflatable weir, so the design phase will be narrowed up to a feasible scope.

3.2.1. Design study

In this paragraph the design is presented which can act as replacement for the weir at Grave. The design is the outcome of four inflatable weir designs made in appendix C. The weirs are based on reference designs proposed in other projects. Two important design considerations are implemented in all four designs that is based on what is found in literature and logical reasoning [62], [45].

- abutments 45 degrees
- one side clamped

Multi criteria analysis

The four design possibilities are conducted to a Multi Criteria Analysis (MCA). A weighted score is given to the criteria of each design. With the sum of the weighted scores from the criteria, a total is formed. With this number a ranking is formed for the design options. The MCA covers the simulation step and the evaluation step. In appendix C the full analysis can be found.

A note has be given to the ship collision criteria, which is most important in this research. The expected higher ship class Vb, discussed in paragraph 2.3, is in the range of push convoys [41, p. 23] and is a plausible scenario for ship collision in the future. Likely the weir has to be resistant against this higher ship class. This research anticipates on the plausible higher ship class in the Meuse in the future, by using the ship geometry of the push convoy, which is clear from the experiments done in chapter 6.

Overview design

The design for the inflatable weir at Grave can be seen as example for the replacement of other Poirée parts in the Meuse. In the next two figures, the final conceptual design is given extracted from the information in this chapter. Dimensions of figure 3.5 are related to figure 3.2 and dimensions of figure 3.6 are related to figure 3.3.

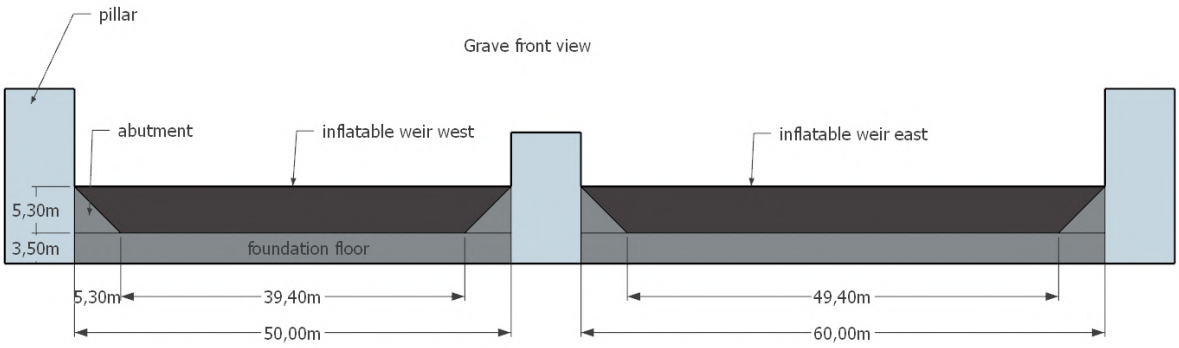

Figure 3.5: front view final design

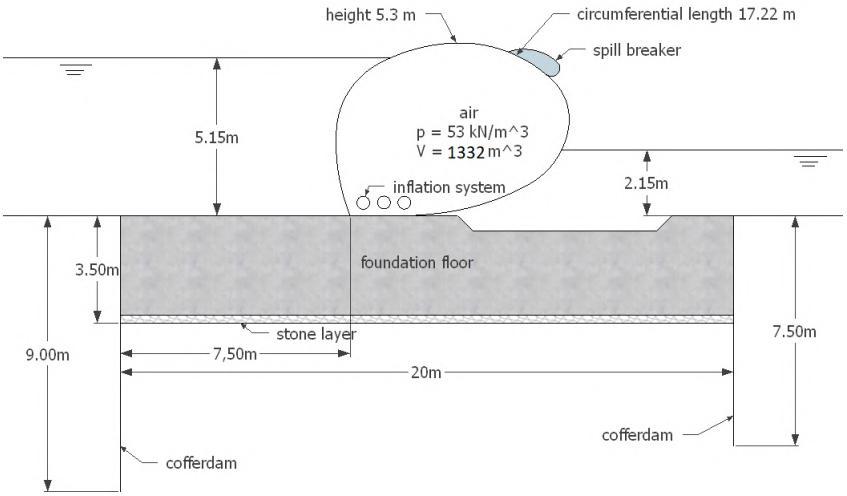

Figure 3.6: side view final design

3.3. Design aspects

This paragraph deals with the sub-parts of the inflatable weir, which are in extend important for the analysis of the ship collision. The sub-parts are categorized in shape membrane, abutments, clamping structure, filling medium and sheet material. The sub parts give insight how the inflatable weir works and is going to look like.

3.3.1. Shape membrane

In this paragraph an overview is given for the shape of the rubber membrane of the inflatable weir design Grave and how it is found. The theory behind this shape can be found in appendix D. Basically the shape is based on a cross sectional view of the membrane. The forces acting in the cross sectional view define the shape of the membrane. Generally these forces consisting of water or air, see figure 3.7. Since water and air can deform to the shape of the contact surface, these forces work perpendicular to it as shown in the figure. The perpendicular forcing makes it easy to work with the theory derived for determining the shape of the

membrane. Further the water pressure is assumed to work hydrostatic, so the force generated by the water increases linearly in depth. In formula form the water pressure is described by:

$$p_w = \rho_w g h_w \tag{3.1}$$

where: p_w = water pressure [N/m^2]
ρ_w = density water [kg/m^3]
g = gravitational constant [m/s^2]
h_w = depth in the water column [m]

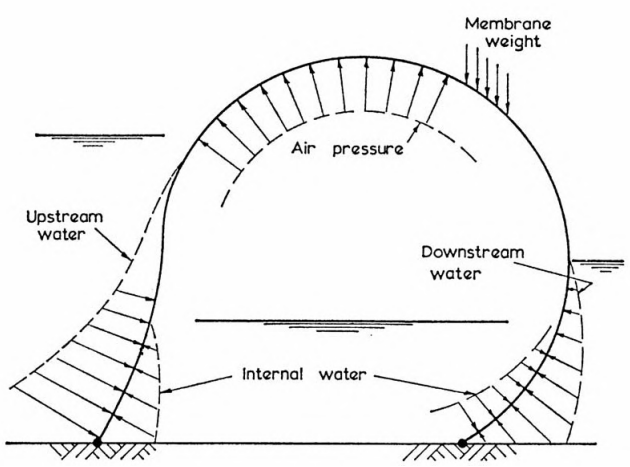

Figure 3.7: force overview [17]

In figure 3.7 the membrane is curved in a specific form. The curvature of the form can be directed inward of the membrane or outwards. When the outer pressure is larger than the inside pressure the membrane will curve inward and vice versa. See in the figure the higher water level on the left, which gives a higher outside pressure than the inside pressure and the membrane is curved inward. The forces taking into account for the curvature of the membrane are defined as follow:

- internal water pressure
- internal air pressure
- outside water pressure
- own weight membrane
- forces in membrane

The air pressure is defined by the air pressure inside minus the atmospheric pressure. With this the atmospheric pressure is already compensated by the inside pressure, so the atmospheric pressure is not presented as a force. The air pressure in formula form is defined as:

$$p = p_{in} - p_{atm} \tag{3.2}$$

where: p = resulting pressure [N/m^2]
p_{in} = internal pressure [N/m^2]
p_{atm} = atmospheric pressure [N/m^2]

Parameters

Without knowing how the shape is going to look like, two essential parameters of the membrane are initially determined: internal pressure 'p' and tensile force 'T', see figure 3.10. When the tensile force is known, the initial angle 'ϕ_0' can be determined from force equilibrium. The length of the sheet 'L' is determined from the found shape according to the theory. A rule of thumb is that the length is four times the height of the membrane for single line clamped and air filled [62], see also appendix D

The internal pressure is determined based on the desired height of the membrane. The internal pressure is about the same as the head for the air-filled type membrane [37]. The internal pressure for the air-filled type is then, where H is the desired weir height [m]:

$$p_{in} = 1000H \; [N/m^2] \tag{3.3}$$

If the downstream side is dry then the pressure in the membrane needs to be about 20%–60% higher than the carried water head. This is to compensate for tensile anchoring reactions, self-weight of the membrane and some other load components [45].

In recent literature a formulation is defined for the tensile force of the membrane. The formulation is made by Gebhardt, where the tensile force is dependent on the relation between the difference of upstream and downstream water level and the internal pressure [35]. With the following formula the tensile force is calculated for an air-filled type membrane:

$$T = \frac{1}{2}\alpha\rho_w g H^2 \tag{3.4}$$

where: T = membrane force [N/m^2]
α = internal pressure coefficient $\frac{p_{in}}{H_{up}}$ [-]
ρ_w = water density [kg/m^3]
H = weir height [m]

In figure 3.8 a relation is given between the theoretical shapes and the internal pressure coefficient. The parameter 'R' indicates the radius of the membrane. In case the membrane is only surrounded by the atmospheric pressure and internal pressure, then the internal pressure coefficient (α) goes to ∞. This is logical, since according to the theory of force equilibrium a circle should be found. More information about the research of the tensile force is found in appendix C.

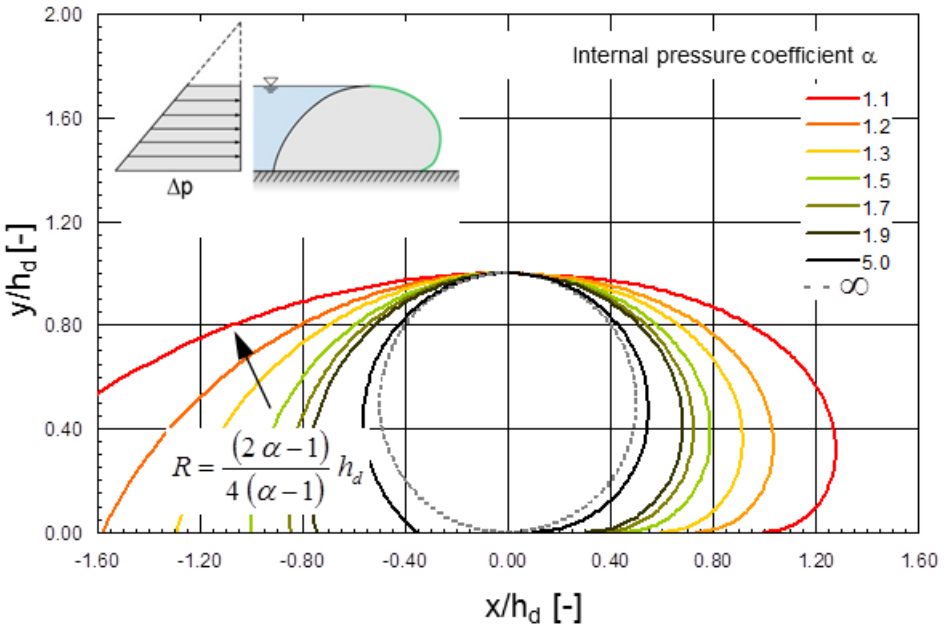

Figure 3.8: geometry as function of internal pressure coefficient for air-filled type membrane [35]

Now the tensile force is determined by equation 3.4, the last parameter 'ϕ_0' can also be calculated by horizontal equilibrium for a one side clamped membrane, see also figure 3.10.

$$\frac{1}{2}\rho_w g H_{up}^2 = T(1+\cos\phi_0) + \frac{1}{2}\rho_w g H_{down}^2 \tag{3.5}$$

where: ϕ_0 = angle membrane upstream [°]
H_{up} = water depth upstream [m]
H_{down} = water depth downstream [m]

Taking ϕ_0 to the left hand side gives:

$$\phi_0 = \cos^{-1}\left\{\left(\frac{1}{2}\rho_w g\left(H_{up}^2 - H_{down}^2\right)\right)/T - 1\right\} \tag{3.6}$$

For a two side clamped weir there are two unknown angle values. The second angle value can be found with vertical force equilibrium. For this the Kettle formula can be used. Since the design will be one line clamped, the two side clamped will not be further discussed.

Shape inflatable weir Grave

With the theory described in appendix D and the determined initial parameters, the shape of the membrane should be found. In the appendix a demonstration is made for a circle with the theory based on the weir height at Grave.

The cross sectional shape of the inflatable weir at Grave is found by force equilibrium of elements. The shape is discretized into a finite number of elements (dS) where the coordinates and pressure are determined on the nodes, see figure 3.9. To calculate those coordinates the following formulations are applied, where dS^* is the elongated element length:

$$\phi_{i+1} = \phi_i - \frac{dS^*}{dS}\frac{p}{T}dS \tag{3.7}$$

$$x_{i+1} = x_i + \frac{dS^*}{dS}\cos\phi_i \tag{3.8}$$

$$z_{i+1} = z_i + \frac{dS^*}{dS}\sin\phi_i \tag{3.9}$$

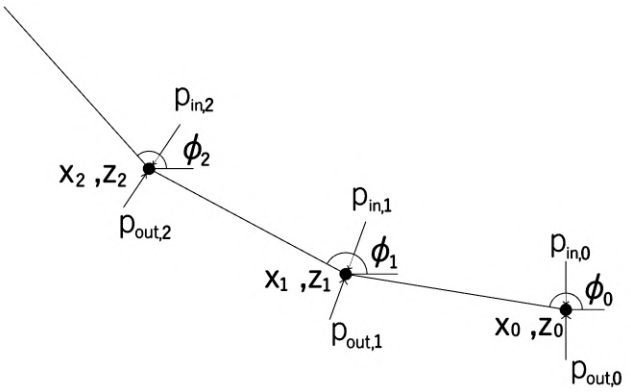

Figure 3.9: element model

At Grave there is an upstream and downstream water level. This creates three different situations around the length of the membrane, where the third situation is the contact with the atmospheric pressure. As done in the theory, the starting point is the clamping line. The resultant pressure for the three different situations are then defined as follows:

$$case = \begin{cases} 1 & \\ 2 & if\ z_i > H_{up}\ and\ case\ =\ 1 \\ 3 & if\ z_i < H_{down}\ and\ case\ =\ 2 \end{cases}$$

$$p = \begin{cases} p_{in} - (H_{up} - z_i)\rho_w g & for\ case = 1 \\ p_{in} & for\ case = 2 \\ p_{in} - (H_{down} - z_i)\rho_w g & for\ case = 3 \end{cases}$$

The unknown starting conditions tensile force (T) and internal air pressure (p_{in}) have to be determined with equations 3.4 and 3.5. Here also results the initial angle ϕ_0 from. In table 3.1 the parameters are shown and in figure 3.10 the found shape is shown.

Parameter	-	value	unit
Design height	h_d	5.3	m
Upstream water level	H_{up}	5.15	m
Downstream water level	H_{down}	2.15	m
Internal pressure	p_{in}	53	kN/m^2
Circumference length	L	17.22	m
Tensile force	T	139	kN
Initial angle	ϕ_0	1.8	rad

Table 3.1: parameters

The initial length of the sheet is taken as four times the membrane head (4H) and is divided into 1000 elements. At the ends of the elements nodes are situated, where equilibrium of forces is determined, see figure 3.9. Starting at the clamping line, the coordinates of the nodes are calculated with equations 3.7, 3.8 and 3.9. The calculation of new coordinates is stopped when $z_i > z_{i-1}$ and case = 3. The coordinates are then linearly connected and so the shape is found, see figure 3.10. The length of the sheet can be found by multiplying the number of elements used to get the shape times the stretched length of an element dividing by the strain ($n^*dS^*/(1+\epsilon)$). The length of the sheet found here is 17.22 m. The x-coordinate, where the z-coordinate is for the first time below 0, is 1.45. This means the sheet lays for 1.45 meters on the foundation.

The following observations are found that deviate from the desired value. The last z-coordinate did not finish at smaller than zero, but 5 cm above the zero (ground) line. This is pretty close to the bottom and is an acceptable deviation, stated that the theory is not perfect for the circular shape. The maximum height is 5.8 m which is a considerable deviation from the desired height of 5.3m.

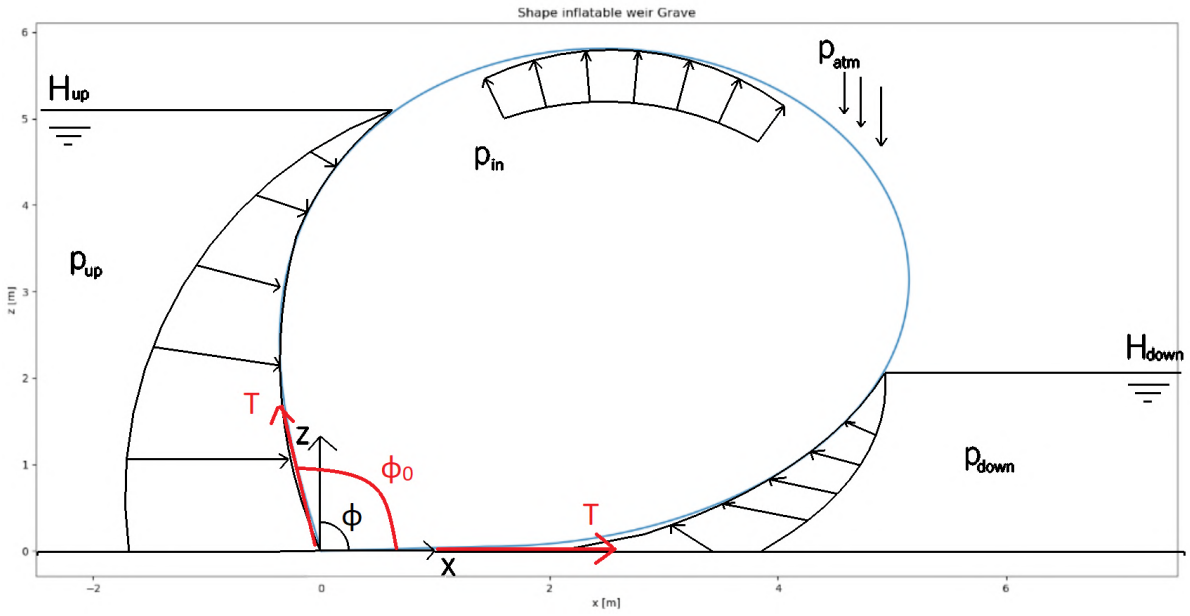

Figure 3.10: shape inflatable weir Grave standard

It is criticized that the values found by the theory deviate too much from the desired values. In appendix D a parameter optimization is executed, to find the shape with the desired height and last z-coordinate. The tensile force is varied between 90 kN and 190 kN and the initial angle between 0 and π. Both are varied with 100 sub steps, so that a 100x100 matrix is created with shapes. Nonetheless there was no shape better fitting the shape curve then the shape found here.

3.3.2. Volume membrane

The volume of the inside of the inflatable weir can be found by the shape of the membrane in cross section and the length of the inflatable weir in longitude. The internal area of the cross sectional shape is first determined

with Greens theorem. In his theorem the internal area can be calculated in a discretized form:

$$A_{in} = \frac{\Sigma x_i z_{i+1} - x_{i+1} z_i}{2} \tag{3.10}$$

Using the coordinates calculated in figure 3.10 and Greens theorem the area of the cross sectional membrane found is 25.6 m^2. For a circle the area would be $\pi r^2 = \pi(5.3/2)^2 = 22m^2$, so the area calculated with Greens theorem seems valid. The volume is then calculated by: internal area multiplied with length of the sheet minus the abutments plus a fourth times the abutments, because of its double 45 degrees inclination. The total air volume is then, see dimensions in figure 3.5:

$$V_{in} = A_{in}(49.4 + 2\frac{1}{2}\frac{1}{2}5.3) = 1332\ [m^3] \tag{3.11}$$

3.3.3. Clamping

This paragraph describes the clamping design of the inflatable weir. A look is first taken if the two side clamped membrane is a competing option against the single clamp line. Then the design of the clamping line is discussed.

It is possible for the inflatable weir to clamp it one or two sided (upstream or upstream and downstream of the river). To get an impression of a one- and two sided clamped weirs, see figure 3.11. The left shows a three dimensional one side clamped weir and the right shows a cross section two side clamped weir. The clamping for both the one- and two sided clamped weirs is extended up to including the abutments [62]. For the one- and two side clamping lines both advantages are derived:

- For the one side clamp less clamping line is needed
- For the two side clamp the membrane stays reachable for inspection and the membrane circumference is shorter

In the figure 3.11 it is shown that the weir with one side clamp can lay flat on the bottom. For two side clamp the sheet lays in folds as has been done in Ramspol, see figure E.5. Ramspol is a storm surge barrier, where it is possible for having a higher water level on both sides of the barrier. With a one line clamp the sheet can turn over direction if the current is from a wrong direction, therefore a two line clamp is chosen. For weirs a one line clamp is convenient, since the water flow comes all the time from one side. Hence a one line clamp for the inflatable weir at location Grave is used in the design. The use of one clamping line makes the use for guide rollers unnecessary as described in appendix C.

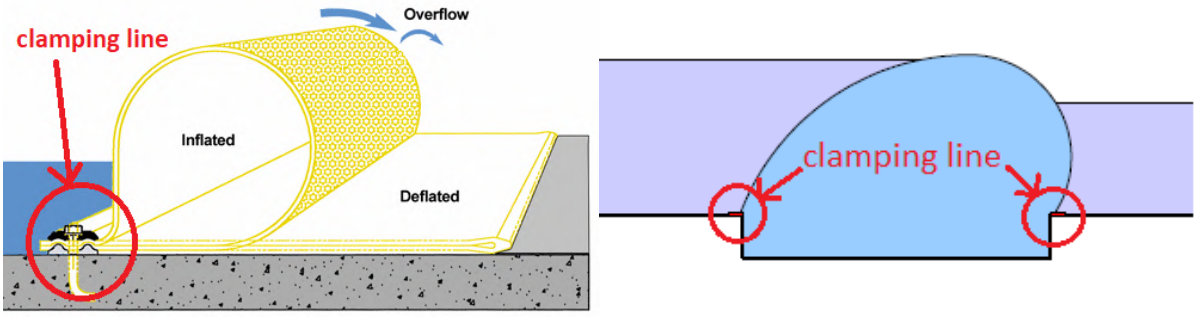

Figure 3.11: one side clamped on the left and two side clamped on the right [62]

Clamping design

For the clamping structure itself the same clamping will be taken as Ramspol. The manufacturer (Bridgestone) of the sheet of Rampsol has much experience with this clamping structure. Other clamping structures, that are not chosen, are given in appendix C. An optimization was tried to make for the design of the clamping structure at Ramspol. However the calculation models could not adequately verify another design, which could reduce the costs. The research was aborted and the clamping structure from the manufacturer was still taken.

The clamping structure is given in figure 3.12. This is the clamping used for the horizontal part for Ramspol. For the abutment part a different clamping structure was chosen, because of the wave steps, see appendix

E. In this design no wave steps do apply. Pre-stressed bolts are penetrated through the sheet and both plates to tighten the clamp. The pre-stressed bolts are placed with a centre-to-centre distance of 150 mm. Several measures are important for protection:

- The clamp should be made of stainless steel to prevent corrosion
- Water repellent grease is used under the cap nuts to prevent water entering
- An elastic wrapping band is put around the anchor holes to allow for stretching of the anchor
- The sheet has a higher thickness at the clamping points

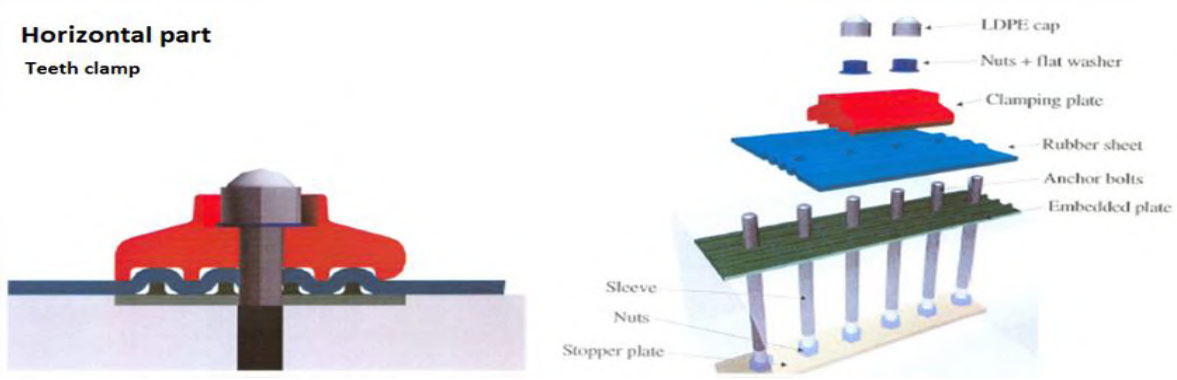

Figure 3.12: wave clamping horizontal part [38]

3.3.4. Abutments

The abutments form a new challenge for the inflatable weir. Traditional steel weirs have straight abutments, which suits to the location for the design of the inflatable weir. However for the inflatable weir a straight abutment causes sacking of the sheet in deflated state. An angle is desired to prevent sacking of the membrane sheet. A too large abutment will on the other hand block the flow passing through the river. Both reasons argue a desired slope of 45°, see figure 3.13.

Another option is to round the sheet membrane on both ends to the bottom. How this looks likes is given in appendix C. This design creates however a leakage at the corners of the weir. In maintain conditions the discharge will than be per abutment around 44 m^3/s, times four at location Grave is 176 m^3/s in total. This comes close to the average discharge of 230 m^3/s. When a lower discharge needs to be maintained this design is insufficient. The design with 45° abutments is thus best suited.

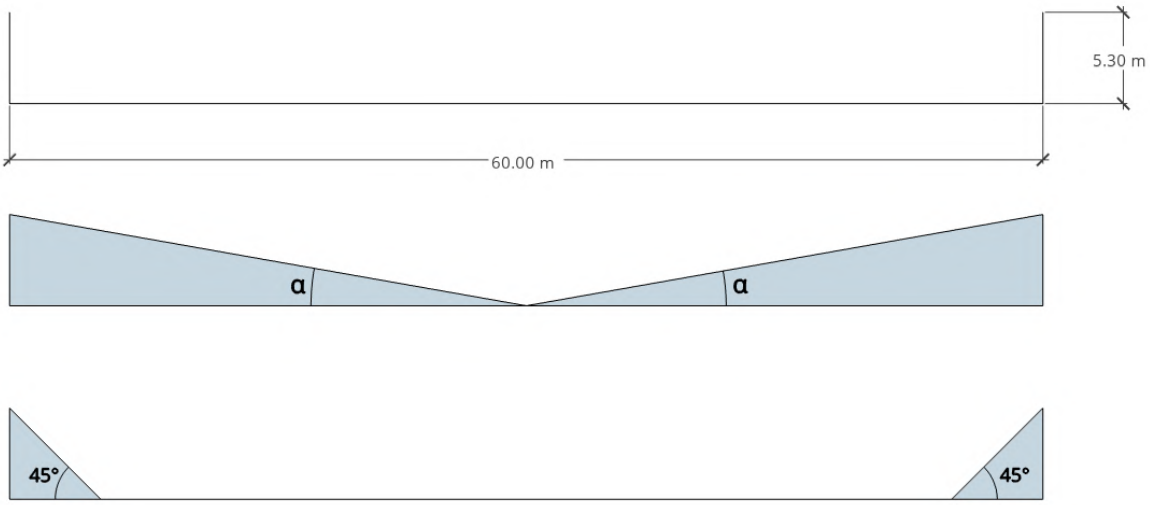

Figure 3.13: slope angle abutments front view

Still the sheet will sack in deflated state, because of its longer length needed in deflated state than in inflated state see figure 3.14. Jongeling demonstrated in a study of 1998 that an over length would solve the problem for the sheet that hangs at the abutment in deflated state [61]. This is done by also putting the width direction of the abutment clamping line under 45 degrees. In deflated state there will be then enough sheet length to store the sheet flat on the bottom of the foundation.

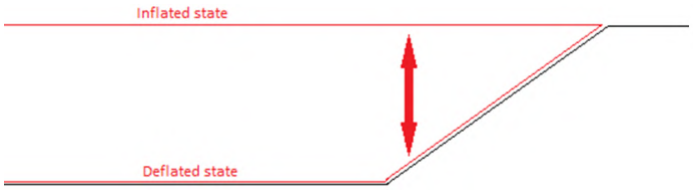

Figure 3.14: under length deflated state [38]

However, with this design the 3D shape of the membrane is not without imperfections. At the transition with the abutment there will be folds, due to the excess length of the slope, see figure 3.15. Two things are a consequence of this:

- At these folds stresses concentrate that are unfavourable for the sheet. Appendix E shows how is dealt with those folds at Ramspol. That is a two clamped inflatable dam, so it is not suitable in this case.
- The membrane on the span of the horizontal foundation can move freely in respect to the membrane at the slope of the abutments. This configuration simplifies the force transfer from the horizontal membrane to the inclined membrane, to zero in case of enough excess length.

Bridgestone gave a schematization of how the inflatable membrane will look like on an inclined abutment of 45 degrees and one side clamped. For this see figure 3.16.

Figure 3.15: fold at transition [11]

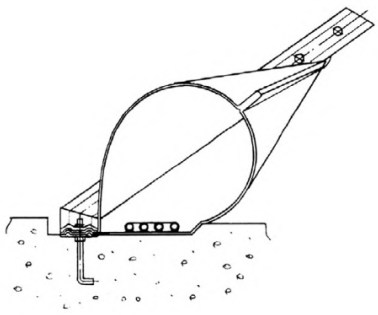

Figure 3.16: Bridgstone abutment schematization [45]

3.3.5. Filling medium

The membrane has to be filled inside with something to stay inflated. The membrane can be filled with water, air or a combination of both. For the inflatable storm surge barrier at Rampsol a combination of both is chosen. The behaviour of the membrane is related to the chosen filling medium inside. Characteristics of the different configurations of fill media are given below:

Water

- It will cost energy to pump out the water of the membrane.
- It will sag due to its own weight
- Larger circumferential length needed
- Probability of resonance due to dynamic loading
- Water is in-compressible

Air

- The internal air pressure should be great enough to withstand the hydrostatic pressure. The consequence is high tensile forces.
- V-notching can occur due to dynamic loading, see figure 4.4
- Increase in temperature expands air

Water and air

- Differential pressure can be minimal
- Danger of sloshing, with probability of resonance

The choice for the medium is dependent on several factors, see table 3.2.

Aspect	Water	Air	Water and Air
Inflation and deflation	-	+	0
Crest height	-	+	+
Circumferential length	-	+	0
Self weight	-	+	0
Stability of the weir	+	-	+
Weather conditions	+	-	-
Compressibility filler	-	+	0

Table 3.2: water, air or water and air filled

For the inflatable weir design it is most suitable to choose air as filling medium. The crest height is the most important one. For a water filled membrane the pressure is limited to the upstream head. In case of overflow, which is commonly for weirs, a higher internal pressure is needed than can be reached with air. A combination of both is also possible, but with overflow conditions sloshing and resonance can occur. The disadvantage of air is that due to hot weather the sheet can melt. A reference is made to Tempe town lake in Arizona, where the rubber dams collapsed. The sun caused the rubber to deteriorate over about 10 years, until one of the rubber dams snapped. In appendix B, a photo of the situation together with elaboration is given. However the weather conditions in the Netherlands are different.

3.3.6. Membrane material

One of the most important parts of the weir is the material where the sheet is made of. Usually there is chosen for a sustainable type of rubber with a thickness of 10 to 20 mm, that is ozone-, oil-, and water resistant. For the design in this research the sheet of Ramspol is taken as design material. The sheet for Rampsol is determined by using materials in scale model tests, see appendix E. Eventually it was chosen to use Nylon fibres as reinforcement for the sheet. The covering layer consists of rubber for its elasticity, see figure 3.17.

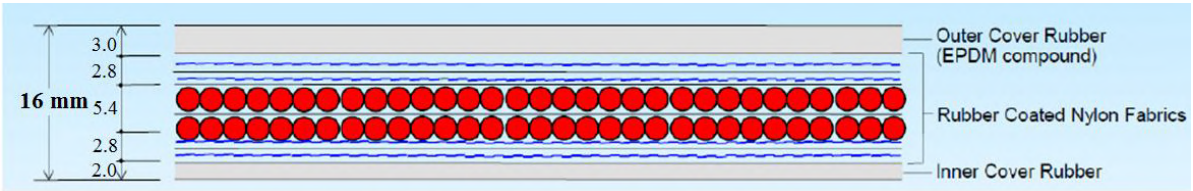

Figure 3.17: sheet cross section [5]

The circumferential and longitudinal yarns are connected with separate fibres, therefore they can stretch independently of each other. This is important to know for modelling the inflatable weir in chapter 7. The sheet including the rubber and fibers are mainly good in absorbing tensile forces. It is demonstrated that the bending stiffness is not an important influencing factor for the sheet. This holds for the sheet, see table 3.3, with the condition $EI \leq 50*10^6$ Nmm^2 [38, appendix 5]. The sheet strength in longitudinal direction should be 30% of the strength in circumferential length according to Japanese rule of thumb.

The fibers are assumed to be wet in the river environment, so the wet conditions hold from table 3.3. The strength of the material is defined by tests done for the sheet of the Ramspol barrier [5, p. 3.2]. From the tests

it is concluded that the speed of loading does not have a great effect on the strength properties. The cyclic loading does have influence on the height of the membrane that can be reached. Cyclic loading induces creep on the sheet that reduces the length of the sheet and so top height decreases. Samples are hung near the dam to test their strength under influence of water environments over the years. The expected lifetime was 25 years, but with the result of the test another 25 years are expected. For further information about the manufacturing and rubber of sheet referenced is to appendix E.

Direction		Tensile strength [kN/m]	E-modulus [kN/m]	bending stiffness (EI) at 5 C° [Nm]
Warp	dry	1870	5700	15
	wet	1602	3800	15
Longitudinal	dry	935	3200	17
	wet	809	2000	17

Table 3.3: fiber strength

3.3.7. Foundation

The foundation of the inflatable weir is also of importance for the design. It gives the inflatable membrane solid ground to lay on. The top of the foundation needs to be smooth to prevent cutting of the sheet. Therefore the concrete foundation as already is installed at Grave is a suitable option. The foundation has in general three main function:

- prevent sliding
- prevent rotation
- prevent settlement

To achieve a safe foundation the above three function should be full filled. The options to reinforce the concrete foundation for the described functions are:

- Cofferdam: in figure 3.3 Grave
- Piles: in appendix figure E.6

The cofferdam works well for transferring horizontal forces and the piles are good for transferring vertical forces as well as horizontal forces. At Ramspol there is chosen for inclined piles as foundation structure, see appendix E. The inflatable barrier at Ramspol is partly filled with water, which is much heavier than air. Large vertical forces are absorbed by the foundation floor that is why piles are probably used.

Since the design for the inflatable weir at Grave, air is used as filling medium, a much smaller vertical load need to be transferred. At this moment a steel weir is located at Grave, which should be heavier than an air inflated weir. As the foundation at Grave already have demonstrated its stability especially in horizontal direction and the vertical load would not much increase with the new inflatable weir, so the existing foundation is feasible for the design.

3.3.8. Maintenance and operation

In this paragraph the maintenance and operation is given for the inflatable weir design. The design is clamped to the foundation and is in inflated state as starting point. In figure 3.18 a standard design for an inflatable weir is given, comparable with the design used in this research. The use of a single line clamped membrane makes it difficult for inspection as discussed in paragraph 3.3.3. Only the outside of the membrane can be inspected in inflated state and when there is no water overflow. Especially the clamping lines need extra attention, since those are all lifetime under water. The advantage is that no guide rollers are used to control lowering the sheet.

To inflate the weir, internal pipes are needed to blow in air and/or water. These inflation pipes are shown in figure 3.18. The pipes are connected to an air compressor on the landside. When the membrane needs to be inflated, air is blown into the sheet and the weir will rise. The function of the spill breaker is described in paragraph 3.3.9.

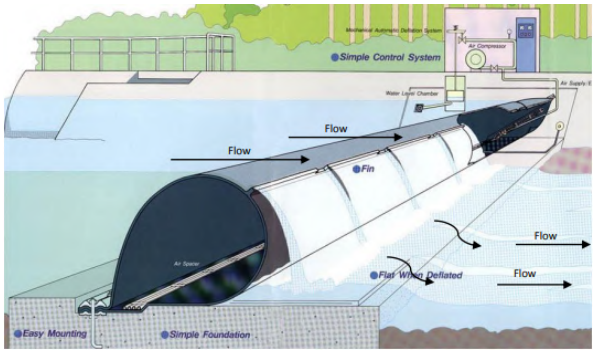

Figure 3.18: impression spill breaker and filling medium pipes [9]

3.3.9. Dynamic effects inflatable weir

Dynamic effects of the weir occur due to overflow. The overflow of water over the weir is present at the moment the upstream water level is higher than the inflated weir. With a lower water level downstream a jet is produced that plunges over the weir on the downstream water. The overflow conditions creates a centre-floating-acceleration and induces a suction force on the curved membrane. The overflow is tried to stay stationary, but this almost impossible by the varying discharges upstream. Due to the interaction of the overflow with the membrane, vibrations can develop. In the worst case the vibrations of the membrane are in phase with the vibrations of the water overflow. The vibrations enhances each other which is called resonance and collapse of the weir is possible. Resonance can be prevented by putting spill breakers on top of the inflatable weir, see figure 3.18 and B.3.

3.4. Conceptual design inflatable weir

For this research the standard inflatable weir design is chosen, see figure 3.19, which has also the highest MCA score. This standard design for inflatable weirs is commonly used around the world [45]. This design can span the whole river up to a certain length, mostly 100m. For the location at Grave this will not be a problem for the 50 and 60 meter long opening. When the opening gets to large, intermediate columns are needed where inflatable weirs are placed in between. The standard (common) design is a design that already proved its functionality [45].

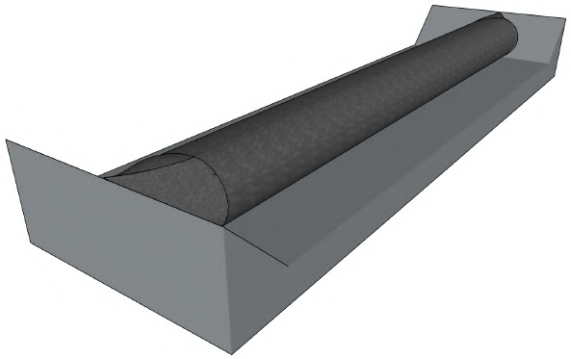

Figure 3.19: standard design

3.4.1. Safety factors

Worldwide, Japan has the most inflatable weirs. Japan developed further the concept of inflatable weir. In the end they made their own Japanese standard guidelines for designing of inflatable weirs. According to the code, the design tensile strength should be 9 times the static load for a two dimensional cross section. This also covers the material aspects and additional loadings (such as waves). The decision for 9 is mostly based on empirical results [63]. For Ramspol an own safety factor was made, see appendix E. The safety factor is based on the folds at the transition and the dynamic effect of the barrier [63]. In total a safety factor of 4.6 was given for the design condition.

3.5. Discussion

In this chapter a design is presented for an inflatable weir at location Grave. The existing weirs are made of steel and exists for about 100 years. The design of the inflatable weir in this chapter is a fairly general one. In theory, the design can be implemented to the Poirée parts of the weirs in the Meuse as well. For that, an optimization is probably needed for the other locations, because they are dealing with different circumstances and dimensions. An option is to have a steeper inclined abutment slope. This is done for the inflatable weirs in Germany, see Bannetze weir, which has a 1:3 slope to increase the discharge capacity. For now it argued that the 45 degrees slope give the optimal design decision based on literature.

For the design of the inflatable weir at Grave itself, an adjustment of the location could be beneficial. Then the 1:1 replacement is neglected, by placing the design a little upfront of the design location. Here the Meuse is wider and the reduction of flow area by the abutments will be compensated. On the other hand, a new foundation is needed that significantly increases the costs. It may be the best option to use standard (common) design of the inflatable weir in this chapter. Then additional flood plains will be necessary to compensate for the decreased discharge capacity by the abutments. In situations of extreme run-off, those flood plains can be used.

4

Analytical model ship collision on inflatable weirs

In the this chapter an analytical model will be represented to analyse the ship collision on the inflatable weir. The first paragraph 4.1 gives an introduction to the ship collision analysis at. The location as well as the basic formulation is elaborated. In next paragraph 4.2 the analytical plate model presented for ship collision on inflatable weirs. Then the reference (1D) collision model is described for check on the results. In paragraph 4.3 the parameters are determined necessary for the analysis. Following with a calculation of the models and the parameters in paragraph 4.4. Lastly a preliminary calculation is done for the ship waves and bottom protection in paragraph 4.5 and 4.6 respectively.

4.1. Set-up

The collision at Grave, see chapter 2, is taken as reference for the ship collision analysis. During that collision the ship hits the right weir of Grave in the middle, see figure 2.11. According the investigation at Grave, the ship collision was head on [64]. The same set-up is represented in figure 4.1 right picture. This ship collision scenario is likely to give the highest impact on the weir and is used for the rest of the analyses done in the remaining of the research.

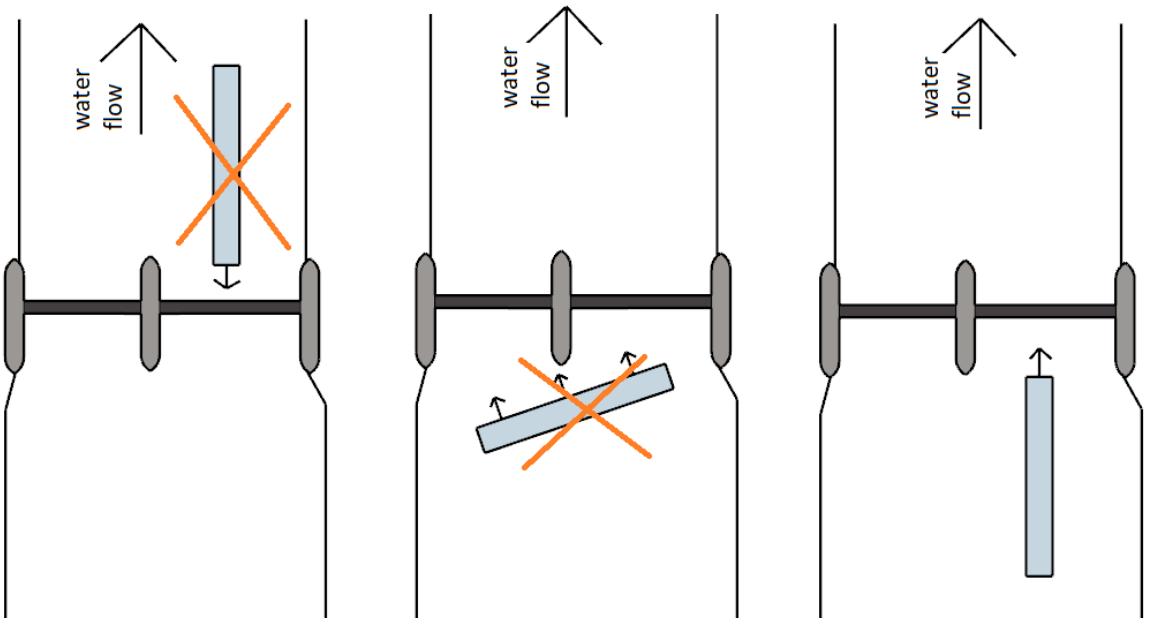

Figure 4.1: collision scenarios

Another option would be inclined collision as the collision at Linne, see figure 2.12. However the ship is more likely to impact the pillar harder than the inflatable weir. This collision is schematized in the middle of figure 4.1. The last option is a collision from the downstream side of the inflatable weir, see left of figure 4.1. In this case it is only possible for an unloaded ship to navigate to the inflatable weir. The draught for a loaded ship is too high and the ship will ground somewhere on the way. Also, there is a downstream current, so the velocity of the ship will likely be less than navigating from upstream. The combination of a lower mass and velocity gives a smaller impact.

4.1.1. Model expression

The ship collision model is made with energy and force laws, that describe the ship as a moving object and the inflatable weir as still standing object. In the model the ship is modelled as kinetic (or moving) energy and the inflatable weir as potential (or still standing) energy. A derivation will be given here how these energies relate to each other. Here, a force is derived, so that the stress on the sheet can be determined. First the kinetic energy of the ship is defined, here also the water is included. When the ship is moving through the water some extra water volume is taken along with the ship (added water mass). The energy that the ship is moving is defined by its mass and velocity squared:

$$E_{kin} = \frac{1}{2}(m_s + m_w)v_s^2 \tag{4.1}$$

where: E_{kin} = kinetic energy of ship and water [N/m]
m_s = mass ship [kg]
m_w = mass water [kg]
v_s = velocity ship [m/s]

Then the potential energy is defined of the sheet. This is defined by the stiffness and stretch of the sheet squared. Think of it like a spring that is given a certain stretch of a unit length. If it let loose the spring bounces back and the energy releases.

$$E_{pot,w} = \frac{1}{2}ku^2 \tag{4.2}$$

where: $E_{pot,w}$ = potential energy of inflatable weir [Nm]
k = stiffness sheet [N/m]
u = stretch of the sheet [m]

The kinetic energy of the ship is absorbed by the inflatable weir. It is for now assumed that the kinetic energy is fully absorbed in potential energy of the sheet of the inflatable weir. The damping in the system is assumed small and therefore zero. Usually the damping consists of the ship, water and inflatable weir. Neglecting this gives a more conservative approach. In formula form a derivation is made to find an expression of the stretch of a unit length sheet of the inflatable weir, which is later needed to find the force acting on the sheet:

$$\begin{aligned} E_{pot,w} &= E_{kin} \\ \frac{1}{2}k\epsilon^2 &= E_{kin} \\ u &= \sqrt{\frac{2E_{kin}}{k}} \end{aligned} \tag{4.3}$$

With the stretch of a unit length acting on the inflatable weir, the force can be found. Force is defined by stiffness times stretch (displacement). When using the expression for stretch from equation 4.3 follows the force on the membrane:

$$F = ku = k\sqrt{\frac{2E_{kin}}{k}} = \sqrt{2kE_{kin}} \tag{4.4}$$

In the Eurocode it states that the added water mass moving along with the ship can be approximated by 10% of the ship mass [12]. From this follows that equation 4.1 can be rewritten to:

$$E_{kin} = \frac{1}{2}1.1m_s v_s^2 \tag{4.5}$$

In appendix F more approximations are given for this added water mass based on numerical and physical models.

4.2. Collision model on inflatable weir

In this paragraph the basic model for the ship collision of the inflatable weir is elaborated. Also the (reference) 1D-model is given to check on the more elaborated 2D-model. In both models the following assumptions are made:

- Movement of the inflatable weir as a whole, so the structure behaviour is assumed linear. In reality the curvature of the membrane and behaviour of the rubber is non-linear.
- The internal pressure of the inflatable weir, induces an uplift on the bow of the ship in reality. In the model it is assumed the ship will only move in the x-direction. In other collision models it is also done like this [32]
- The ship in the analysis is rigid compared to the inflatable weir. This means that only the inflatable weir can deform during the collision and the ship remains its shape.
- An increase in air pressure would likely happen during impact and folds at the abutment can unfold. This pressure increases and folds are for now neglected.

4.2.1. Analytical plate model ship collision

In this paragraph the actual (2D)-model is described used to determine the strain in membrane sheet. The strain is most important to know, since it indicates if the sheet will rip apart. A note has to be given that not only the force due to collision can rupture the sheet. Sharp edges of the ship such as the bow thruster, can cut the sheet. For the scope of this research the bow thruster is for now neglected. Also the bow shape of the ship has influence on the actual strain on the sheet. The bow influence is further determined in chapter 7.

The inflatable weir is modelled as linear elastic spring in the xz-plane and xy-plane or side view and top view respectively. The springs are supported by a pinned support. This way the spring model can rotate around the pin, but is fixed in the sectional planes at the supports. An overview of the model from side view is given in figure 4.3 and from top view in figure 4.2. The contact height is defined as:

$$\delta = D + H - H_{up} \tag{4.6}$$

where: D = draught ship [m]
H = height inflatable weir [m]
H_{up} = upstream water depth [m]
δ = contact height ship-inflatable weir [m]

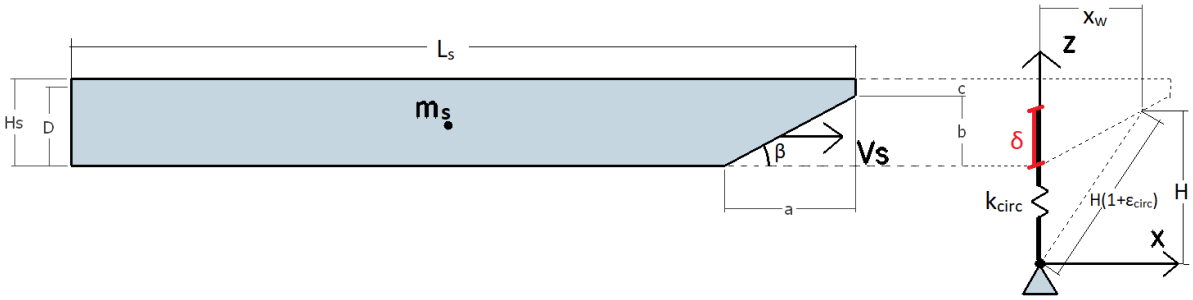

Figure 4.2: ship collision model side view

The displacement (strain) of the springs (yarns) are independently of each other in circumferential and longitudinal directional, as described in paragraph 3.3.6.So for the total stiffness the stiffness in the circumferential and longitudinal direction can be added to each other. How much the yarns stretch depend on the ship-structure displacement x_w. It is of importance to know the strain in the sheet, to know if it will not rupture. In figure 4.7 and F.5 the maximum strain is determined as 20% for the design sheet. The amount of strain in circumferential direction according to the model is:

$$\epsilon_{circ} = \frac{\sqrt{H^2 + x_w^2}}{H} - 1 \tag{4.7}$$

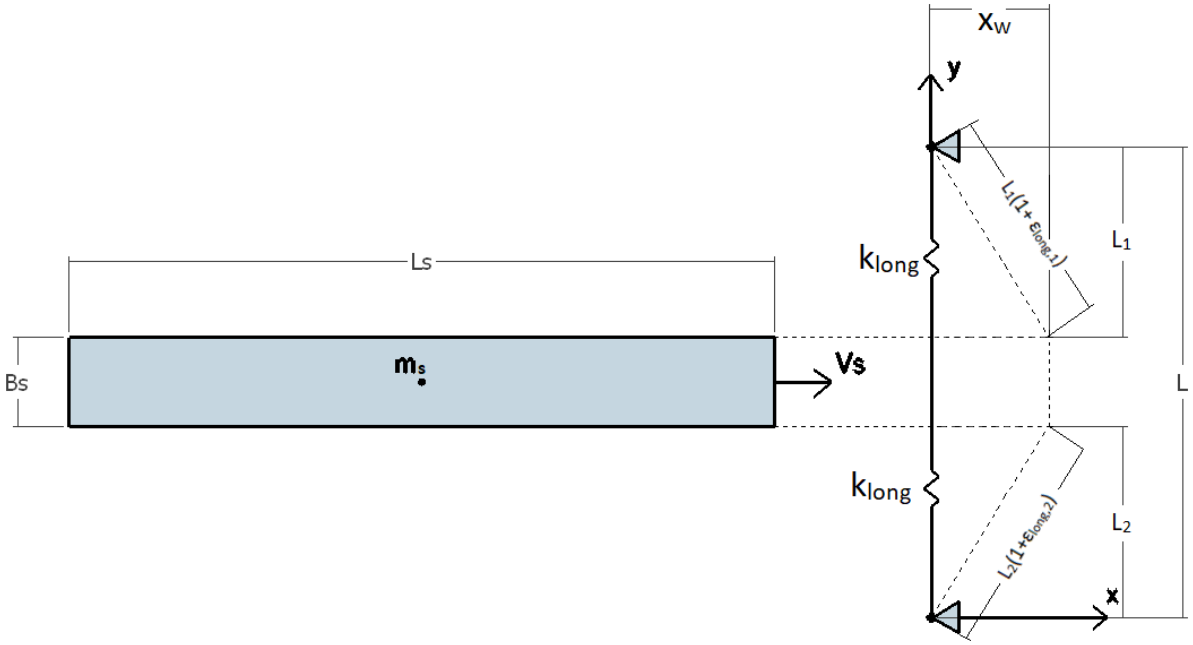

Figure 4.3: ship collision model top view

For the spring in longitudinal direction, the displacement is dependent on the impact location. The strain in longitudinal direction is defined for one side as:

$$\epsilon_{long,1} = \frac{\sqrt{L_1^2 + x_w^2}}{L_1} - 1 \tag{4.8}$$

and for the other side:

$$\epsilon_{long,2} = \frac{\sqrt{L_2^2 + x_w^2}}{L_2} - 1 \tag{4.9}$$

When the ship hits in the middle of the inflatable weir, then the strain of both sides is defined as $\epsilon_{long,1} = \epsilon_{long,2}$. The force acting on the inflatable weir is determined as:

$$F = \sqrt{2(k_{circ} + k_{long})E_{kin}} \tag{4.10}$$

The resistance of the inflatable weir is the contact width (B_s) or height (δ) of the ship-inflatable weir interaction multiplied by the stiffness of the yarns multiplied by x-component of the springs multiplied by the strain, in formula form:

$$F_R = B_s k_{circ} \frac{x_w}{\sqrt{H^2 + x_w^2}} \epsilon_{circ} + \delta k_{long} \left(\frac{x_w}{\sqrt{L_1^2 + x_w^2}} \epsilon_{long,1} + \frac{x_w}{\sqrt{L_2^2 + x_w^2}} \epsilon_{long,2} \right) \tag{4.11}$$

Filling in equation 4.7, 4.8 and 4.9 in equation 4.11 and equalling to equation 4.10, the displacement x_w can be found. Then the strains are also known.

V-notching

The supposable deformation is based on the V-notching phenomena seen in Ramspol, see figure 4.4. In figure 4.5 the phenomena is schematized from the top, where the arrows indicate water flow. V-notching is a result of the situation where the internal pressure is extremely lower than the external pressure. This is the case when the Ramspol storm surge barrier inflates itself and meanwhile from the higher level water is flowing through a gap of the barrier. In the situation of a ship collision the membrane is already inflated, but the external pressure is extremely increased by the ship collision. The inflatable weir is likely to form a V-shape, during ship collision.

Figure 4.4: V-notching Ramspol [62]

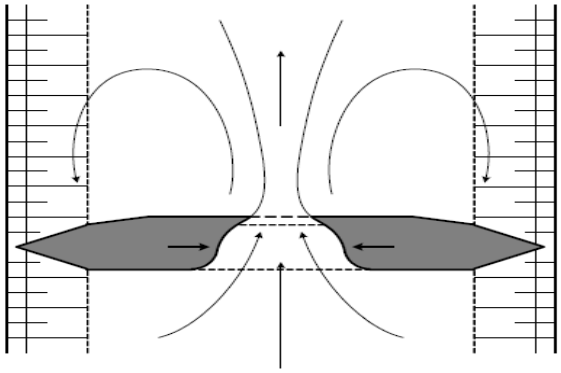

Figure 4.5: V-notching schematization top view [62]

4.2.2. Reference model

The 1D-model is the reference model, which represents the behaviour only in x-direction of the ship-inflatable weir interaction. The force acting on the weir is converted in a strain, with a simple spring stiffness formula. The strain in the reference model is the same as the displacement of a unit length. The strain becomes then the force from equation 4.10 divided by the total stiffness, where the components of the total stiffness are multiplied by the contact height/length the stiffness works on:

$$\epsilon = \frac{F}{B_s k_{circ} + \delta k_{long}} \tag{4.12}$$

where: k_{circ} = stiffness in circumferential direction [kN/m]
k_{long} = stiffness in longitudinal direction [kN/m]
B_s = width of ship, see figure 4.3 [m]

In figure 4.6 the representation is made of the simplified reference model.

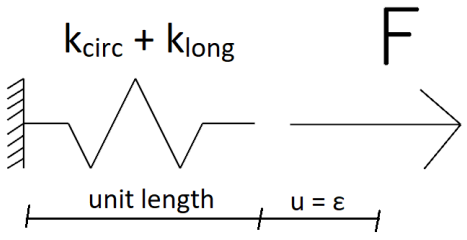

Figure 4.6: 1D-model

4.3. Parameters ship collision analysis

In this paragraph the necessary parameters are described for the ship collision analysis. The parameters are then used for a first calculation with the plate model and the reference model.

4.3.1. Stiffness sheet

The yarns which are acting as springs in circumferential and longitudinal direction have a certain stiffness, which are determined based on tests. The stiffness of the modelled springs for the inflatable weir is based on the sheet properties. The stiffness is determined by samples which are loaded until failure. For the design sheet, given in paragraph 3.3.6, sample tests are already done for the Ramspol project. Figure 4.7 and 4.8 shows the stress-strain relation of the design sheet for six different samples in circumferential- and longitudinal direction respectively. The samples show that for increasing stress the strain becomes less, which is a non-linear feature of the sheet. For ship collision the sheet stiffness is assumed linear and the ultimate strain is taken. Based on this strain the stiffness of the modelled springs is determined.

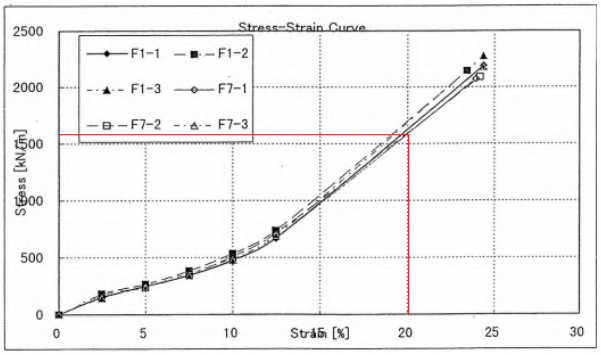

Figure 4.7: stress strain relationship sheet circumferential [62]

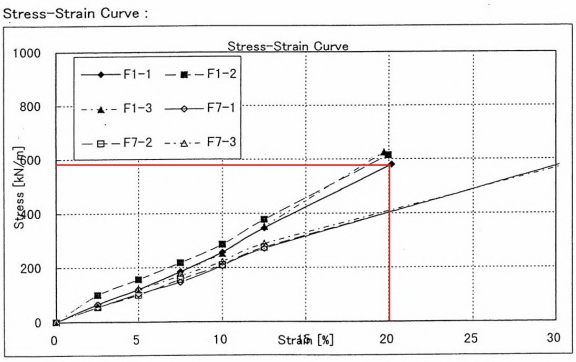

Figure 4.8: stress strain relationship sheet longitudinal [62]

As can be seen from the test, the maximum strain is 20% until break. The stiffnesses become then

$$\text{stiffness circumferential } (k_{circ}) = 1500 \,/\, 0.2 = 7500 \text{ [kN/m]}$$
$$\text{stiffness longitudinal } (k_{long}) = 600 \,/\, 0.2 = 3000 \text{ [kN/m]}$$

4.3.2. Velocity ship

The velocity of the ship is chosen according to the ROK 1.4 by Rijkswaterstaat [27]. In figure 4.9 the maximum ship velocity is shown per CEMT-class for the ship collision. This velocity is leading, only if the ship CEMT-class is not exceeding the CEMT-class of the navigation route. The ship needs a required water depth and width, where the CEMT-class of the navigation route is based on, to achieve the maximum velocity. For the Meuse no higher CEMT class ships are navigating through the Meuse than the CEMT-class of the navigation route, see paragraph 2.3. So this velocity numbers are valid for the ship collision model in this research. In appendix F and E more velocity numbers are given, but for different situations.

Class	0	I	II	III	IV	Va	Vb t/m VII
Veclocity [m/s]	fixed impact force	4,1	4,8	5,1	5,3	5,5	4,5

Figure 4.9: maximum ship velocity according to ROK [27]

4.3.3. Ship size and mass

For the various ships, tables are made to assign a ship class to the ship. There are three type of ships distinguished [41, p. 18]:

- motor cargo ships
- pushed convoys
- coupling connections

The ship that collided with the existing weir at Grave was a motor cargo ship, see chapter 2. For the analysis of ship collision on the inflatable weir, the pushed convoy is used. These are ships with in front of it convoys that are being pushed by the ship and are expected to allow a Vb class in the future of the Meuse. The CEMT-classes for these ships with corresponding size and mass are cited in the Richtlijnen Vaarwegen booklet from Rijkswaterstaat [41]. The CEMT-classes for pushed convoys that are allowed in Meuse are shown in figure 4.10. For the calculations, the used CEMT-classes are circled in red.

CEMT-class	type push convoy	width (m)	length (m)	draught loaded (m)	dead weight tonnage (ton)
IV	Europe I	9.5	70.0	3.0	1450
Va	Europe II	11.4	76.5	3.5	2450
Va	Europe IIa	11.4	76.5	4.0	2780
Va	Europe IIa Extended	11.4	90.0	4.0	3220

Figure 4.10: pushed convoys [41]

4.3.4. Bow

The bow geometry is based on the pushed convoy. The choice of the bow is of importance for the interaction during ship collision. The contact area differs, which yields in different results. There is also the V-bow shape that is commonly used for motor cargo ship. The total fleet in the Netherlands consists of both motor cargo ships and pushed convoys. For information about fleet set-up see appendix A.

The full bow shape for the pushed convoy can be found in appendix F. The geometry of the bow shape is based on pronunciation by the United Nations in a European agreement about international water traffic [66]. In the model it is assumed that the bow has a triangular shape as can be seen in figure 4.2. The parameters a, b and c in the figure are determined with report of the United Nations and are as follows:

- a is 19.7 m
- b is 4.4 m
- c is 1.14 m

From the report it is also shown that the radius of the edges is 50 to 60 cm, which makes the edges less sharp. Therefore the ship will less likely cut the sheet of the inflatable weir by the edges of the bow.

Further it is stated in chapter 2 that the maximum draught, with a deepened Meuse, is 3.5m. The height of the oblique part of the bow (b) is 4.4m, so the tip of the bow is always above the inflatable weir during impact.

4.4. Results collision analysis

In this paragraph the results are gathered for the analysis of ship collision. Three different parameter set-ups are calculated according to the three different classes from figure 4.10. The current maximum draught (3.0m) allowed in the Meuse is used as normative condition. Then the ship mass is calculated by (maximum draught Meuse / maximum draught CEMT-class) * maximum deadweight CEMT-class, see table 4.1. The according collision velocity of the ship is taken from figure 4.9.

CEMT class	draught [m]	mass ship [ton]
IV	3	1450
Va	3	2100
Va extended	3	2415

Table 4.1: parameters

Plate model

The outcome from the 2D model is described here for the three different CEMT classes. An example calculation for class Va extended is shown below. To find the unknown value x_w the goal and seek function in Excel is used. It was stated that the ships hit the middle of the weir, so L_1=L_2 and $L_1 = \frac{L-B_s}{2} = \frac{60-11.4}{2} = 24.3[m]$. Equation 4.11 can then be rewritten to:

$$\begin{aligned} B_s k_{circ} \frac{x_w}{\sqrt{H^2+x_w^2}} \epsilon_{circ} + 2\delta k_{long} \left(\frac{x_w}{\sqrt{L_1^2+x_w^2}} \epsilon_{long,1}\right) - F_R = 0 \\ 11.4 * 7500 * \frac{x_w}{\sqrt{5.15^2+x_w^2}} * \left(\frac{\sqrt{5.15^2+x_w^2}}{5.3} - 1\right) + \\ 2 * (3 + 5.3 - 5.15) * 3000 \left(\frac{x_w}{\sqrt{24.3^2+x_w^2}} \left(\frac{\sqrt{24.3^2+x_w^2}}{24.3} - 1\right) \right) - 27696 = 0 \\ x_w = 5.54[m] \end{aligned} \tag{4.13}$$

The displacement and strains found for the three different CEMT classes are given in table 4.2

CEMT class	ship displacement [m] x_w	strain circumferential [%] ϵ_{circ}	strain longitudinal [%] $\epsilon_{long,1}$ $\epsilon_{long,2}$
IV	5.27	41	2.15
Va	5.37	42.29	2.41
Va extended	5.54	44.66	2.57

Table 4.2: 2D model output

During ship impact the final strain of the circumferential yarns is including the tensile force in static condition, see figure 3.10. The final strain becomes then:

$$\epsilon_{circ,total} = \epsilon_{circ} + \frac{T}{k_{circ}} = \epsilon_{circ} + \frac{139}{7500} = \epsilon_{circ} + 1.9\% \tag{4.14}$$

Or to say 1.9% has to be added to the circumferential strain in the table above.

In 3D the inflatable weir looks like a curtain in the yz-plane, see figure 4.11. In this figure the ship and sheet of the inflatable weir are shown before impact. In figure 4.12, the situation is shown at impact. This is the supposable deformation form in 3D according to the plate model.

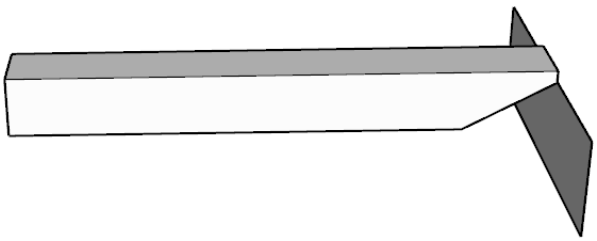

Figure 4.11: schematized inflatable weir 3D before collision

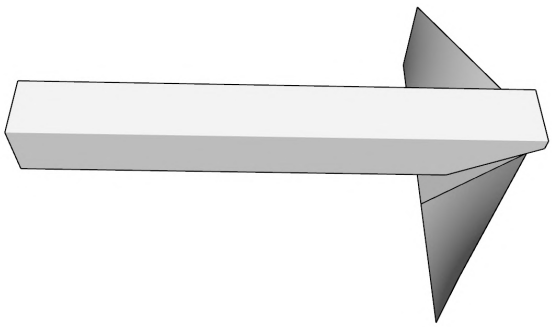

Figure 4.12: supposable deformation 3D

It is noted that the strain is definitely exceeding the limit strain given in table 4.2. The question is still if this model is an accurate representation of the real physical mechanism. The model has to be compared with numerical or physical models, described in chapter 5 and 6. In chapter 7 the analytical model described here is calibrated on the physical model tests.

In this chapter it is assumed that all the energy of the ship is translated into strain of the sheet. The displacement found (x_w) is the maximum displacement of the weir and the ship. At that displacement the velocity of the ship is zero. According to this model the ship will bounce back by the elastic property of the sheet. In the physical model test in chapter 6 it is shown that the ship bounces back partially, but not further than the weir itself.

Reference model

The outcome from the reference model is described here for the three different CEMT classes. An example calculation for class Va extended is made using equation 4.12:

$$\epsilon = \frac{F}{B_s k_{circ} + \delta k_{long}} = \frac{27696}{11.4 * 7500 + (3 + 5.3 - 5.15) * 3000} = 0.2917 \tag{4.15}$$

In the table below the outcomes of the strain (elongation) of the reference model is given for the three different CEMT classes

CEMT class	strain total ϵ [%]
IV	25.63
Va	27.2
Va extended	29.17

Table 4.3: reference model output

4.5. Ship waves

The ship waves are a result of the ship navigating through the river and can have a potential significance on the collision. Ship waves are generally categorized in two forms:

- Primary wave: the water level compression around the ship. The wavelength is around ship length L_s
- Secondary wave: the waves generated from the bow and hull. Those waves are much shorter in length than the primary waves

The primary waves are especially important in narrow channels. Here the conservation of energy happens over a small cross sectional area resulting in larger water level compression and return current. In the Meuse river this narrow channel approximation is not the case. This is determined by the blockage coefficient, which looks at the area of the ship under water in ratio to the total water area, see figure 4.13.

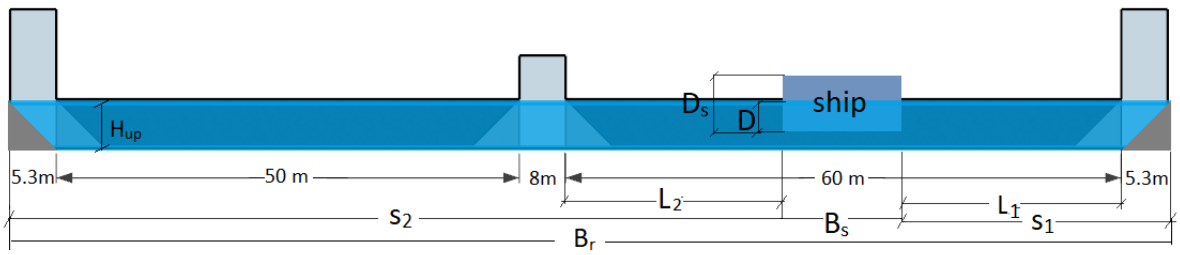

Figure 4.13: overview ship collision

For the location at Grave with the largest ship at the moment of writing (CEMT Va), the blockage coefficient is around:

$$\frac{A_s}{A_r} = \frac{11.4 * 3}{5.15 * (110 + 2 * \frac{1}{2} * (2 * 5.3))} = \frac{34.2}{621} = 0.03 \tag{4.16}$$

where: A_s = area ship under water in latitude cross section [m^2]
A_r = area of the water in latitude cross section [m^2]

Or the same as 3%, which is not significant.

On the other hand, the secondary waves have a bigger impact. In appendix F it is elaborated how these waves are generated. The height of these secondary waves are determined experimentally. A formula from experiments is derived to calculate the wave height, which is described in RWS/DHL 1988 [18]. In equation 4.17 the height of ships waves are calculated. The height is calculated for the cusps of the waves, which is the superposition of diverging and transverse waves.

$$\frac{H_w}{h} = \zeta \left(\frac{s}{z}\right)^{-1/3} Fr^4 \tag{4.17}$$

where: H_w = wave height [m]
z = effective water depth [m]
ζ = coefficient which represents ship's geometry [-]
s = distance side ship to bank [m]

The wave height increases with the velocity of the ship reaching its limit at Fr = 1. The Froude number ($Fr = \frac{v_s}{\sqrt{gh}}$) is a measure for the inertia in ratio to the gravity. Here 'h' is described as the effective water height accounting for the slopes at the edges of the river ($h = \frac{A_c}{B_r} = \frac{621}{110+5.3*4} = 4.73m$), where B_r is the river width. The Froude number is then Fr=5.5/(9.81*4.73) = 0.81. The coefficient for ship geometry is dependent on the kind of ship. The coefficient is dominated by the draught and bow of the ship. For a push convoy the ζ coefficient is around 0.5. Now all the values can be calculated for the wave height equation 4.17 and is shown in table 4.4.

	IV	Va	Va extended
A_s/A_c [-]	0.04	0.05	0.05
Fr [-]	0.78	0.81	0.81
s_1 [m]	27.9	26.95	26.95
s_2 [m]	86	85	85
$H_{w,1}$	1.15	1.35	1.35
$H_{w,2}$	0.79	0.92	0.92

Table 4.4: wave height secondary wave cusps

With the wave height, also the wave load can be calculated. A conservative rule of thumb approach is used for this. The wave force is calculated when the wave top is reaching the inflatable weir. The load is considered stationary and the maximum wave force is, where 'H' is the height of the inflatable weir:

$$F_{wave} = \frac{1}{2}\rho_w g H_w^2 + H\rho_w g H_w \tag{4.18}$$

For the highest wave, which is on the right of the ship (s_1), the wave force is calculated as 77kN/m. The ship load per running meter is $\epsilon_{circ}/100 * k_{circ} = 0.41 * 7500 = 3000kN/m$. The wave force is negligible compared to the ship load.

4.6. Bottom protection

Besides the ship-weir interaction, there are also the side effects of the water. The waves are already described in previous paragraph. However there will be also an overflow of water after collision. Eventually the ship lays on the weir, causing flow gaps at the sides of the ship, this is seen at the experiments in chapter 6. In this paragraph a first estimation is made of the overflow and the needed bottom protection downstream.

According to the theoretical shape of the sheet during compression in figure 6.22, the mean drop height is 1/3 of the total drop height. The flow velocity is calculated with, for a ship with draught of minimum 3.0m and where $\overline{h}$ is the mean water depth:

$$\frac{v^2}{2g} + \overline{h} \longrightarrow v = \sqrt{2g\overline{h}} = \sqrt{2 * g * \frac{(H_{up} - H_{down})}{3}} = \sqrt{2 * 9.81 * \frac{(5.15 - 2.15)}{3}} = 4.43[m/s] \tag{4.19}$$

With equation 2.2 and the equation of Shields:

$$d_{50} = \frac{v^2}{\Phi \Delta C^2} \tag{4.20}$$

where: Δ = dimensionless specific grain weight $\frac{\rho_s - \rho_w}{\rho_w}$
Φ = threshold value before grains start to move (0.03) [-]
C = Chézy coefficient [-]
d_{50} = Nominal grain size diameter [m]

the grain diameter d_{50} becomes 0.96m. This means 1 to 3 ton stones, where Grave is not fulfilling this according to table A.1. However Shields equation is based on uniform flow. In this case the flow is rapidly decelerated downstream. The overflow plunges first downstream of the weir in the water, see figure 4.14. At the location where the overflow plunges is close to the foundation and the colloidal concrete at Grave. This has higher resistance then loose stones. If the bed protection is still damaged, an option is to place nets with rocks behind the weir. A Master Thesis by Oorschot researched this for the bed protection of Grave in detail[16].

An example can be taken from Ramspol during closure with the presence of the V-notching phenomenon, see figure 4.4. This creates a design flow velocity of 3.3 m/s. However it is sufficient to use 300-100 kg stones.

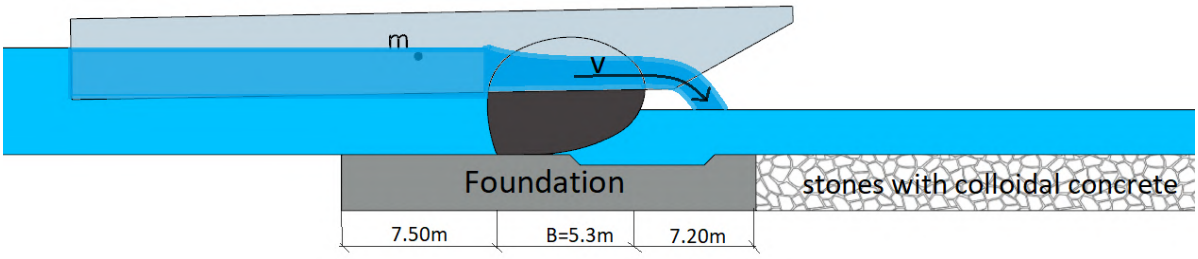

Figure 4.14: water overflow at gaps

4.7. Discussion

The plate model describes the membrane in a simplified way for the ship collision analysis. For the ship only one degree of freedom is considered in the (horizontal) x-direction. In chapter 7 the analytical model is further extended with the (vertical) z-direction. It is now assumed the bow always hits the top of the weir. In reality, this first contact moment depends on the curvature of the membrane. Also, the contact changes in time. That is, the further the ship is over the weir, the lower the contact point. The contact point is of great importance for the displacement of the ship and inflatable weir and strain in the sheet. According to the model it is the lower the contact point, the lower the displacement, but the strain remains the same in circumferential direction. However, it can be argued that more energy is transferred to the sheet, with a low contact point.

Another influencing factor are the folds that are present in the membrane. In chapter 3 the folds are already described and in the model tests they seem present, see chapter 6. In appendix H it is shown that these folds do not unfold during collision. It can be argued that no longitudinal strain develops in the analytical model. Another thing to mention is that the ship collides in the middle of the weir. In a scenario where the ship hits close to the abutments, a higher longitudinal strain will develop according to the analytical model. It is then the question if still no longitudinal strain will develop, if the middle of the weir can move freely in longitudinal direction.

In the analytical results, it seems that the inflatable weir is not resistant against collision with a ship. The circumferential strain is too high, which result in rupture of the sheet. Options to mitigate the effects of ship collision can be:

- put a second sheet under the first sheet like an inner tube (of a bicycle).
- Making a second inflatable weir behind the other weir.
- Deflating the weir before collision.
- Investigating the optimal sheet thickness.

The last option is preferred, in scope of this research. In the next chapters more details will be gathered for the ship collision analysis.

5

Numerical model ship collision on inflatable weirs

The chapter presented here deals with the modelling ship collision in numerical software. For this research software Ansys 2019 R3 is used. The chapter is mainly aimed to get insight how to model such a ship-inflatable weir interaction and not to obtain meaningful results. The beginning of the chapter gives the different analysing techniques in paragraph 5.1. In the next paragraph 5.3 the parameters are given implemented in the model for analysing ship collision. Thereafter the model used is schematized and some pitfalls are elaborated in paragraph 5.4. The computation time is an important consideration in software simulation, therefore paragraph 5.5 is dedicated to it. The last paragraph 5.6 discusses the results of the simulation .

5.1. Analysing methods

For the ship collision on an inflatable weir event Ansys, a numerical program to model this, is used, but the problem itself is a difficult one. Different analysing methods are available through Ansys, all with their own solution techniques. For the ship collision event the transient analysis will be used. In this paragraph different analysing methods are put next to each other to substantiate the decision. Each method has its pros and cons. Ship collision on inflatable weirs involves many aspects that can't be modelled all in one model. So beforehand it is wise to determine which analysing technique gives a first result from Ansys. Three analysing methods are considered, that shows potential of modelling the first steps in the numerical software:

- explicit dynamic analysis
- static analysis
- transient analysis

Dynamic analysis is seems suitable for materials with a limited amount of deformation such as steel. Analyses that are done in this mode are for example car crash simulations. Steel has a low elastic strain capacity after reaching the limit, then the steel will deform plastically. This plastic deformation is can be seen in the folds of the car during and after the car crash. This impact is of relatively short duration, where ship collision on an inflatable weir event is of longer in duration. It will take seconds before the ships stops. Besides the rubber can have large elastic deformation even over 100%.

The second analysing method is static analysis. This method is seems suitable for loads that does not change in time and location. In that case the ship has to apply a constant load on the weir. However this load change in time and direction.

The last analysing method is the transient structural. This analysing method is capable of handling loads in time. This method seems most suitable for analysing ship collision on the inflatable weir for now. It is possible to model the ship in transient structural with an initial velocity and let it collide into the inflatable weir. The disadvantage is that contact elements in transient can only have a fictional coefficient of 0.05. In explicit dynamics this number could be higher.

5.2. Geometry and mesh

In this paragraph the geometry, mesh of the ship and the inflatable weir is explained. Why this geometry is used is also an item in the paragraph.

Geometry

The geometry of the ship is taken the same as used in the analytical model. The sizes are taken from the largest ship from table 4.10. Only this ship is taken, because of the extensive computation time in Ansys, see paragraph 5.5. The sizes for the ship are:

- length 90 m
- height 5.54m
- width 11.4m

Besides the geometry of the ship, it has also a draught. This draught is important for the contact surface with the inflatable weir. In the next chapters 6 and 7 the maximum draught is set to 3.5 meter. This is when the Meuse river is deepened. For the geometry, in the numerical model, the ship is placed 3.5 meter from the top of the inflatable weir plus freeboard ($H\text{-}H_{up}$). Additionally, the ship is place in front of the inflatable weir in the, just as in the previous and next chapters. It is placed as close as possible to the inflatable weir, to reduce computation time.

For the inflatable weir it was more difficult to determine the geometry. Initially the shape that has been taken was calculated in figure 3.10. That is the shape in figure 5.1. In the simulation program the cross section was pressurized from within, but large numerical instabilities developed. Therefore it was chosen to do schematize the inflatable in the numerical model also as a plate, the second geometry in figure 5.1. The sheet was tested in the simulation program with the right thickness. Again numerical instabilities were found. The last modification was to increase the thickness ten times the initial one, last geometry in figure 5.1. This helped to perform an analysis without numerical instabilities.

Further the other dimensions were kept the same. This is the length of membrane which is kept 60 m and the height of the membrane that is 5.3m.

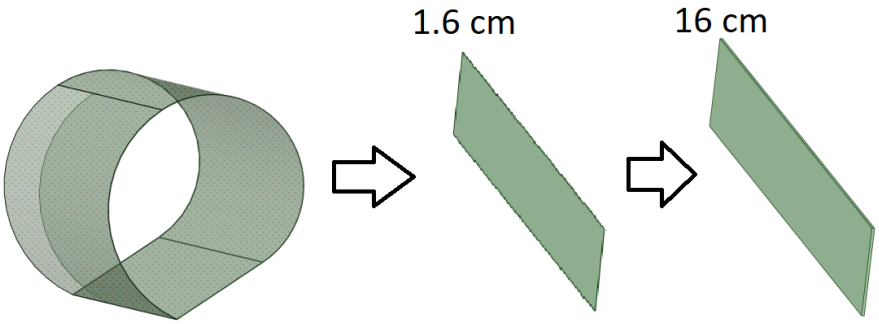

Figure 5.1: geometry conversion

Mesh

The mesh is an important part of simulation analysis. The mesh is like a net divided in a certain amount of areas. In the simulation program each small element area is a calculation for the timestep initiated. So more a finer mesh grid makes the model more accurate, but also more computational demanding. A rougher mesh grid with large areas is faster in computation time, but less accurate. A balance has to be sought for the mesh, which is determined in this paragraph.

The first thing to note is that the default mesh shape is chosen. These are rectangular areas. Other shapes are triangular or diamond formed. It was investigated which part of the geometry gets a fine mesh and which one a rougher mesh. The ship hits the weir only with the bottom hull in the numerical model, so this gets a fine mesh. The rest of the ship doesn't need a mesh and is there only to represent stiffness and mass. The inflatable weir sheet only needs a fine mesh at contact elements, which is the location of impact. It was tried to do this in figure 5.3, but the sheet will then rupture. Hence, for the whole sheet a fine mesh will be chosen.

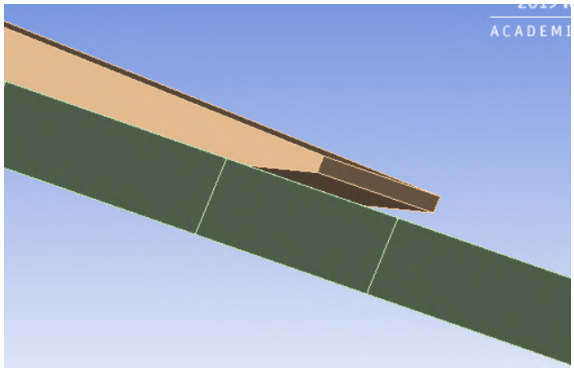

Figure 5.2: reduced contact area sheet

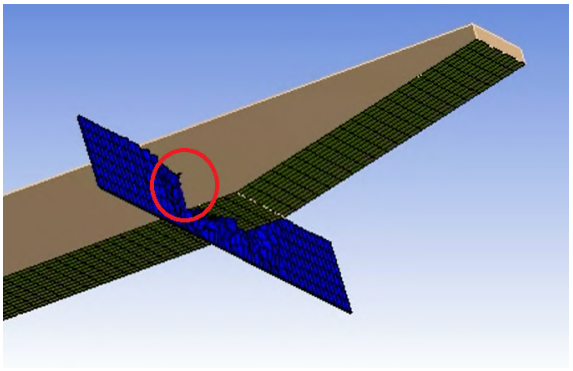

Figure 5.3: result reduced contact area

The element size of the fine mesh is taken 1 by 1 meter. To produce initial solutions with this mesh may take 5 minutes on a normal laptop. That is a manageable time. The whole computation will may take 1 hour, with this mesh. In view of this computation time, the mesh is not taken smaller.

5.3. Parameters ship and inflatable weir

This paragraph described the parameters used to model the inflatable weir and the ship.

Mass of ship and weir

The mass of the ship is determined by its draught. With the draught of 3.5m, the mass can be calculated with the help of chapter 7, where the mass is 3112 ton. With the mass known, the specific weight of the ship can be determined. This is important since it is needed as input parameter for the model. According to the model the ship volume is 5190 m^3. The specific mass is the calculated by $m_s/V = 3112e3/5190 = 600kg/m^3$. In appendix C it is demonstrated that the own mass of the rubber sheet can be neglected for the shape theory. During the ship collision the mass of the sheet will play some role, but is negligible compared the mass of the ship. For the simulation model the specific weight has to be filled in, this is 1009 kg/m^3 for the rubber used [5].

Velocity

The velocity of the ship is taken from the figure 4.9 from the previous chapter. The velocity is based on the Va extended class and so the velocity used is 5.5m/s

Frictional coefficient

The frictional coefficient is initially guessed, since there is no literature available for the event. For the first guess the coefficient is taken as 0.3 . However transient structural does only allow a frictional coefficient up to 0.05, so this is chosen as the maximum friction coefficient see appendix G. Later in chapter 4 it is found in figure 7.7 that the mean bow coefficient is 0.055, which is not very far from 0.05 in the Ansys model.

Damping

In the system no damping is used, it is assumed small as also done for the analytical model. Including no damping would likely give a conservative approach.

Rubber stiffness

For the rubber the same strength has to be achieved as used in chapter 4. In Ansys it is possible to define different kind of model theories for the rubber. In this research Yeoh 1st order method is used. The material constant C10 had to be filled in to get a stiffness of the rubber. The C10 value is adjusted until stress strain relationship is the same as in figure 4.7. In this case 100% strain is taken as calculation point. In figure 5.4 the stress is given for 100% strain with C10 = 2.25e5. The stress is around $7.9e6Pa = 7.9e6N/m^2 = 7900kN/m^2$, which gives a stiffness of 7900 kN/m. That is around the same as in the analytical model (7500 kN/m).

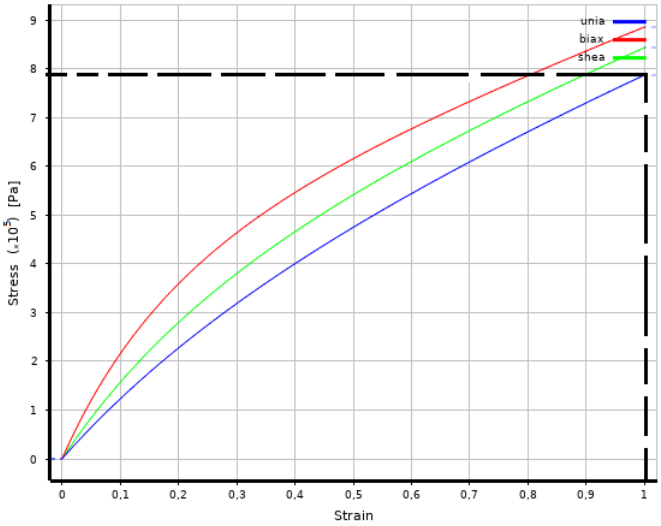

Figure 5.4: stress strain Yeoh 1st order

5.4. Collision Model

In this paragraph the collision model in the Ansys simulation software is explained. Also simulations that did not generate a stable result are given notice.

5.4.1. Schematization

The Ansys model represent about the same schematization as in chapter 4. The ship is about the same as it would be in reality. The inflatable weir is schematized in figure 5.5 as side view and figure 5.6 as top view, for in the numerical model. The stiffness of the sheet in the model is uniform in the circumferential and longitudinal direction. The air pressure is modelled as springs that work perpendicular to the sheet. As last in this schematization the supports are made rigid, so no rotation at the supports.

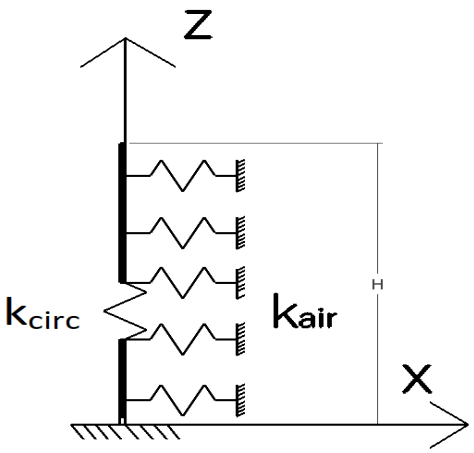

Figure 5.5: side schematization Ansys

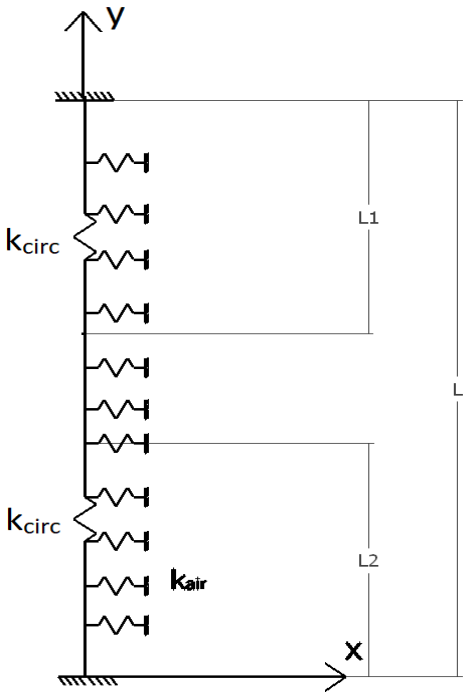

Figure 5.6: top schematization Ansys

The stiffness of the spring, which represents the air pressure inside membrane is determined as follow. First it is known that the inside pressure of the membrane should be 53 kN/m^2. Further, it is assumed that the inflatable weir is compressed the same amount as the contact height δ, see chapter 4. Only the maximum ship is analysed, so the contact height becomes $\delta = D + H - H_{up} = 3.5 + 5.3 - 5.15 = 3.65$. The spring stiffness then becomes $p_{air}/\delta = 53/3.65 = 14.5 kN/m^2$.

Another option is to assume the weir is pushed together by half the width of the weir (B/2). This gives a higher spring stiffness. When running the model an instable ship-weir contact develops. Eventually the sheet rips. In the next paragraph the air pressure is tried to model as a pressure. This did not find to be stable.

5.4.2. Test models

In this paragraph two test models are presented one for the tensile force and one for the air pressure.

Tensile force

In the sheet a tensile force is present, which is not automatically in the Ansys model. The air is modelled as springs and those don't generate tension in the sheet. In chapter 3, the tensile force is statically determined as 139 kN/m. The tensile force is modelled in the numerical model as a pressure on the top edge of the sheet. The pressure becomes $T/t = 139/0.16 = 869 kPa$, where 't' is the thickness of the sheet in meters. The model with this pressure is shown in figure 5.7 as schematization. The velocity of the ship is put 0 m/s, to prevent any disturbance in the result. Then the model was started and after 0.2 seconds it gave an error. The result was a fractured sheet as is shown in figure 5.8. An option is to reduce the tensile pressure, but this would not comply with the theory.

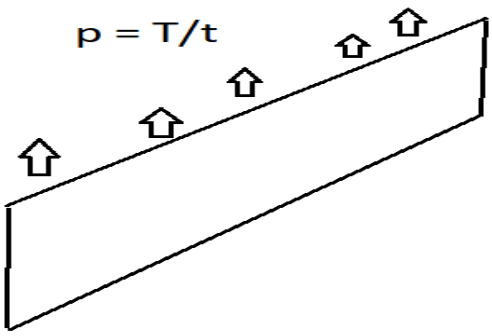

Figure 5.7: tensile force modelled as pressure

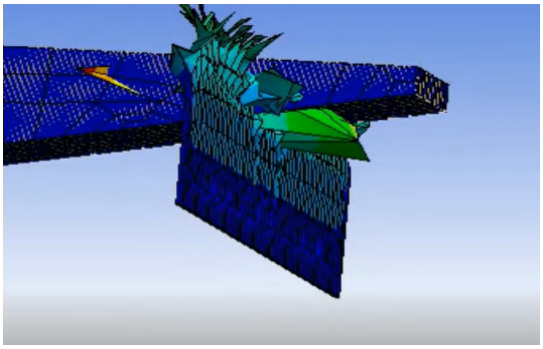

Figure 5.8: instable solution tensile force

Air pressure

Another model was executed with only air pressure at the side of the sheet, see figure 5.9 for schematization. The same air pressure is used as defined in chapter 3. The velocity of the ship was put at zero. Then the model was executed and the graphical solution is shown in figure 5.10. The solution is instable after 0.3 seconds. It shows a blown sheet, which does not look like the initial plane anymore.

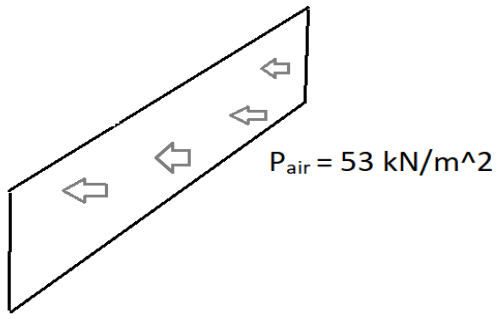

Figure 5.9: air pressure modelled

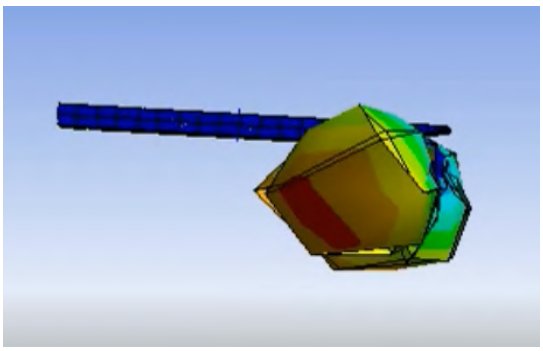

Figure 5.10: instable solution air pressure

5.4.3. Set-up and boundary conditions

The final model is shown in figure 5.11. The model is shown before it is executed. In this situation the ship is close to the inflatable weir, which is done on purpose. The time when the ship does not hit the inflatable weir is 'wasted' computation time. The movement of the ship is in x-direction and is zero in the other directions. At time t=0 the ship is given an initial velocity of 5.5m/s. In the model only this velocity is present and there is no propulsive force of the engine included. After the simulation is finished the ship has glided over the weir, the results are shown in paragraph 5.6.

Two boundary conditions are given to the bottom of the ship. The first one states that there if no vertical displacement of the mass centre of the ship. Otherwise the ship will fall downwards, because there is no water present in this model. The second boundary condition says that the rotation 'ϕ_y' is zero, that means there is no rotation around the y-axis. Without this boundary condition the ship will rotate endlessly due to the given moment by the air springs.

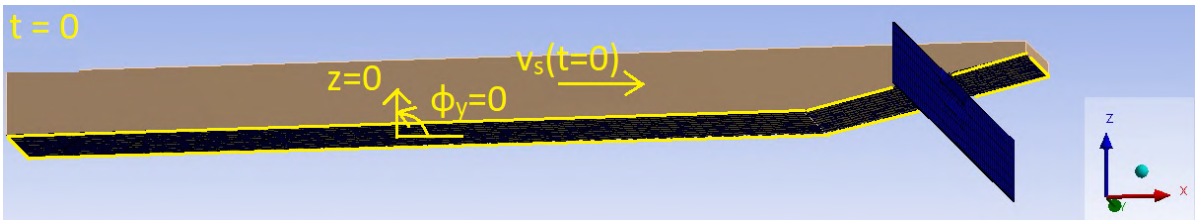

Figure 5.11: begin of analysis

5.5. Computation time

The computation time is one of the main issues in Ansys, which has to be dealt with. In this paragraph it is explained how to reduce this computation time and how much computing power is potentially needed.

The computation time is mostly dependent on three things: the mesh, the stepping time and computing power. The mesh as already explained in paragraph 5.2 is the size of the element within the plane. More elements mean more computing time in general. The stepping time is the other factor influencing the amount of computations needed. Here it is about finding the right stepsize so that the solution will not change anymore, but not a too small stepsize otherwise the computation takes forever. In Ansys it is possible to some extent determine automatically the step size. For the ship collision model this is done and shown in appendix G in figure G.3. The minimum sub steps is 2000 and the maximum 2e5.

The last things thing that is adjustable is the computing speed, this has mostly to do with the GPU's that are available. For this part a reference is made to Ramspol. In that time also Ansys modelling was done and big computation power was required. The transient dynamic computation for a 2-D cross section with a 4096 second duration, cost approximately 100.000 iterations on a model with approximately 10.000 degrees of freedom according to the macros report [26]. The required storage capacity is then 30 GB. The time to calculate this raw data is approximately 2 to 3 weeks on a PC with 1 GHz processor. More information about the Ansys modelling for Ramspol can be found in appendix E Assuming the ship collision Ansys simulation takes the same computation power as for the Ramspol model. A 2-D model running 20 seconds costs approximately (20/4096)*3= 0.015 weeks is 2.5 hours with a 1 GHz processor. Nowadays computer processors can be up to 4 GHz and come with 18 cores, Intel core I9-10980XE extreme edition processor. Running a simulation on 1 core takes now 2.4/4=0.615 hours or 35 minutes. In this research 16 of the 19 will then be needed to do all simulations in parallel, as in the experiments see chapter 6. The total time still is 35 minutes. The 2-D model is 1 meter width, for the full length of the weir 60 meter is needed. That should logically mean a 60 times higher computation time, and not even the 3D effects are taken into account. Running a 3D-simulation with this developed numerical model, would at least take 1.5 days on one core.

The computation with the simplistic ship collision model in this chapter on the laptop took about 1 hour with 4 cores of 2.5 GHz. That is the simplistic model takes 4x2.5/4=2.5 hour to compute on one core of the 4 GHz processor. This is a step faster, than that a complex 3D model would be used. For fast 3-D results a NASA computer would be helpful to decrease the computing time.

5.6. Output and analysis

In this paragraph the results are analysed of numerical ship collision simulation. The end result is presented as well as the relevant graphs for the inflatable weir and the ship.

The simulation has been executed for 20 seconds simulation time, so it has enough time to glide over the inflatable weir. The ship itself is 90 meter and the distance it can maximum travel is velocity x time = 5.5 x 20 = 110 meter. In figure 5.12 a screenshot is taken at 8.5 seconds of the simulation. It shows the ship heads over the curtain and the curtain shows not much resistance. The curtain itself flaps back and forth around the ship, due to the disturbance given of the ship.

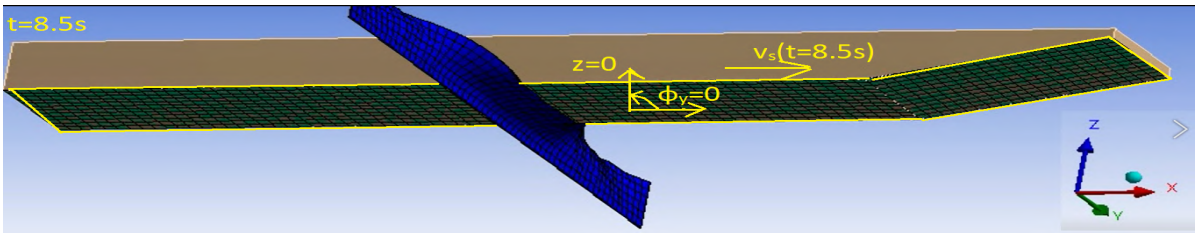

Figure 5.12: intermediate of analysis

In figure 5.13 the simulation is shown at t=20 s. It is noticed that the ship has glided fully over the sheet and the sheet is still intact. The sheet shows some folds at top. This is the after effect of the impact. The springs that represent the air pressure try to return the sheet to the initial state. That will take an infinite time since there is no damping in the system.

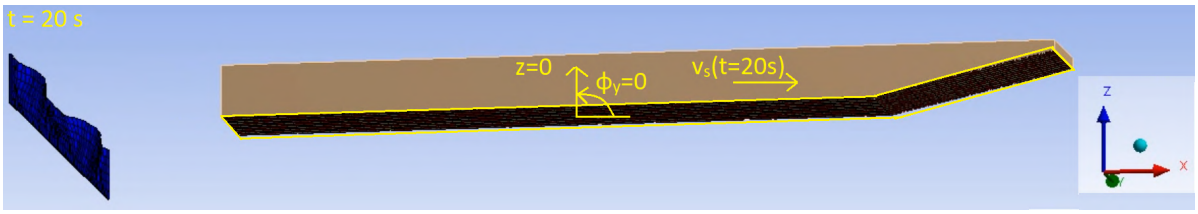

Figure 5.13: end of analysis

5.6.1. Graphs

Here the graphs are explained that can be distracted from the ship collision simulation. In figures 5.15, 5.17 and 5.16 three lines are shown, that have a specific meaning. It is worth mentioning what those lines mean beforehand.

- Green line: maximum value of all elements in time
- Blue line: mean value of all elements in time
- Red line: minimum value of all elements in time

All the graphs in this paragraph is extracted from the same simulation.

The next two figures 5.14 and 5.15 represent the velocity of the ship and deformation of the sheet in x-direction respectively. It can be seen that the velocity of the ship first shows a little drop in velocity and then stays about the same. The drop is possible explained by the bow of the ship. First the ship hits the weir with the bow. The air springs work perpendicular to the sheet and so to the bow. The springs generate a negative force component in the x-direction when hitting the bow, which decelerates the ship. Thereafter the springs work perpendicular to the bottom of the ship and no x-component is created. It seems friction has little effect on the velocity.

In the deformation graph of the sheet, the values stay about the same. At the beginning the maximum deformation is increased until almost the weir height. This likely means that, due friction and strain the sheet of the inflatable weir displaces more than the draught of the ship + freeboard (δ). It can also be seen that there

is a negative displacement of the sheet. This may results from the folds that develop underneath the sheet at the ship-weir contact.

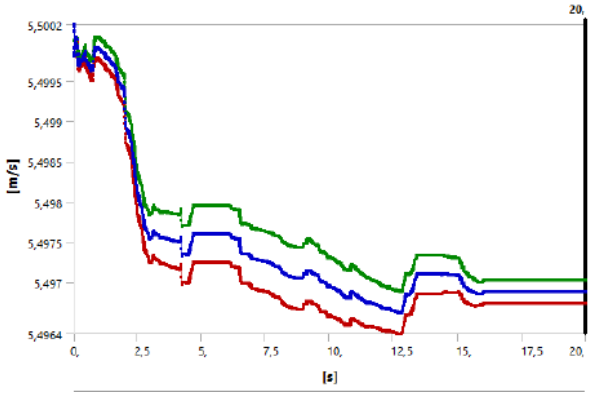

Figure 5.14: velocity x-direction ship

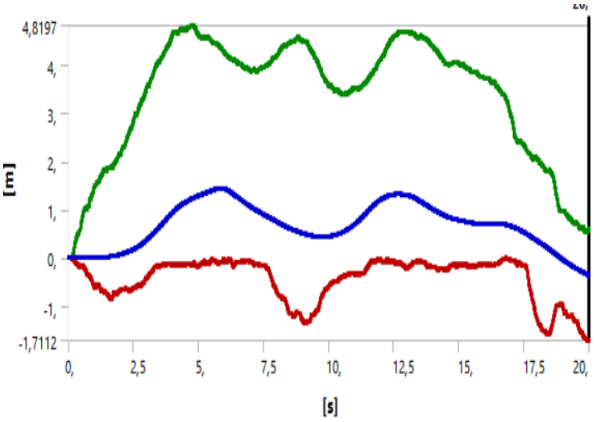

Figure 5.15: deformation x-direction of the sheet

In the next two figures 5.16 and 5.17 the stress in z- and y-direction or stated otherwise stress in circumferential- and longitudinal direction are given respectively. In both graphs it is shown that the mean stress is around 0. The maximum and minimum values are fluctuating. The graph for the maximum absolute stresses in y-direction shows about the same magnitude in pressure as in the z-direction. Calculating the pressure to a strain in circumferential direction gives 1.5e5 Pa * 0.16 m = 24000 N/m = 24 kN/m, dividing this by the stiffness gives a strain of 24/7500=0.32%. That is actually very low compared to the results found in chapter 4.

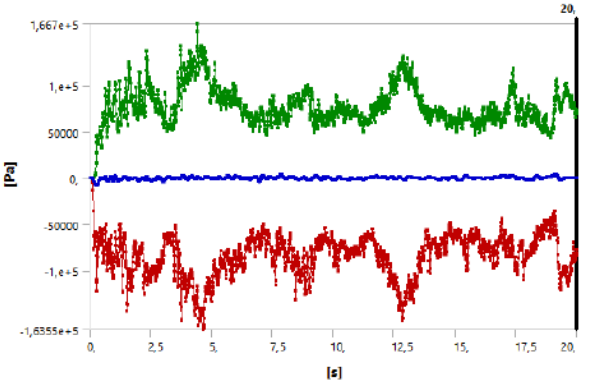

Figure 5.16: stress in z-direction

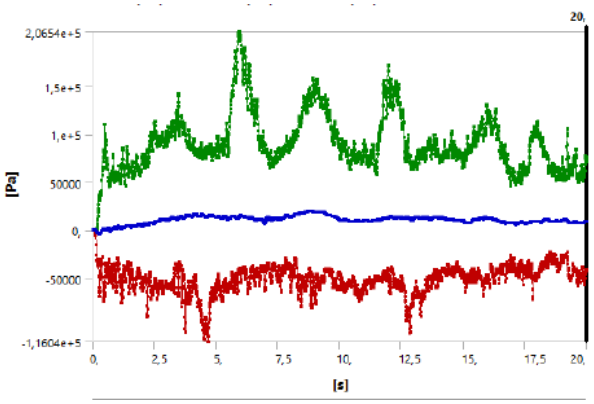

Figure 5.17: stress in y-direction

5.7. Discussion

The model in Ansys is a sophisticated tool for analysing this event. The collision can be divided in multiple parts that each can be researched. It is hard to put all effects in one model. It was chosen to see what the effects were on the sheet if the ship will glide over the sheet. The model that was created simulated these results, but it is doubtful drawing conclusions from the results. One noticeable result is the velocity, that almost did not decline during impact.

This chapter covered some pitfalls encountered in modelling ship collision on inflatable weirs in numerical software. For a better model, a deep understanding of the program is needed. More accuracy is likely needed in the results, therefore physical model tests are done in chapter 6. These tests are verified with an optimized analytical model in chapter 7.

6

Physical model ship collision on inflatable weir

In this chapter the physical model tests belonging to this research are described. One of the reasons is that the numerical model didn't match the analytical results. First, to get an understanding of what is analysed in the experiments, take a look at the cartoon in paragraph 6.1.3. The full video experiments are uploaded to the 4TU-datacentrum (`https://data.4tu.nl/portal`). The first paragraph 6.1 describes how the scale model is determined and how it looks like. The scale factor is one of the main considerations in scale modelling. Then for the built scale model a test procedure is set out in paragraph 6.2 with the desired parameters to be tested. In the following paragraph 6.3 the processing of the videos are described. In the last paragraph 6.4 the data is analysed of the sixteen ship collision experiments done on the inflatable weir.

6.1. Model test set-up

In this paragraph the set-up of the physical model test is elaborated. The model is based on the ship collision at Grave at the right weir, see figure 4.1. For making a scale model a scale factor has to be chosen. This factor represents the ratio between the model are done and the prototype. In general it is said that the bigger the scale model the better, but this is not always possible. A compromise has to be made between what is a manageable scale and what is a good scale for the representation of the hydraulic and hydrodynamic phenomena.

Figure 6.1: overview physical model

In the time for the Ramspol project a scale model with a factor of 25 was used. This scale was determined as manageable and still representing the physical phenomena accurately. Other reasons use a certain scale can be the possibility of representing the constructive details correctly, the accuracy of the measurement devices and the dimensions of the research facility [62]. The length (Ramspol: 80m [38] and Grave: 60m) and height (Ramspol: 10m [51] and weir 5.3m) of the weir location is significantly smaller than Ramspol. Both two observations are reasons to also use the scale of 25 in this scale model. In figure 6.1 the overview is shown of the built 1:25 scale model.

6.1.1. Scaling

One of the most important features to be scaled is the air inside the membrane. The air pressure and volume can't be scaled linearly and according to the law of Boyle these two are inversely proportional to each other. The air volume is scaled with n_V=3249 instead of n^3=25^3 and the air pressure with n=25 to satisfy the law of Boyle. Extra air volume needs to be added in the scale model, to compensate for the smaller scale ratio. In total 3.81 times the inflatable weir volume itself in the scale model needs to be added. This is done with air boxes on the side see figure 6.1. For full explanation about scaling of the air in the membrane see appendix H.

For researching the membrane on ship collision, besides air also the elastic properties of the sheet need to be modelled. In the scale model the membrane sheet has to satisfy the following conditions:

- Sheet is closed, so the required air pressure is maintained
- Scaled strain stiffness, in special in circumferential
- The scale model sheet has the same friction coefficient as the prototype

In the scale model only the strain rigidity in circumferential direction is scaled with n^2=25^2 correctly. The thickness had to suffer and is significantly thicker than the desired scale thickness. Bending stiffness could also be important for studying inflation and deflation of the membrane, but that is not in scope of this research. See appendix H how to scale those properties.

The velocity of the ship is scaled accordingly with $\sqrt{n}$. The scaling of the velocity can be done by the Froude number $\frac{v}{\sqrt{gL_s}}$ or the Reynolds number $\frac{\rho L_s v}{\mu}$. The Froude number is a measure of the resistance and the Reynolds number defines the turbulence. The viscous forces do play a lesser role in the scale model than the acceleration forces, therefore the velocity is scaled in ratio with the Froude number [30]. See appendix H for further explanation.

The mass of the ship is scaled with $n^3 = 25^3 = 15625$ and dimensions are scaled linearly, hence $n = 25$. In the figure 6.3 and 6.2 a side view and top view is shown with the dimensions of the scale model.

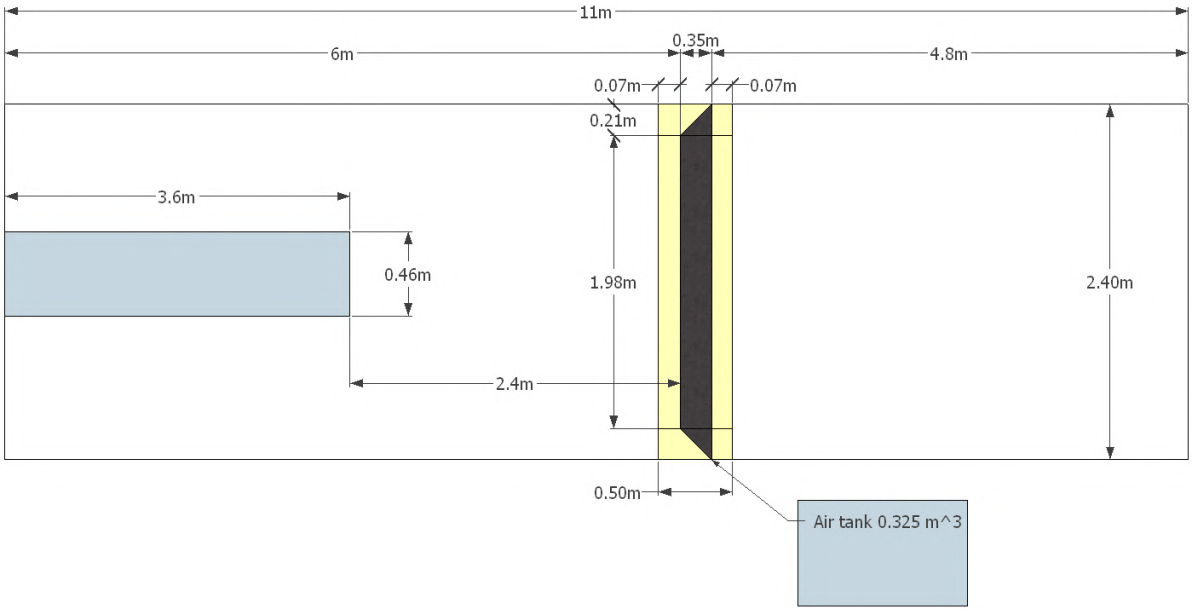

Figure 6.2: top view model

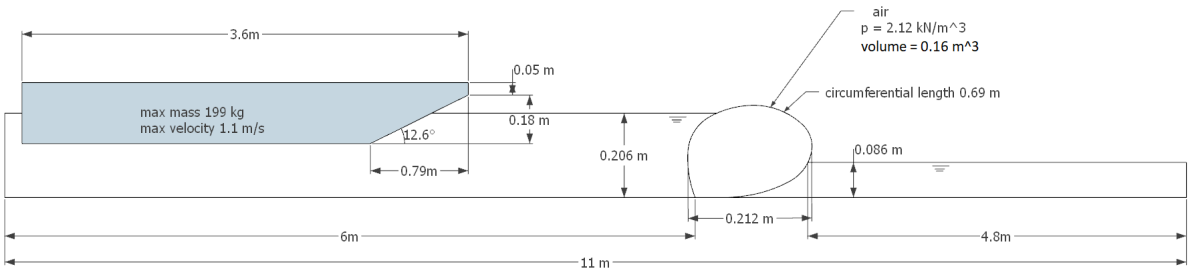

Figure 6.3: side view model

6.1.2. Scaling results

In this paragraph is explained what the scaling results are of the scale model. Not everything could be scaled to the exact number. Such as the air pressure deviated from the desired scale pressure. Second, the scaled thickness of the sheet and so the weight of the sheet are larger. Lastly, the stiffness in longitudinal direction is larger. However, the latter three are of minor importance.

The air boxes on both sides of the weir contain half of the added volume ($0.325 m^3$). The air boxes are cubes and the inner sides are all $\sqrt[3]{0.1625} = 0.55m$ long. An air blower is put between an air box and the inflatable weir with a T-profile. The blower was put on and the pressure was measured with a barometer, see appendix H. The highest pressure that could be reached is $1.7\ kN/m^2$, this is around 20% less than the desired pressure. It was noted that the height of the membrane at this pressure is 0.22m or 5.5 m in the prototype. In the shape calculation in chapter 3 the height was 5.8 m, but then for a higher air pressure in the prototype.

Figure 6.4 shows a picture of the inflatable weir, used in the scale model. The foundation is made of 18mm plywood (multiplex in Dutch) planks. The sheet is connected with a single line aluminium strip (3 mm thick) to the foundation. The centre-to-centre distance of the screws are put 10 cm aside each other. The screws are 20 mm long to prevent piercing the foundation plywood.

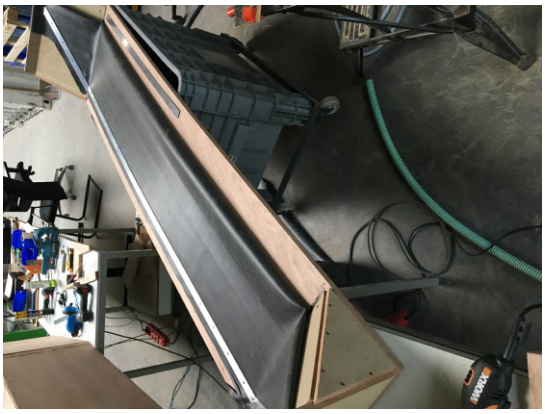

Figure 6.4: inflatable weir dry

The figure above also shows the sheet, a detailed view of the thickness of the sheet if given in figure H.7 of appendix H. The real thickness is 1.52 mm. This is 1.52/0.64= 2.4 times larger than the desired scaled thickness. The strain stiffness of the sheet is $8\ N/mm^2$ according to the supplier (EPDMtotaal). This means a strain rigidity of 8*1.52=12N/mm=12e3 N/m which is the desired in circumferential length, but not in longitudinal length. No yarns are presented in the scale model, so only one strain rigidity could be defined.

The length of the sheet for a circle would be $\pi H = \pi 5.3 = 16.65m$. The length from the calculations with the shape as in figure 3.10 come closer to the length of a circle than the length of literature, see equation D.10 [62]. For this reason the calculated length. Also the shape of the membrane is calculated with equations 3.7, 3.8 and 3.9 for the dimensions of the 1:25 scale model. Here the length that is found is 0.712 m, which is very close to the scaled length. The discussed parameters are shown in table 6.1 with there prototype value.

	unit	scale (n=25)	prototype	scaled value
Length sheet	[m]	n	17.22	0.69
Thickness sheet	[m]	n	0.016	0.00152
Strain rigidity circumferential	[kN/m]	n^2	7500.0	12
Strain rigidity longitudinal	[kN/m]	n^2	3000.0	12
Air pressure	[kN/m^2]	n	53	1.7
Air volume membrane	[m^3]	n^3	1332	0.085
Air volume total*	[m^3]	n_V=3249	1332	0.41

Table 6.1: parameters sheet

6.1.3. Experiment recording

This paragraph describes one of the sixteen experiments done for ship collision on an inflatable weir in the water lab in cartoon form. The video recording is shown in figure 6.5 as snapshots for the maximum draught (D=0.14m) and maximum velocity v_4, which is explained in the next paragraph.

In the first snapshot only the bow of the ship is shown before impact. It already travelled around 2 meters to gain its desired velocity. In snapshot two the ship is almost hits the inflatable weir. The added water mass and bow wave already hits the weir and pushes it a little horizontally. Next, the bow of the ship hits the weir in snapshot three. Here the interaction starts with the transfer of the impact energy and the ship is pushed a little upwards by the air pressure inside the weir. Also this snapshot shows that the bow wave splashed over the weir. Then in snapshot four the ship is still gliding over the weir and is pushed a little further upwards. The bow of the ship is practically over the weir. In the fifth snapshot the ship has lost most of its momentum and is on its tipping point. This is where the ship has the maximum displacement over the weir. It also shows that part of the ship over the weir is falling downwards by gravity. Between snapshot six and five the ship and weir moved a little bit backwards, due to the elongation of the sheet that behaves elastic. The last snapshot shows the ship in rest position on the weir. At this moment there is water flowing over the weir by the created gaps at the side of the ship.

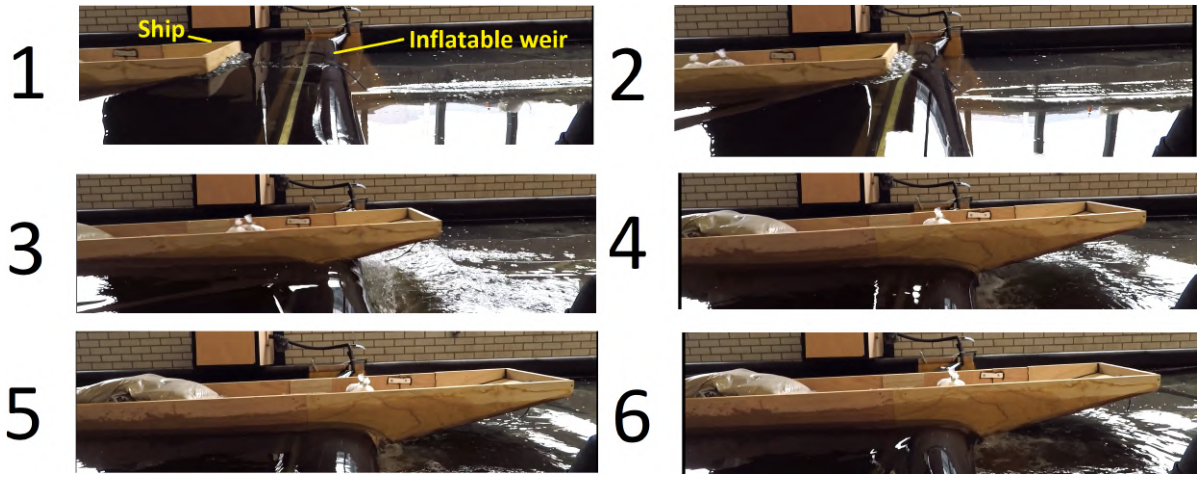

Figure 6.5: cartoon collision experiment

6.2. Experiment method

The experiments are repeated two times. This includes all the measurements with the sixteen different combinations of mass and velocity of the ship. The first set of experiments showed some inconsistencies in the measurements, therefore a second set of experiments was done with an improved experiment set-up.

The measurements that did not show inconsistencies in the first experiments are kept in this chapter. The measurements from the first set of experiments that did show inconsistencies are put in appendix H and the measurements done with the improved (second) set of experiments are shown in this chapter instead. The improved set gives the following changes in the experiment:

- more calibration points for the velocity
- trying to achieve a higher air tightness, by making new air boxes
- top view camera is better positioned, for better view
- more accurate resolution measurement for the discharge over the weir
- ruler on the foundation floor to measure weir displacement more accurate

6.2.1. Test parameters

For the scale model the dimension are used of push convoy class Va extended, see figure 4.10. The experiments are done with sixteen different combinations of the mass and velocity of the ship.

Mass

The four different scaled draughts corresponding to the scaled ship mass are 0.08, 0.10, 0.12 and 0.14 meter. Here 0.08 meter scaled is the minimum draught for an unloaded ship and the 0.14 meter is the maximum draught available in the Meuse after deepening the river, see section 2.3. The draught is used as means to convert to the mass. The volume of the ship that is under water creates an upward force that has to be equal to the mass of the ship, this is called the law of Archimedes.

First, the volume of the ship that is under water has to be determined. Therefore the angle of the bow is needed, see figure 4.2 and 6.3. The angle is calculated with: $\beta = \tan^{-1}(b/a) = \tan^{-1}(4.4/19.7) = 12.6°$. Then the mass of the ship can be calculated with the volume of the cubic part plus the bow of the ship that is underwater times the specific weight of water. In formula form this reads:

$$m_s = (D(L_s - a) + \frac{1}{2}D\frac{D}{\tan(\beta)})B_s\rho_w \tag{6.1}$$

where: m_s = mass of ship [ton]
D = draught of ship [m]
L_s = length of ship [m]
β = angle of bow [°]
B_s = width of ship [m]
ρ_w = density of water [kg/m^3]

The mass corresponding to the draught is given in table 6.2. These masses are achieved with sandbags, see also appendix H.

draught [m]	mass [kg]
0.08	109
0.10	138
0.12	168
0.14	199

Table 6.2: parameters ship

Velocity generation

The velocity of the ship is generated with a rope that pulls at the prow of the ship. The rope is turned over at two pulleys at the end of the basin see figure 6.6, where it is connected to a bucket. The ship is pulled to the other end of the basin see figure 6.2 and the bucket is filled with sandbags. Subsequently the ship is let loose and the gravity of the bucket pulls the ship forward.

Figure 6.6: tower for fall height

The drop height of the bucket is around 2m and the ship has 2.4 m free length to navigate before it hits the inflatable weir. This means there is 0.4 meter distance left before the ship hits the weir, where no propulsive force is present. Besides, it has to be noted that for a heavier bucket the rope somewhat elongates and the drop height can reduce up to around 0.1 meter. So the non-propulsive distance takes up to 0.5 meter. 0.5 meter in front of the prow a tape is put on the rope, see figure 6.7. The time is measured between when the tape is on top of the foundation and the prow is on top of the foundation. The velocity is then calculated by dividing the distance (0.5 m) by the time interval. The measured velocity is actually not conservative since it decelerates between the distance of the tape and the prow.

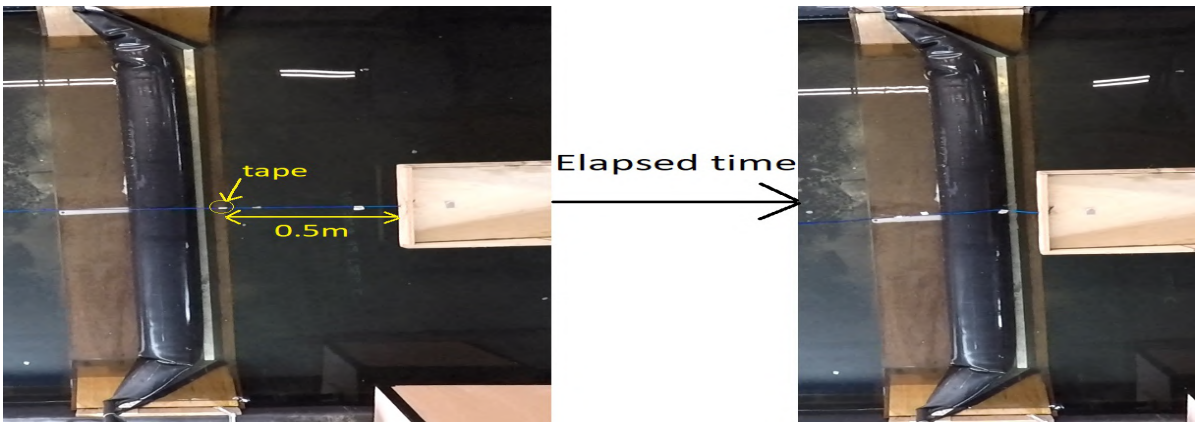

Figure 6.7: time between last 50 cm

There is a small deviation from the straight pulling of the rope at the prow of the ship. The deviation is calculated as follows: 0.18 cm high is the rope from bottom ship. The height from the bottom deviates from:

- H_{up} + (0.18-D_{max}) = 0.206 + (0.18-0.14) = 0.246 cm
- H_{up} + (0.18-D_{min}) = 0.206 + (0.18-0.08) = 0.306 cm

In the first experiment the pulley itself is 24 cm from the bottom. So the maximum angle is $\tan^{-}1(0.06/(11-3.6-2)) = 0.6^{\circ}$ with a maximum vector downwards of sin(0.6) = 0.01=1% of the total force. In the second experiment the pulley is put 0.27 cm from the bottom to reduce the downward force contribution to max 0.5%.

Velocity calibration

For the scaled velocity four different values evenly spaced 0.275, 0.55, 0.825 and 1.1 m/s are desired. The last is the maximum velocity for ship collision according to figure 4.9. In the first experiment the velocity is calibrated with four different weights 2, 5, 10 and 15 kg respectively in the bucket. For explanation on the execution of the experiments, see appendix H.

For every draught the four different weights in the bucket and are tested. In appendix H those weights in the bucket are plotted against the measured velocity of the ship with. In the second experiment set also the velocity measures from the first experiment set are included, so containing in total 8 data points for every draught. Those data points are marked as blue dots in the next four graphs.

Then for the (blue) data points a natural exponential function is plotted on each graph, where D is the draught in the scale model. The R^2 indicates the accuracy of the function, the closer to one the more accurate. Then the weights are calculated for the desired velocities. These velocities are used for the experiments later in the chapter. The data point for these velocities are given as orange dots. It is noted that the closer the velocity to zero, the bigger the deviation from the desired velocity. Besides, the accuracy of the desired velocity is not much increased with the first experiment measurements in appendix H.

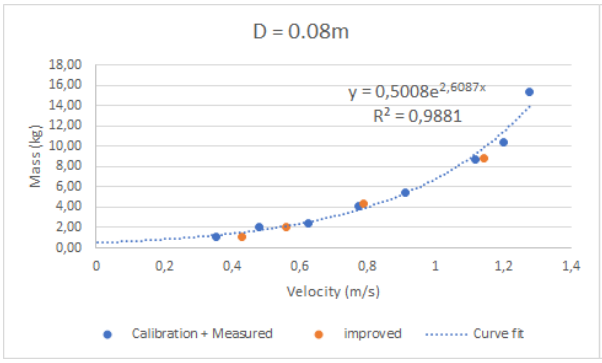

Figure 6.8: calibration 0.08 m

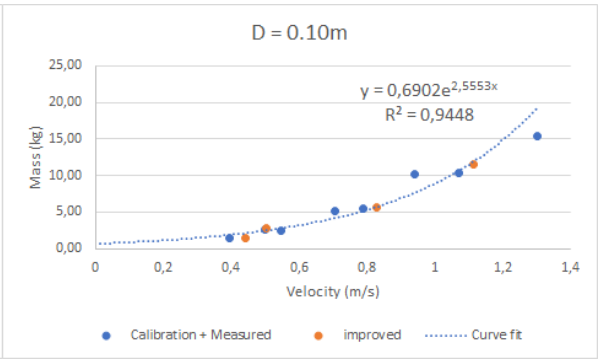

Figure 6.9: calibration 0.10 m

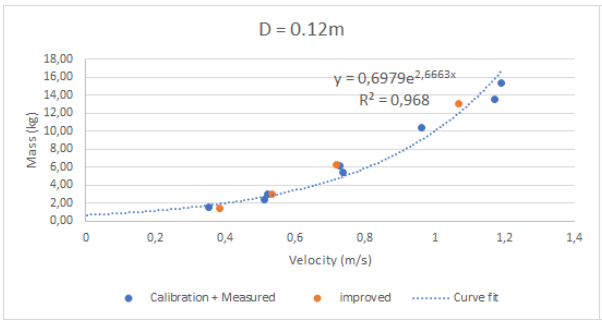

Figure 6.10: calibration 0.12 m

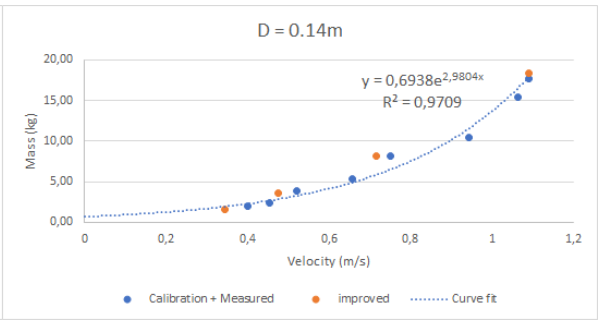

Figure 6.11: calibration 0.14 m

6.3. Processing methodology

In this paragraph it is explained how the data is gathered. The following items are measured from the model experiments:

- the maximum displacement in x-direction of the ship over the weir
- maximum (uplift) displacement in z-direction of the prow of the ship
- estimation of maximum displacement weir in x-direction
- discharge over the weir if applicable
- estimation of the increase of air pressure

For the displacement of the ship over the weir the number of pixels is counted. A known dimension on the video has to be measured to convert pixel to length scale. The width of the foundation plate (54 cm) is used for this conversion, see figure 6.12. The maximum displacement of the ship is measured from the prow to the clamping strip, see figure 6.12.

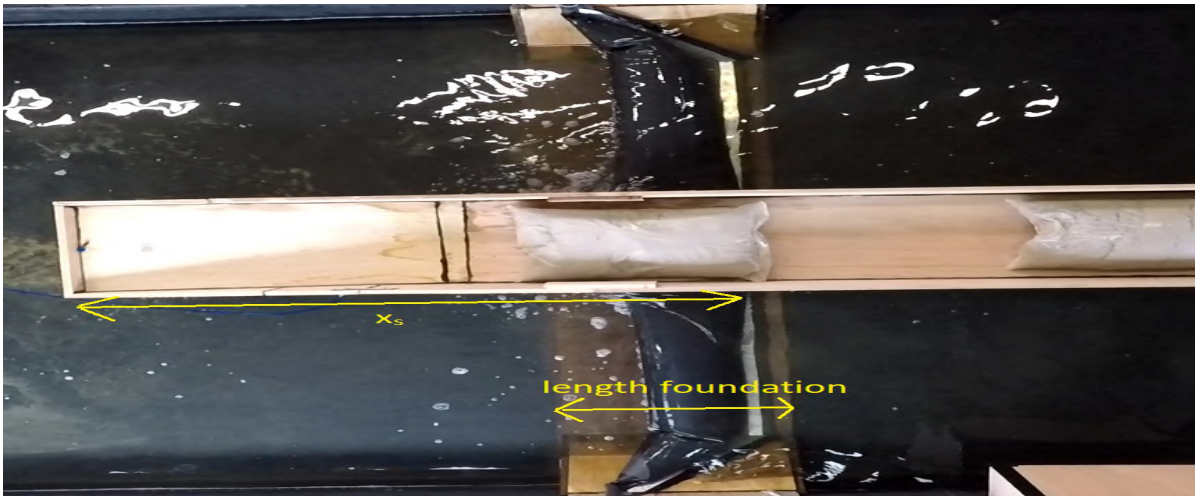

Figure 6.12: displacement ship top view

The maximum displacement in vertical direction of the ship is measured with a side view, see figure 6.13. The prow is taken as known length in the video, so the pixels can be converted to length. The dot that is fixed on the prow gives the reference point for the vertical displacement. The maximum vertical displacement is the distance between the dot before the ship hits the weir. The moment the ship hits the weir and the prow is at maximum height.

The displacement of the weir in x-direction is measured with the ruler in figure 6.13. The ruler is laid down in the middle of the weir in longitudinal direction, this is also where the middle of the ship hits the weir. The initial length visible before impact is measured of the ruler. Then during impact the minimal length of the ruler is measured. The distance between the initial and the minimal length is the horizontal displacement of the weir.

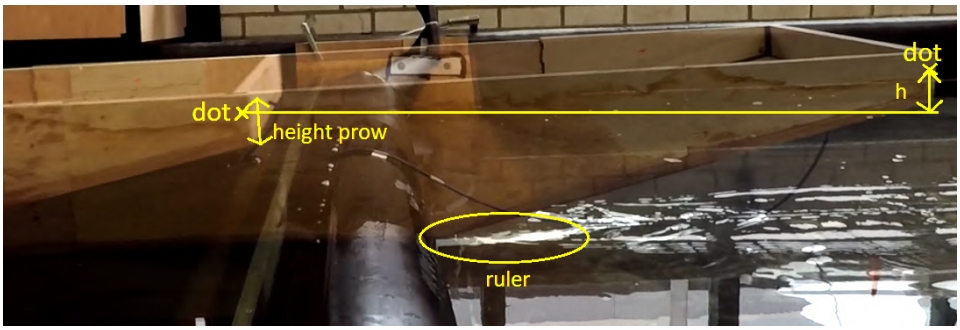

Figure 6.13: uplift prow of ship (h) by impact with weir and ruler to measure weir displacement

The displacement of the weir in z-direction by the ship is given in figure 6.14. After the impact the ship is laying on the weir and gives a compression. The reference height of the ship before impact is compared to the height ship in rest on the weir after impact. This difference in height is measured from the top deck of the ship between the two phases.

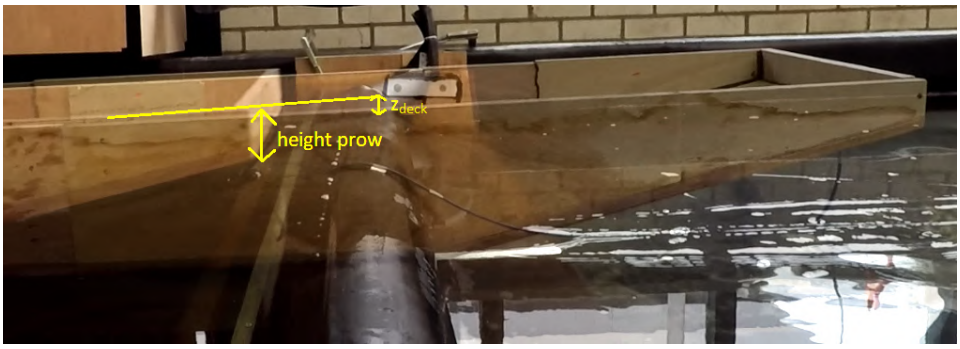

Figure 6.14: displacement measurement ship on weir

The discharge over the weir is measured by the water depth increase downstream over a time period after the impact. This gives an average discharge over the weir due to ship collision. In figure 6.15 it is shown where the water depth is measured. The initial height from the wall to the water level (D1 and D2) is taken as reference. When the ship rest on the the weir, water will flow over the weir. The time to let the water surface increase is varied between 25 and 50 seconds. The new height from the wall to the water level (D1 and D2) is measured and gives the water depth increase.

Figure 6.15: water depth measurement

Conclusion

The displacement of the ship in both x- and z-direction and displacement of the weir is accurately measured, since a reference length could be determined. However, the displacement of the weir became more difficult to read with higher velocity of the ship. The high velocity created a large bow wave topping over the inflatable weir. This wave overtopping blurred the view of the ruler, which was used as reference length for the displacement of the weir. See also figure 6.5 the ruler in snapshot 2 and blurred in snapshot 3.

6.4. Data analysis

The videos are analysed and the graphs obtained from it are given in this paragraph. Every line in the graphs represent a different draught of the ship. The velocity of the ship for every data point is given on the x-axis. The variable that is measured is given on the y-axis.

6.4.1. Displacements

In figure 6.16 the horizontal displacement of the ship over the clamping line is given. This represents the absolute maximum distance from the clamping line to the prow of the ship. The dashed line shows when the bow of the ship is over the weir (length bow + B/2). The graph shows an increase of displacement for a higher velocity. The kinetic energy scales with the velocity squared, so more momentum forward is generated and gives a bigger displacement.

The graph does not show the correct displacement over the weir. The weir is a little further away and the bow is inclined. It is assumed the top of the weir is half the width away from the clamping line (B/2). Then the displacement correction becomes:

$$x_{cor} = \frac{B}{2} + \frac{b-D}{\tan(\beta)} = \frac{1}{2}0.21 + \frac{0.176-D}{\tan(12.6)} \tag{6.2}$$

where: x_{cor} = correction for displacement ship over weir [m]
B = width of weir [m]
b = height of inclined part bow [m]
β = angle of bow [°]

This has to be subtracted from the maximum displacement (x_s) to obtain figure 6.17. It is shown that now the line with the highest draught is more on top instead on the bottom of the graph. This is because for a lower draught the ship has travelled already a while before hitting the weir.

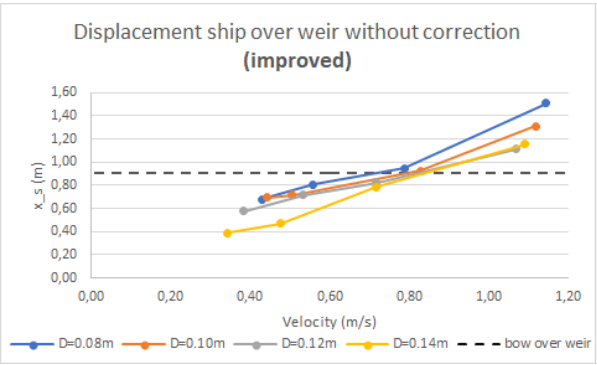

Figure 6.16: displacement over weir without correction

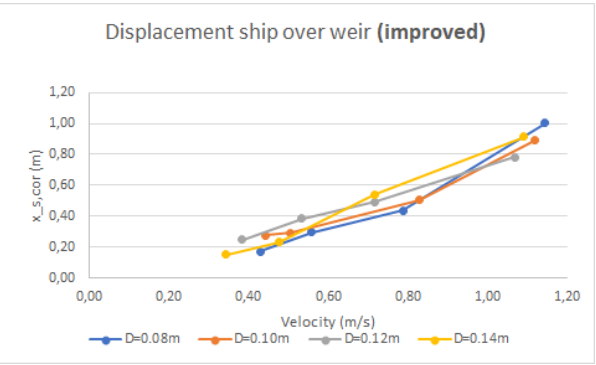

Figure 6.17: displacement over weir

In the next figure 6.18 the maximum vertical displacement of the prow is given. The maximum vertical displacement of the prow lays around the point, where the bow is just over the weir. The first measurements it showed that there was an outlier at D=0.12m, see appendix H. In the improved measurements this outlier is more flattened out, but still is higher than D=0.14m. A reason for this can be, that the impulse is around the same for D=0.12m and D=0.14m (contact area and compression of weir). In combination with a lower mass gives a higher upswing of the prow.

It can be seen from the graph that the vertical displacement increases for a higher velocity, this is logical since a higher reaction impulse is give to the ship. Also the general trend shows for a smaller draught/mass a smaller vertical displacement. This confirms that a lower impulse and contact area gives a smaller vertical reaction impulse.

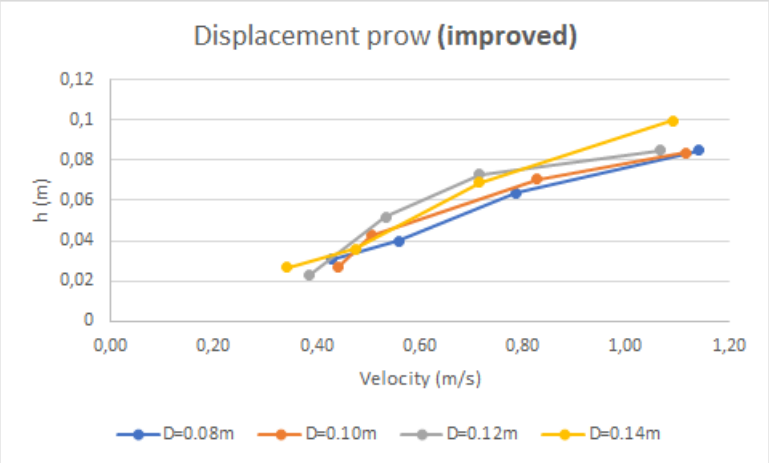

Figure 6.18: displacement prow

The maximum displacement of the weir in horizontal direction is given in figure 6.19. The displacement is generated by the ship, that pushes the weir forward and flattens the weir to the ground simultaneously. Also there is an elongation of the sheet, due to the friction of the ship with the weir, that gives an extra displacement. The greater influence for weir displacement is from the first effect.

the graph show an increasing displacement of the weir for an increasing draught/mass and velocity. Those parameters increase the kinetic energy and so the impulse will be greater. Logically the weir has a larger displacement. It is also noted that the weir displacement flatten out for increasing velocity. At some point the deformation is maximum for the displacement (the weir is pushed flat to the bottom). At that point only the elongation can contribute to extra displacement.

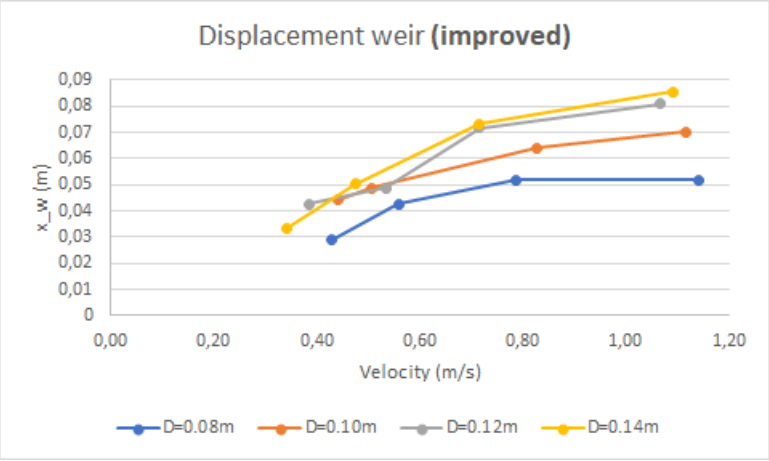

Figure 6.19: displacement weir

6.4.2. Discharge and friction

In this paragraph the discharge and friction is calculated when the ship lays on the weir after impact. The steps are made in chronologically order.

First, the total vertical displacement of the weir by the ship is calculated, see figure 6.20. If the bow of the ship is not fully over the weir then the compression by the draught of the ship is $x_{s,cor}\tan(\beta)$. The extra compression (z_{deck}) has to be added for the total displacement, in formula form:

$$z_w = \begin{cases} x_{s,cor}\tan(\beta) + z_{deck} & for \quad x_{s,cor}\tan(\beta) < \delta \\ \delta + z_{deck} & for \quad x_{s,cor}\tan(\beta) > \delta \end{cases}$$

where: z_w = compression of weir [m]
$x_{s,cor}$ = displacement ship over weir with correction [m]
β = angle bow ship [°]
z_{deck} = relative displacement deck ship on weir [m]
δ = contact height ship-inflatable weir [m]

The general trend shows that the further the ship is over the weir, the more compression of the weir. This is logical, because more weight is leaning on the weir.

Second, the average discharge is calculated, see figure 6.21. This is done by the water level increase in the downstream basin over a time period, described in the previous paragraph. In formula form the average discharge can then be calculated with:

$$Q = \frac{(\frac{(D1+D2)_{new}}{2} - \frac{(D1+D2)_{old}}{2}) A_{basin}}{t} \tag{6.3}$$

where: Q = discharge [m^3/s]
$D1$ = water depth measurement location 1 [m]
$D2$ = water depth measurement location 2 [m]
A_{basin} = top view area of downstream basin [m^2]
t = time [s]

Old is before impact and new is a certain time after the impact. The water level increased in the downstream basin only for the v_3 and v_4 velocity. Then only the vertical displacement of the weir was then large enough to create an overflow. It is remarkable that the discharge of the lower draughts are higher, only the highest draught has a higher discharge. It might be possible that a higher draught up to D=0.12m, gives a smaller gap of the flow are due to the curvature of the weir in longitudinal direction.

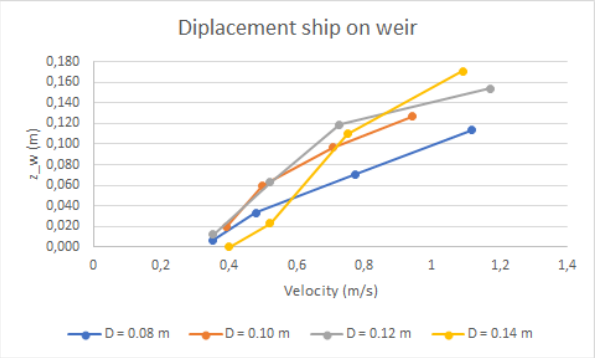

Figure 6.20: displacement ship on weir

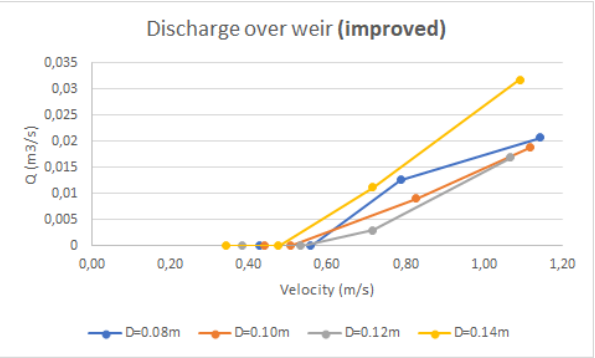

Figure 6.21: discharge over weir

The area where the water flows through after impact is schematized in figure 6.22. In this way the flow velocity can be calculated exactly. An angle is assumed of 45 degrees where the membrane sheet curls back linearly to the normal state. The gap in the weir, where the water flows through, is then calculated with:

$$A_{gap,w} = z_w^2 \tag{6.4}$$

Now the flow velocity can be calculated. This is done for the ship with D=0.14m and v_4 velocity. In this way also the maximum friction coefficient in test can be determined. The average flow velocity is calculated with:

$$\overline{v} = \frac{Q}{A_{gap,w}} = \frac{0.032}{0.17^2} = 1.1[m/s] \tag{6.5}$$

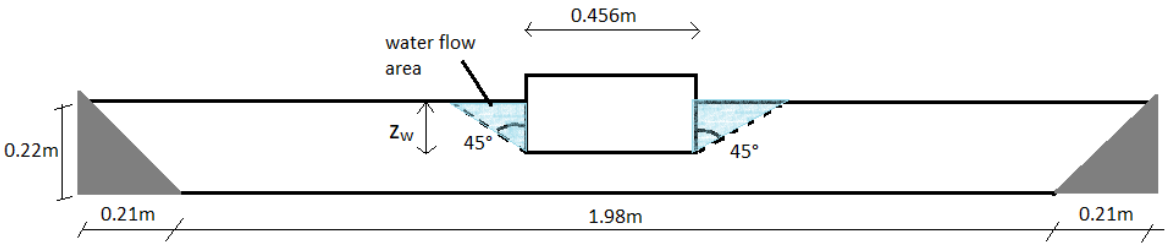

Figure 6.22: geometrical displacement weir from ship

In the following the force is calculated per meter width, since the ship is symmetric. The velocity over the weir gives a drag force (F_D) to the stern of the ship, see figure 6.23. This force can be calculated with the following formula, where drag coefficient is set as 2.0 based on experiments done for bridge piers [6] :

$$F_D = \frac{1}{2}\rho_w C_D A_s \overline{v}^2 = \frac{1}{2} * 1000 * 2 * 0.064 * 1.1^2 = 76[N/m] \tag{6.6}$$

where: F_D = drag force per unit length [N/m]
ρ_w = density water [kg/m^3]
C_D = drag coefficient [-]
A_s = area ship under water ($B_s D$) [m^2]
$\overline{v}$ = average water velocity [m/s]

The hydrostatic force per unit length (F_H) for the stern of the ship is:

$$F_H = \frac{1}{2}\rho_w g D^2 = \frac{1}{2} * 1000 * 9.81 * 0.14^2 = 96[N/m] \tag{6.7}$$

By horizontal force equilibrium the static friction coefficient is determined:

$$\begin{aligned} \mu_{static} F_{up} &= F_H + F_D \\ \mu_{static} p_{in} B &= F_H + F_D \\ \mu_{static} = \frac{F_H + F_D}{p_{in} B} &= \frac{96 + 76}{1700 * 0.22} = 0.45[-] \end{aligned} \tag{6.8}$$

This is the maximum static friction coefficient that can be determined from the experiments. The actual static friction coefficient is higher. This is determined when the ship starts to move over the weir from resting position on the weir.

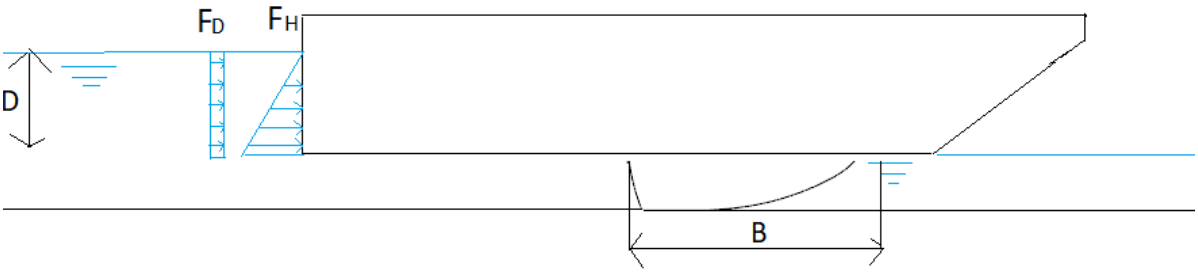

Figure 6.23: side view forces

6.4.3. Overtopping waves

Overtopping is not yet included in the velocity calculation over the weir. Here it is demonstrated that the overtopping is negligible for the determination of the friction coefficient.

The highest waves determined from chapter 4 is 1.35m. This corresponds to the ship collision with D=0.12m and v_4 in the experiments. The height of the overtopping should be half the wave height minus freeboard. The

height of the weir is measured 22 cm, so the overtopping height becomes (1.35/2)/(scale=25) - (0.22-0.206) = 0.013 m. The average width is assumed to be 2 meters where water flows over the weir. The flow velocity is assumed to be the same as the wave velocity, which is calculated for shallow water waves with:

$$c_{wave} = \sqrt{gH_{up}} \tag{6.9}$$

The time that water flows over the weir is measured from the videos. The water flows for around 1 second of the weir. Calculating the over topping volume is done as:

$$V_{over} = 0.013 * 2 * c_{wave} * 1 \tag{6.10}$$

The percentage of overtopping volume of the total volume is given in the next table:

	D=0.08 m	D=0.10 m	D=0.12 m	D=0.14 m
v_3	0.00	0.00	0.00	7.16
v_4	1.38	2.16	4.00	4.25

Table 6.3: percentage overtopping volume of total overflow volume

A 4.25% of volume decrease would also mean the same percentage decrease in mean flow velocity and a (0.9575^2) 8.3% decrease in drag force, see equation 6.6. Translating to the static friction coefficient gives 0.47. This is not a significant difference.

6.4.4. Air pressure

The static air pressure can have an effect on the friction force. The static air pressure is calculated with the assumed reduced volume in the membrane, when the ship rests on the membrane as in figure 6.22. The displaced area in this cross section can be calculated with:

$$A_{gap} = A_{gap,s} + A_{gap,w} = z_w * B_s + z_w^2 \tag{6.11}$$

where $A_{gap,s}$ is the gap of the weir occupied by the ship. Now the displaced area is known, it is assumed this is linearly proportional to the shrinkage of volume in the membrane. The shrinkage factor can be calculated as:

$$f_s = \frac{A_{gap}}{A_w} = \frac{z_{rest} * B_s + z_w^2}{(1.98 + 2 * \frac{1}{2} * 0.22) * 0.22} = \frac{z_w * B_s + z_{rest}^2}{0.48} \tag{6.12}$$

Where A_w is the area of the weir from figure 6.22. This is only the volume shrinkage in the weir. It is determined in appendix H that the added volume is 3.81 times the volume in the membrane of the scale model. To include the added air boxes, the total volume shrinkage becomes:

$$f_{s,tot} = \frac{f_s}{4.81} \tag{6.13}$$

It is assumed the percentage of volume decrease is the same amount of pressure increase, in accordance with the law of Boyle. The pressure increase in static condition for every experiment is given in graph 6.24. It shows a maximum static pressure increase of 5%. This will then also be the change in the static friction coefficient. It can be argued this change is significant. However, the ship still does not move over the weir.

In figure 6.25 the dynamic air pressure is given. This dynamic air pressure is measured from the barometer. The measurement is taken by the naked eye from the videos. The initial water level in the piezometer, before the ship hits the weir, could not be distracted. The camera was too far away from the piezometer to read this. Only when the air pressure increased the water level was noticeable. Around 1 or 2 seconds after the impact, the water level in the barometer shoots up. This is the air that is pushed away from the impact. The high dynamic air pressure increases the stresses temporarily. The dynamic air pressure increase is up to a factor 2 from the initial pressure. This seems very high, but this was not visually observed on the membrane.

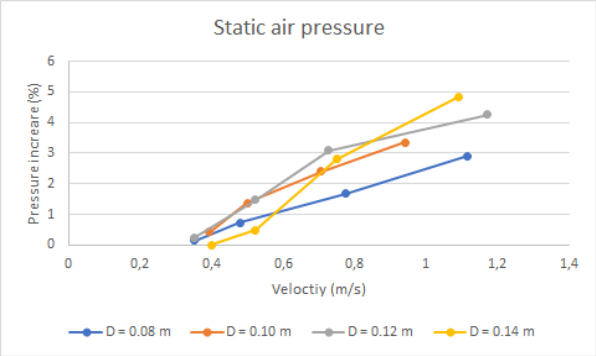

Figure 6.24: static pressure increase

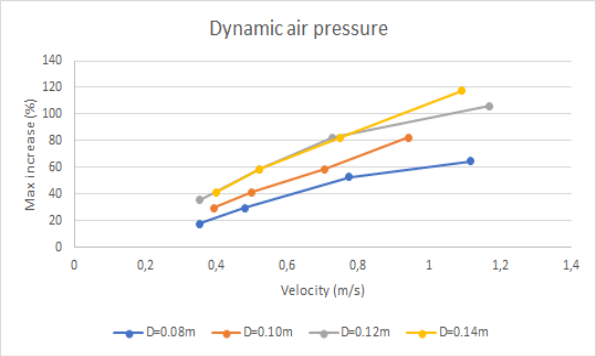

Figure 6.25: increase air pressure

6.5. Discussion

The ship does not pass the weir more than half the ships length, from the experiments. This means that the ship will not pivot around in centre of gravity and ground at the downstream side of the inflatable weir. Therefore, it can be concluded that a higher downstream level, the one in the winter, does not require to be tested. a higher downstream water level makes that the inflatable weir will be standing more upright and a higher hydrostatic pressure from the downstream is present, see figure 6.26. The ship collision will then generate a bigger counter-acting force and a smaller uplift force, so the ship will travel a shorter gliding distance.

Another option is that the ship approaches from the downstream side of the weir at winter conditions. This event is doubtful for two reasons. First, only an unloaded ship can get to the weir without grounding, with a safe under keel clearance of 0.5 m [19]. Second the approach velocity is lower, due to the water velocity resistance coming from upstream.

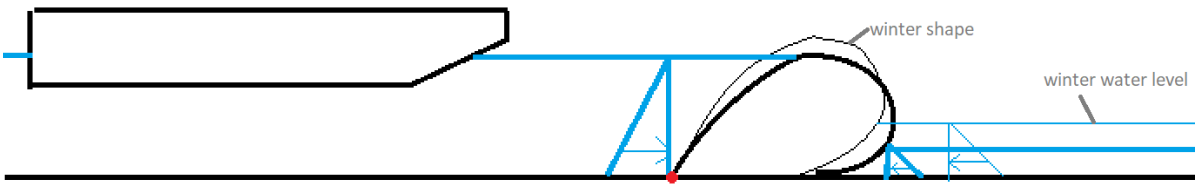

Figure 6.26: winter higher downstream water level

The upstream water level can change as well at location Grave. The upstream water level depends on the discharge in the Meuse. In figure 2.5 in chapter 2, the water level is shown for various discharges. A lower water level upstream will be present for a discharge of 1030 to 1640 m^3/s. A higher water level upstream will be present at even higher discharges. At these discharges the weir will be opened and ship can navigate over the weir. A higher water level will be unlikely, since then the water will flow over the weir.

In the experiment only one size of the ship is tested. Results with other dimensions are not available, but potentially can be extrapolated from the results. First, a longer ship will have a longer arm from the mass centre of the ship to the inflatable weir. This creates a larger upward momentum, but also a larger counteracting force. Second, both a larger and/or a wider ship for the same mass, will have a lower draught. The contact area will be less, and generates a lower upward moment as consequence. It is likely that for small ships especially in length, will top over the weir. With the results of the scale model experiments more detailed analysis are made in the next chapter.

The sheet for the scale model test is unreinforced. The strain in the sheet of the scale model, therefore can be much higher before failure than the sheet in the prototype. It has to be verified with the analytical model if the strain stays below the limit strain of the prototype.

7

Analysis

In this chapter the analysis is performed on the physical model tests in chapter 6 and an extension is given on the model presented in chapter 4. A new calculation set is done, because of the different mass and velocity used in the physical model. It is of importance to do this calculation to calibrate the theory with the physical model.

The first paragraph 7.1 analysis the ship collision on an inflatable weir event in a time schematization. Then the new mass and velocity are given in paragraph 7.2. Building on the time model new factors are added in paragraph 7.3. The new analytical model is calibrated with a potential energy coefficient to account for the uplift and glide coefficient on the physical model test. In the same paragraph the results of the improved analytical model are compared with the results of the scale model tests. In the last paragraph 7.4 last something is said about the desired clamping lines and the strength of the sheet.

7.1. Ship collision analysis

This paragraph describes the analysis of the ship collision on inflatable weirs in time. The analysis is based on what is found in the physical model tests.

The collision starts with the bow colliding into the inflatable weir, see figure 7.1 step 1. The forward energy of the ship pushed the inflatable weir downwards. On its turn the contact area between the bow ship and the inflatable weir is increased up to a maximum assumed of B/2 in horizontal and δ in vertical direction, see graph 7.2 and 7.3. In this moment in time momentum is developed tilting the bow upwards. From step 2 in figure 7.1 the contact area reduces again, but still momentum upwards is generated. There is assumed for a finite small time no contact with the weir, there the ship starts to glide fully over the weir where step 3 starts. Since the ship is tilted somewhat upwards, the forward momentum of the ship will move the front bow just a bit higher for some time. In the meanwhile the ship is decelerated losing its momentum and gravity takes the bow down again. From step 3 onwards the contact area is increased again see figure 7.2, but only in the horizontal direction. When the ship is laying horizontal again, the contact area is maximum again. In the meanwhile the ship glided over the weir, this is step 4 to 5. Step 5 is now achieved and the ships lays on the inflatable weir resting.

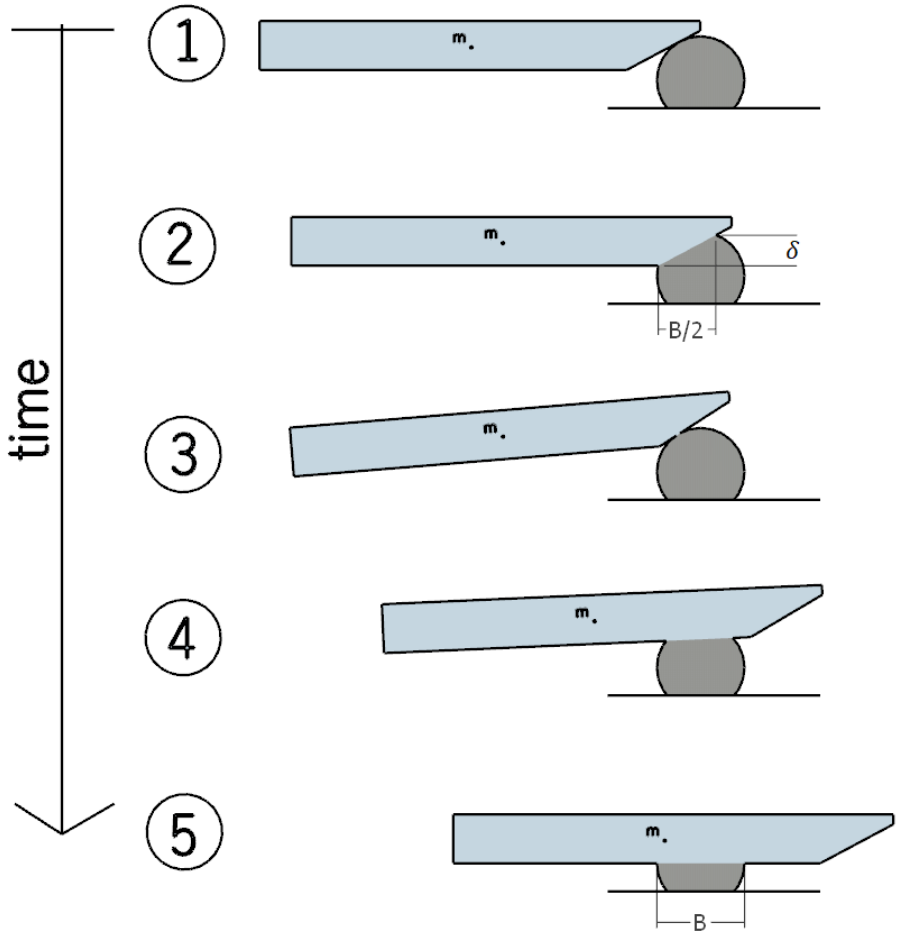

Figure 7.1: ship collision in time

In the first graph below, the impact is divided into two parts. The first part is a half sinusoidal shape, where the ship collides with the weir and is then uplifted. The second part of the graph represents the gliding of the ship over the weir. Most of the kinetic energy is absorbed by the first part of the impact. Here also vertical contact length is present, see the second graph.

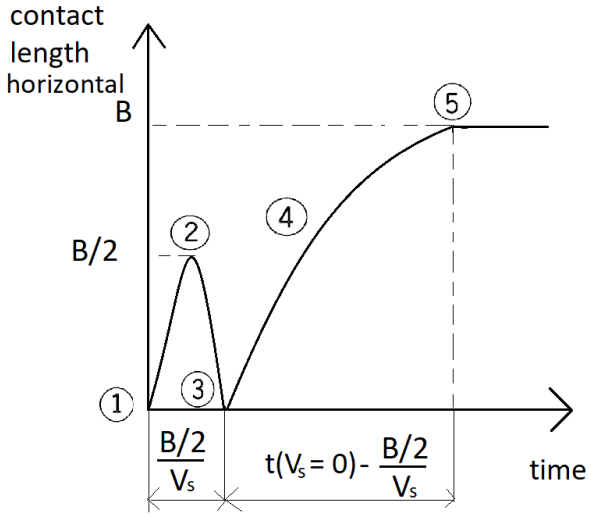

Figure 7.2: horizontal contact length in time

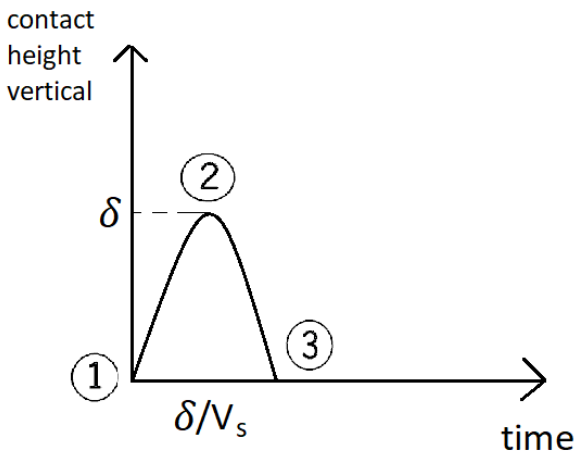

Figure 7.3: vertical contact length in time

Duration

The duration of the whole collision impact is given to get impression of the time scale. In a paper of Vrouwenvelder a formula for the impact time is given [4]. The time is based on a plastic deformation of steel structures. This means that there is only impact of the ship and no spring reaction of the impacted structure. For the inflatable weir collision time step 1 to 3 is assumed small in relationship to the rest of the collision, so the spring reaction is dismissed.

For the calculation of time, the maximum mass and velocity of the ship from the next paragraph is taken. The air stiffness is defined by the average contact area of the ship times the air pressure. Then the impact time is:

$$\Delta t = 0.5\pi\sqrt{m_s/k_{air}} = 0.5\pi\sqrt{m_s/(B/2) * B_s * p_{in}}0.5\pi\sqrt{31120/((5.3/2) * 11.4 * 53)} = 6.9[s] \tag{7.1}$$

where: m_s = mass of the ship [kN]
k_{air} = spring stiffness of the air inside membrane [kN]
B = width inflatable weir [m]
B_s = width ship [m]
p_{in} = air pressure in membrane [kN/m^2]

The impact time of first part of the collision is assumed:

$$\frac{B/2}{v_s} = \frac{5.3/2}{5.5} = 0.48[s] \tag{7.2}$$

Is around 7% of the total collision time, which can be considered low compared to the total collision time.

In the physical model test, this collision scenario took 1s, until max displacement x_{max} of ship over the weir. Scaled back to prototype gives 1x5=5s, this deviates from the calculated collision time. An explanation for this deviation can be: in the calculation is assumed a horizontal spring-mass system and in the experiment the direction of the spring-mass system changes and the spring magnitude itself.

7.2. Modified mass and velocity

In the physical model tests four different values are used for the mass and velocity. It was convenient in the physical model test to choose these values. In this analysis the values are scaled back to prototype values and are used in the calculations. The four different draughts, that are used for the analysis, are given in table 7.1. To calculate the prototype mass corresponding to the draught of the ship equation 6.1 is used.

draught [m]	mass [ton]
2.0	1703
2.5	2160
3.0	2630
3.5	3112

Table 7.1: parameters ship

The velocity is divided in four different numbers, with equal step size. The last velocity is the maximum velocity for the ship class of Va (extended) used in the physical model tests and in this chapter for the improved model. The four different velocities are: 1.375, 2.75, 4.125 and maximum 5.5 m/s.

7.3. Improved ship collision model

In the improved ship collision model two factors are added. The conversion to potential energy and glide coefficient which is determined by physical model tests. This paragraph explains what is included in the improved model and how it is used.

7.3.1. Potential energy conversion

Potential energy by air pressure

In the beginning of the collision there is the air pressure creating a momentum on the ship. This will raise the front of the bow up. The moment in the ship collision analysis is point 2 in figure 7.1. During this uplift a

counteracting force is created on the stern of the ship, this is the water uplift pressure. These two forces have to be in balance and the uplift height can be calculated, see figure 7.4. With the uplift, the potential energy generated can be calculated.

An analogy is made with lock gate hawser forces. Here the water that is pumped in creates translation waves. This will tilt the ship around its y-axis. Further elaboration is shown in the lecture notes lock gates of the course Hyraulic Structures [67]. First the force generated by the air pressure is defined as:

$$F_{up} = p_{in}\sqrt{\left(\frac{B}{2}\right)^2 + \delta^2} \tag{7.3}$$

It is assumed that the centre of mass is in the middle of the ship. Then the horizontal distance from the force to the centre of mass is calculated with:

$$G = \frac{1}{2}L_s - \frac{1}{2}\frac{B}{2} - \frac{b-\delta}{\tan(\beta)} \tag{7.4}$$

And the lever arm of the force is:

$$C = G\cos(\beta) \tag{7.5}$$

With the above expression the momentum upwards can be calculated:

$$M_{up} = F_{up}C \tag{7.6}$$

For the counteracting force, the water uplift pressure from the stern is calculated. The total force is then the amount of extra volume that is displaced times the specific weight and gravity:

$$F_{down} = \frac{1}{2}h_{air}\frac{1}{2}L_s\rho_w g \tag{7.7}$$

The counteracting moment is found by multiplying the water uplift force with the lever arm to the centre of mass:

$$M_{down} = F_{down}(\frac{1}{2}\frac{2}{3}L_s) = F_{down}\frac{1}{3}L_s \tag{7.8}$$

Now an expression is found for the upturning moment and down turning moment of the ship. With these two components an expression can be found for the uplift of the front bow. This is done by equalling 7.6 with 7.8 and using 7.7 follows:

$$h_{air} = \frac{M_{up}}{\frac{1}{2}L_s\rho_w g\frac{1}{3}L_s} = \frac{M_{up}}{\frac{1}{6}L_s^2\rho_w g} = \frac{F_{up}C}{\frac{1}{6}L_s^2\rho_w g} \tag{7.9}$$

$$E_{pot,air} = \frac{1}{2}m_s g\frac{1}{2}h_{air} \tag{7.10}$$

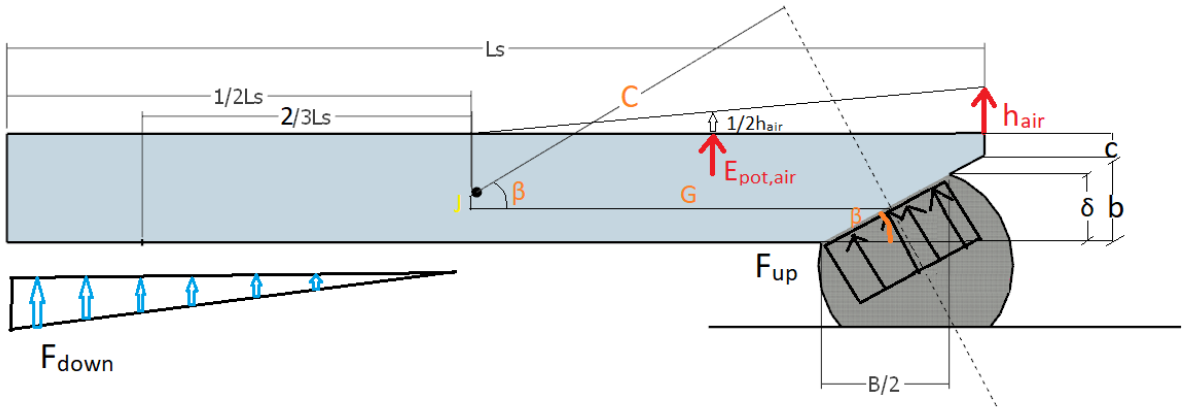

Figure 7.4: forces and moment static

The distance G goes a little bit beyond the centre of mass in the figure. This is due to the fact that the point of engagement of the air pressure force is not on a horizontal line with the centre of mass. The deviation that would be subtracted to the length G is(assuming mass centre is in the middle): $\frac{J}{tan(\beta)}$ Where $J = |\frac{1}{2}(D_s - \delta)|$. It can be demonstrated that this deviation is small, so it is neglected in the actual computation.

Potential energy by ship

The ship itself is also generating potential energy. In fact during the collision the ship kind of surfs over the weir. In collision time this is number 3 and 4 in figure 7.1. The wave in front of the ship creates a water layer between the ship and the inflatable weir. This makes the frictional resistance very low.

The potential energy is found as a component of the kinetic energy. The component is dependent on the angle of the bow, see figure 7.5. In the equation below this potential energy is defined:

$$E_{pot,ship} = E_{kin} * \lambda \tag{7.11}$$

To cover the whole range of β values for the bow figure 7.5 has to be extended. This is shown in figure 7.6, for bow angles larger than 45 degrees. The unknown value λ is defined as:

$$\lambda \begin{cases} \sin(\beta) & for \quad 0 < \beta < 45^\circ \\ 1 - sin(\beta) & for \quad 45^\circ < \beta < 90^\circ \end{cases} \tag{7.12}$$

Also the generated height of the front bow can be calculated with the potential energy. The generated potential energy is expressed as:

$$E_{pot,ship} = \frac{1}{2} m_s g \frac{1}{2} h_{ship} \tag{7.13}$$

Equalling equation 7.11 with 7.13 and using the kinetic energy formulation from equation F.1, then the height of the front bow is defined as:

$$h_{ship} = 2\frac{E_{pot,ship}}{\frac{1}{2}m_s g} = 2\frac{\frac{1}{2}m_s * v_s^2 * \lambda}{\frac{1}{2}m_s g} = 2\frac{v_s^2 \lambda}{g} \tag{7.14}$$

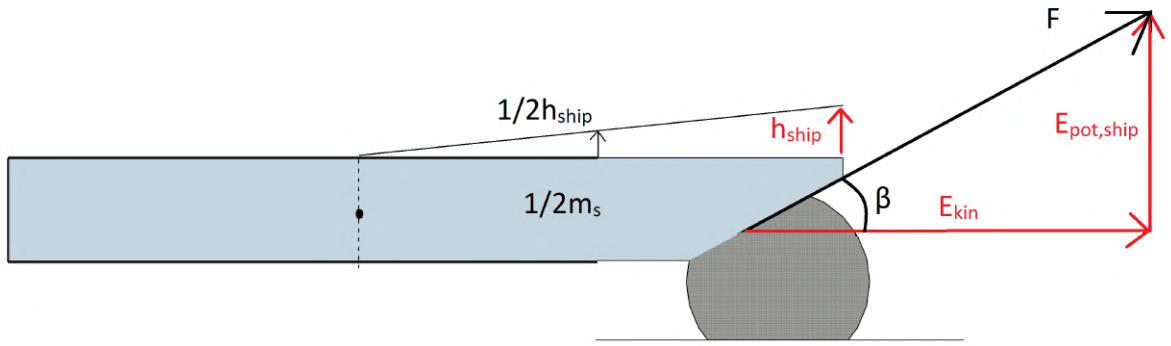

Figure 7.5: potential and kinetic energy distribution

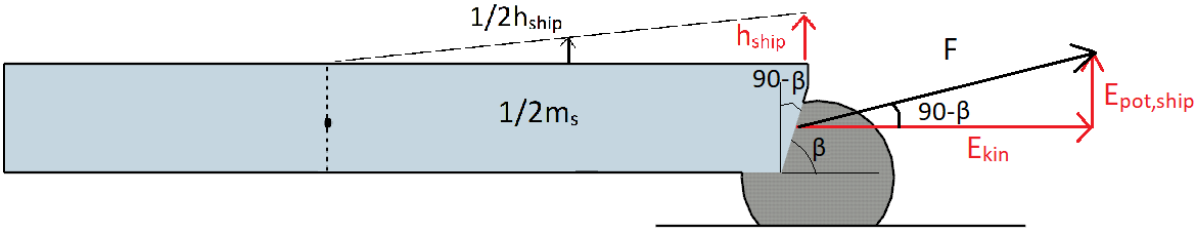

Figure 7.6: adjustment energy transfer analysis

The total uplift of the front bow is found by adding the uplift generated potential energy by the air pressure and the kinetic energy of the ship:

$$h = h_{air} + h_{ship} \tag{7.15}$$

Also the total potential energy is found by adding the potential energy generated by the air pressure and the kinetic energy of the ship:

$$E_{pot} = E_{pot,air} + E_{pot,ship} \tag{7.16}$$

7.3.2. Glide coefficient

The glide coefficient is added to account for the ship gliding over the weir. In standard expressions for ship collision only the colliding into the structure is included. This paragraph describes how the glide coefficient is calculated.

First the conservation of work and energy is used. With this the force transferred to the membrane can be found:

$$F_w = \frac{E_{kin} - E_{pot}}{x_{s,cor}} \tag{7.17}$$

where: F_w = the mean force transferred from the ship to the membrane [N]
$x_{s,cor}$ = displacement ship over weir with correction [m]

The force calculated according the the theory is:

$$F = \sqrt{2(k_{circ} + k_{long})(E_{kin} - E_{pot}} \tag{7.18}$$

The ratio between the work force and the theory force is the glide coefficient for the bow angle used in this research:

$$C_{glide} = \frac{F_w}{F} \tag{7.19}$$

The bow coefficient is calculated with the experiment values for all sixteen combination in figure 7.7. A general way to find the glide coefficient for all bow angles, with this experiment set is done as:

$$C_{glide,gen} = \frac{\sin(12.6)}{\lambda} C_{glide,mean} \tag{7.20}$$

where the 12.6 is the bow angle used in this research.

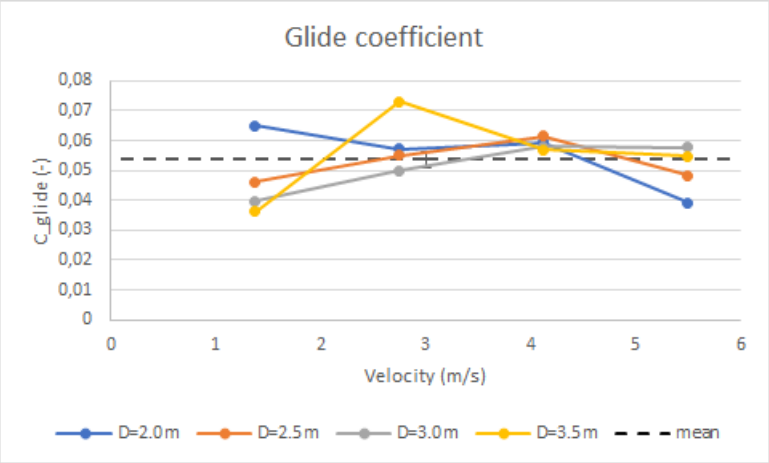

Figure 7.7: glide coefficient

Then the glide coefficient can be included in the force formula. The force becomes:

$$F = C_{glide,mean} \sqrt{2(k_{circ} + k_{long})(E_{kin} - E_{pot})} \tag{7.21}$$

Where $C_{glide,mean}$=0.054 is the mean glide coefficient of the coefficients determined in graph 7.7.

7.3.3. Strain

The new strain can now be calculated with the adjusted force formula in equation 7.21 implemented in equation 4.11. 1.9% strain has to be added for the tensile force in static equilibrium, already discussed in chapter 4. It was concluded from chapter 4, that the longitudinal strain is not significant in the ship collision analysis, so this one is left out as graph. In graph 7.8 the strain is shown calculated with the improved analytical model. It is shown that the maximum strain is well below the limit strain.

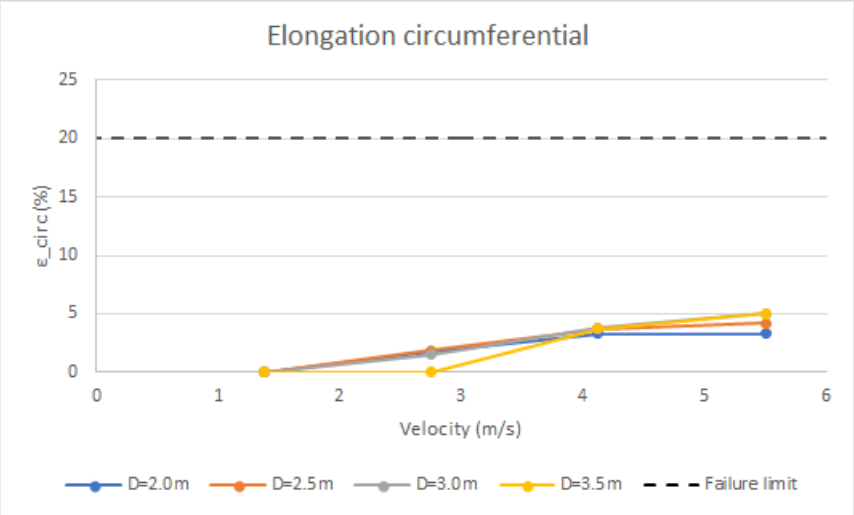

Figure 7.8: elongation circumferential with glide coefficient

7.3.4. Comparison of results

In this paragraph some results are compared from the calculation done in the improved analytical model and the physical model tests.

The uplift of the bow of the ship (h) is calculated with equation 7.9, 7.14 and 7.15. The values of the physical model tests are used to make it comparable. For the dimensions figure 6.3 and 6.2 , for the mass table 6.2 and for the velocity figure 6.8, 6.9, 6.10 and 6.11 is used.

In figure 7.9 the uplift 'h' calculated is compared with the actual measured uplift of the bow of the ship. A positive deviation means the uplift calculated is higher and a negative deviation means the uplift measured is higher. It is noticed in the figure that most percentages are negative. The average deviation is around 25% from the experimental value.

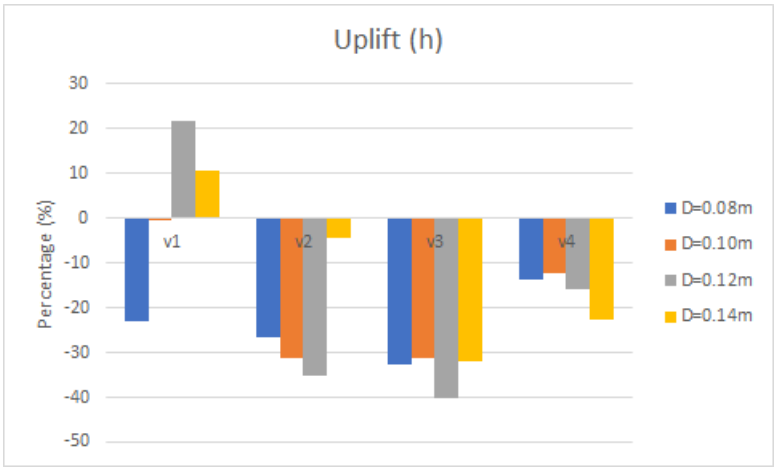

Figure 7.9: comparison uplift bow ship between calculation and measurements physical model tests

Also the new accuracy of the new force equation 7.21 is tested. The same experimental values are used as for the calculation of the uplift of the bow 'h'. The new force equation 7.21 is put in equation 4.11 to calculate the displacement of the weir 'x_w'. In the improved model it is not anymore assumed that the ship and the weir move together. The force transferred from the ship to the weir during collision gives a displacement of the weir, using the improved model.

The results from the calculations are compared with the measured displacement from the weir in the experiments see figure 7.10. A positive deviation means the displacement calculated is higher and a negative

deviation means the displacement measured is higher. It is clear that for the lowest velocity 'v_1' there is an 100% deviation. The potential energy calculated is here bigger than the kinetic energy and so no displacement of the weir is calculated. The rest of the deviation are on average 15%

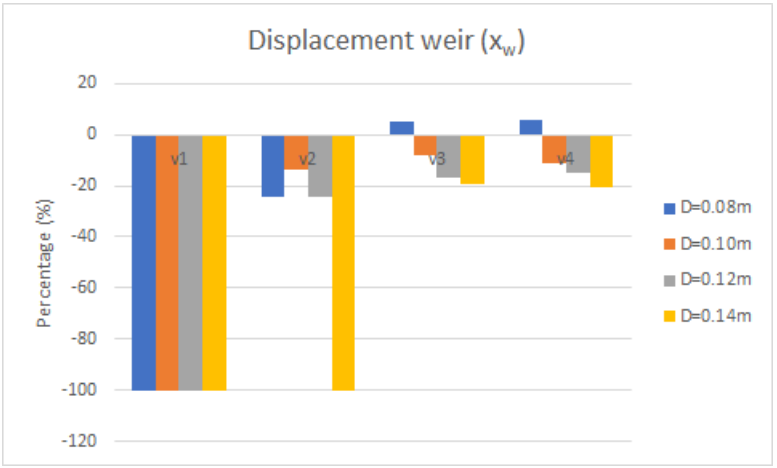

Figure 7.10: deviation x_w

7.4. Clamping and sheet strength

This paragraph determines the required clamping for ship collision. It will be checked if the sheet used in the design is resistant to collision force from the improved analytical model

The force in the clamping is determined with the static tensile force plus the ship force that is acting on the clamps per meter width, so:

$$F_{sheet} = T + F_{ship} \tag{7.22}$$

The static tensile force is already calculated in chapter 3 (139 kN). The maximum ship force is for the maximum mass and maximum velocity. The maximum ship force to the clamps is derived from the strain of the sheet in figure 7.8, $F_{ship}=k_{circ}x\epsilon_{circ}=7500x0.052=390$ kN/m.

The design strength of the bolts in the clamping line is calculated with:

$$F_{t,\mathrm{Rd}} = \frac{k_2 \cdot f_{\mathrm{ub}} \cdot A_{\mathrm{b}}}{\gamma_{\mathrm{M2}}} \tag{7.23}$$

where: k_2 = coefficient for head of bolt is 0.63 [-]
f_{ub} = nominal tensile strength bolt [N/mm^2]
A_b = stress surface of bolt [mm^2]
γ_{M2} = partial safety factor [-]

The Japanese prescribe a safety factor of 2 between the working load of the bolts of the clamping system and the yield strength of the bolts [25]. This is γ_{M2} in the formula. Looking at figure C.6 the bolts are totally straight rods so k_2 is 0.63. The nominal tensile strength for the bolts is designed as 500 N/mm^2.

In chapter 3 it is also given that the bolts are 150 mm apart from each other, so the force $F_{bolt}=F_{sheet}x0.15$. Equating the design strength $F_{t,Rd}$ with the bolt force gives the stress surface of the bolt, which is $A_b=503$ mm^2. The diameter is then expressed as:

$$D_{bolt} = \sqrt{4A_b/\pi} = \sqrt{4 * 503/\pi} = 25.3[mm] \tag{7.24}$$

Also the plate, which clamps the sheet, has to be calculated. The design strength of the plate is calculated width:

$$B_{p,Rd} = \frac{0.6\pi d_c t_p f_u}{\gamma_{M2}} \tag{7.25}$$

where: d_c = smallest span [mm]
t_p = plate thickness [mm]
f_u = tensile strength of plate [N/mm^2]

The tensile strength of the plate is assumed the same as for the bolt. The span of the plate is assumed as 150 mm to preserve a watertight sheet. The smallest plate span is then, where 25.3 mm is the bolt diameter, (150-25.3)/2= 62.3 mm. Equating the plate strength to the force the sheet in equation 7.22 gives a plate thickness of 18 mm. An overview of the clamping system is given in figure 7.11

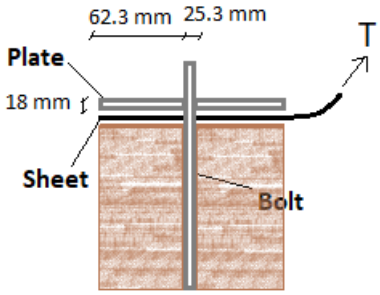

Figure 7.11: clamping dimensions

The total maximum force is determined in equation 7.22. This is the static force plus the maximum ship collision force. The design strength in chapter 3 is given as 1602 kN/m. Including the Ramspol safety factor the check of the strength of the sheet can be determined. In appendix E the safety factor is determined including the folds. From the physical model tests it was observed that the folds did barely move, see appendix H, therefore this factor can be excluded. The safety factor becomes then 1.25. The check of the sheet strength reads as follow:

$$\frac{R_t}{1.25F_{sheet}} = \frac{1602}{1.25 * 529} = 2.42 \tag{7.26}$$

This is far above one, which means the design sheet is then resistant against the applied ship collision force.

7.5. Discussion

The analysis done in this chapter is mainly extracted from the observations done in the previous chapters. A collision scenario is represented in the beginning of this chapter, that describes the general effect during the ship collision. This scenario is based on what is the most likely collision event. For a very low ship velocity it was shown in the scale model experiment, that the ship is not really gliding over the weir and bounces back. The other extreme would be a very short ship that jumps over the weir and grounds on the downstream side.

The optimized model includes the effect of uplift of the ship during collision. The model describes everything statically. In reality, the dimension time is present which makes the event dynamically. It can be argued that a dynamic model is going more into details of the ship collision. For example the contact area of the ship with the weir will be more accurately represented, which are now schematized in figure 7.2 and 7.3. On the other side the static model is more suited for a general overview.

It is shown that the static model describes the physical effects with an accuracy of 30% and 15%. That is not a bad result for a simplified model as used here. To have a model which is perfectly in accordance with the physical model tests, a lot of iteration steps will be needed. Everything in this chapter is still calculated statically, but gives results of the event. There are some issues with determining the right contact area for example. This contact are was not accurately visible in the model experiments, but are determined with logical reasoning. Another thing to mention due to the static calculation, the deviation of the uplift 'h' can be mainly explained. In the static calculation no acceleration terms are included.

8

Conclusions and recommendations

The first paragraph 8.1 describes the conclusions of this study. The second paragraph 8.2 provides recommendations based on the findings of this study.

8.1. Conclusions

In this section the research questions that were posed in chapter 1 are answered and conclusions are presented based on the findings of the research. The first research question was stated as:

1. How can the inflatable weir-ship interaction by ship collision at Grave be modelled to predict the motions of the ship and the inflatable weir?

An analytical model was made to predict the inflatable weir-ship interaction during ship collision. The analytical model is simplified, but still produces results for the motions of the ship and the inflatable weir. The numerical test could not be verified with the analytical model. It is complex to simulate the ship collision on inflatable weirs in numerical software and takes considerable computation time (1 hour) on a laptop with four 2.5 GHz processors. The numerical software showed the ship collision visually in time, where it just ran straight through the sheet. In reality this is not likely to happen. The numerical model set-up in this research seems not suitable for analysis of ship collision on inflatable weirs. Where the physical model test seemed a reliable verification method for the analytical model. The analytical model, described in chapter 7 is improved with help of the physical model tests in chapter 6.

It was assumed, in the analytical model, that the ship and weir had the same horizontal displacement during the impact. However the physical model tests invalidated this and showed a far higher horizontal displacement of the ship over the weir. That is why two factors are added in the improved analytical model. First, a gliding coefficient is included to determine which part of the energy is transferred directly to the sheet of the weir, see chapter 7. The gliding coefficient is mainly dependent on the angle of the bow, but also on the friction between the sheet and ship. Second, the uplift of the bow was noted during the physical model test. So the effect of conversion to potential energy is also added in the improved analytical model. It was found that in the improved analytical model, the movement of the ship in vertical direction deviated with an average of 25% and the movement of the inflatable weir in horizontal direction deviated with an average of 15% from the physical model tests. One of the reasons for this is that the analytical model is static and the physical model tests dynamic.

One thing that is not well determined is the contact area of the ship with the inflatable weir during impact. In the analysis it is assumed the maximum contact area horizontally is half the width of the membrane (B/2). However this cannot be verified accurately with the physical model tests. The contact area could at most be read with the naked eye. As last the performance of the used models is summarized in table 8.1

	Analytical	Numerical	Physical
Results	0	-	+
Time	+	0	-
Degree of freedoms	-	0	+
Accuracy	0	+	0

Table 8.1: comparison models

2. What happens when a push convoy ship collides with an inflatable weir?

The physical model tests in chapter 6 gave the best impression of the ship-inflatable weir interaction. The ship showed a larger displacement over the weir for increased velocity. This dependency is almost linearly. The draught of the ship does have minor influence on the displacement over weir. Second, the uplift of the prow (bow) showed the same dependency, also for an increasing velocity an higher uplift of the ship appeared. For all experiments the ship glided over the weir and came to a standstill on (top of) the weir, then the weir is pushed down by the ship. For the lowest two velocities, only the bow stayed on the weir after collision. The weir was in that case not barely pushed down by the ship. Lastly, there is the displacement of the weir itself. A higher velocity and/or draught showed a larger displacement of the weir. The curve flattened out for a higher velocity. Eventually the ship cannot flatten the inflatable weir further and displacement will only be experienced by strain of the sheet.

Besides the behaviour of the ship and the weir, also the effects of the water is investigated. The experiments showed the ship glides over the weir by a small layer of water. This layer of water became bigger for increasing velocity and draught. The layer of water is also called the added water mass. The videos showed that the added water mass already displaced the weir before the ship hits the weir. Secondly, the water overflow that was calculated in chapter 7, was also noticed in the experiments. Lastly, there was significant air pressure increase during the impact. However this did not express itself in unfolding of the folds present the abutments.

Perspective inflatable weir

The inflatable weir shows an interesting reaction to ship collision in the performed study. The results of the improved analytical model in chapter 7 showed a maximum circumferential strain of 5%, which is within the limit before break (20%). The longitudinal strength was confirmed to be of minor importance to the force transfer from ship collision in chapter 4. With a modified safety factor for the one used at Ramspol, the design tensile strength could also be checked. An unit check value of 2.42 is well above the safe value of 1. The last sub question was to determine the side effects of the water. The ship waves generated, by the movement of the ship, showed no significant influence on the load of the inflatable weir. For the class Va ship, in chapter 4, the average water overflow velocity can increase to around 4.5 m/s. The current bottom protection can be damaged by the overflow, depending how much the flow velocity is decelerated.

This study has taken the first steps into researching ship collision on inflatable weirs. It is of importance to know if the inflatable weir is resistant against ship collision. If not, extra preventing measures are likely needed, which cost money.

Besides the ship collision, a general perspective for the inflatable weir as replacement in the Meuse will be proposed. First, the inflatable weir has an effective functionality. By automatically controlling the air pressure in the weir, the overflow height is regulated. Second, the inflatable weir can be assembled on a flat foundation. Extra costs can be saved by using the existing foundations of the weirs in the Meuse. A disadvantage on the other hand is that the inflatable weir can be vulnerable to sharp edges.

To increase the perspective of inflatable weirs in the Meuse, a next step is to compare it with other weirs suitable in the Meuse. Further investigation is recommended in ship collision on the inflatable weir. A few of them are in paragraph 8.2.

8.2. Recommendations

In this paragraph the recommendations are given based on the executed research. There are a lot of recommendations to mention, because research about this specific scenario has not been considered yet. The most relevant ones are shown below.

Model improvement

- The sheet is assumed to be linearly stiff in the models. In reality the stiffness is nonlinear and this can significantly alter the results. The model can be improved by incorporating the non-linear stiffness of the sheet.
- The improved analytical model is a static model. The verification with the physical model tests is missing out the time component. For a more realistic comparison, an analytical/numerical time model can be built that analyses the ship impact on the weir in time.
- From the scale model experiments it was observed that the system (weir, ship, water) was moving back and forth during the impact. The movement gradually faded out due to the damping of the system. For a more accurate model the damping of the system should be included. It is recommended to study the included damping.
- For larger bow angles, the bow is shorter. An extra effect (coefficient) should be included for that, because the (horizontal) contact area with the bow ship-inflatable weir is less.

Further research recommendations

- The design of the inflatable weir is conceptual in this research and only for the replacement of weir Grave. To further outline the replacement of the weirs in Meuse by inflatable weir, a study can be made on the feasibility. The other weir locations require different dimensions of the inflatable weir and the circumstances also differ.
- Now it is reasoned which scenario has the highest probability of occurrence. For a more accurate answer a probability calculation is needed. For this, the data of the ship is needed and the development of shipment in the future. Based on the data it is possible to determine the probability and the consequences of every scenario. Eventually, a Monte Carlo simulation is recommended to determine the failure curve of every scenario.
- In the research it ship collision from the upstream side of the weir is studied and reasoned most probable. There is a scenario in the winter, where an unloaded ship hits from the downstream side of the weir. It is interesting to research the effect on the inflatable weir in this scenario. The inflatable weir may flip over its clamping line.
- In the research only the hull of the ship is considered. Usually, ships also have a bow thruster. This bow thruster is installed in front of the ship and can be outside or inside of the hull during navigation. The question is, if the bow thruster will hit the weir during impact. And if this happens, will the propeller cut the sheet apart or not?
- The collision at Grave is simulated in this research. The collision of the push convoy at Linne was a different one. Here the ship collided parallel to the weir. It is interesting to research what the effect is of an inclined collision for every angle possible.
- This research made use of an inclined flat bow that is situated on push convoys. Other type of ships have a V-bow. This type of bow is more inclined and curved. The effects of the ship-weir interaction, due to the impact, can be quite different. The ship will have more likely a bouncing back effect. It is recommended to study ship collision on inflatable weirs with this type of bow shape for the ship.
- The power of the engine is not considered in this research and can significantly increase the impact on the weir. Besides, it is possible that the shipper puts the ship in reverse during the impact.
- There was no spill breaker present in the experiment. This can cause extra resistance during gliding over the weir. It is recommended in a further design stage, when the spill breaker is designed, to include this in the physical scale model.

List of Symbols

The next list describes several symbols that will be later used within the body of the document

Greek symbols

α	angle of the bow	$^\circ$
β	internal pressure coefficient $\frac{p_{in}}{H_{up}}$	–
δt	thickness membrane	m
Δ	dimensionless specific grain weight $\frac{\rho_s - \rho_w}{\rho_w}$	–
δ	contact height ship-inflatable weir	m
Δ_t	impact time	s
ϵ	strain of inflatable weir	–
ϵ_{circ}	circumferential strain inflatable weir	–
ϵ_{long}	longitudinal strain inflatable weir	–
γ	Poisson constant	–
γ_{dyn}	dynamic coefficient	–
γ_{M2}	partial material factor	–
γ_{mat}	material factor	–
γ_T	partial factor	–
κ	curvature of sheet	$1/m$
λ	component transferring forward momentum ship to potential energy	–
μ	mean	–
μ_v	viscosity	N/m^2
μ_{static}	static friction coefficient	–
Φ	threshold value before grains start to move	–
ϕ_0	angle membrane upstream	$^\circ$
ρ_w	specific weight water	kg/m^3
σ	stress	N/m^2
σ_d	standard deviation	–
Θ	angle circular shape	$^\circ$
ζ	coefficient which represents ship geometry	–

Latin symbols

γ	Poisson constant (1.0 for isothermal- and 1.405 for adiabatic compression)	–
$\overline{v}$	average water velocity	m/s
a	length bow	m
A_b	stress surface of clamping bolt	mm^2
A_m	base width membrane on bottom unstretched	m
A_r	latitude cross sectional area river	m^2
A_s	area ship under water in latitude cross section	m^2
A_{basin}	top view area of downstream basin	m^2
$A_{gap,s}$	gap area in inflatable weir occupied by ship	m^2
$A_{gap,w}$	gap area in inflatable weir for water flow	m^2
$A_{gap,w}$	total gap area in inflatable weir	m^2
A_{in}	area inside inflatable weir cross section	m^2
A_{leak}	leakage area circular shape	m^2

$A_{shrinkage}$	total area shrinkage prototype inflatable weir	m^2
B	width of inflatable weir	m
b	length of inclined part bow	m
B_m	base width membrane on bottom stretched	m
B_s	width of ship	m
$B_{p,Rd}$	design strength clamping plate	N
C	Chézy value	$m^{1/2}/s$
c	height prow	m
C_b	block coefficient	–
C_C	confinement coefficient	–
C_D	drag coefficient	–
C_E	eccentricity coefficient	–
C_H	hydrodynamic coefficient	–
C_S	ship coefficient	–
$C_{glide,gen}$	general bow coefficient	–
$C_{glide,mean}$	mean bow coefficient from experiments	–
C_{glide}	bow coefficient from experiments	–
c_{wave}	wave celerity	m/s
D	draught of ship	m
d	grain size diameter	m
$D1, D2$	water depth measurement locations	m
D_b	diameter clamping bolt	mm
d_c	smallest span clamping plate	mm
d_m	maximum fender deflection	m
D_s	height of ship	m
d_{50}	nominal grain size diameter	m
D_{max}	maximum draught	m
D_{min}	minimum draught	m
dS	Length of sheet element in unloaded state	m
dS^*	Length of sheet element in loaded state	m
E	Elastic modulus	N/m^2
E_{kin}	kinetic energy of ship and water moving along	Nm
$E_{pot,air}$	potential energy generated by air pressure inflatable weir	Nm
$E_{pot,ship}$	potential energy generated by forward momentum ship	Nm
$E_{pot,w}$	potential energy of inflatable weir	Nm
EA	strain stiffness	N
EI	bending stiffness	Nm^2
F	force of the ship	N
f	energy absorbing efficiency of fender system	–
F_D	drag force	N
F_H	hydro static water force	N
F_R	resistance force inflatable weir	N
f_s	shrinkage factor	–
f_u	tensile strength of clamping plate	N/mm^2
F_w	work force	N
F_{down}	downward force by hydro static water pressure	N
$f_{s,tot}$	total shrinkage factor	–
F_{sheet}	total force sheet	N

$F_{t,Rd}$	design strength clamping bolts	N
f_{ub}	nominal tensile strength clamping bolt	N/mm^2
F_{up}	upward force by air pressure	N
G	horizontal arm upward force to mass centre ship	m
G	perpendicular arm upward force to mass centre ship	m
g	gravitational constant (9.81)	m/s^2
H	height inflatable weir	m
h	total uplift prow	m
H_w	wave height	m
h_w	depth in water column	m
h_{air}	uplift prow by air pressure inflatable weir	m
H_{down}	downstream water depth	m
h_{ship}	uplift prow by forward momentum ship	m
H_{up}	upstream water depth	m
i	slope	–
j	amount of layer areas for circular shape	–
K	compressibility coefficient	–
k	stiffness sheet	N/m
k_2	coefficeitn for head of clamping bolt	–
k_{air}	spring stiffness air inside membrane	N
k_{circ}	stiffness sheet in circumferential direction	N/m
k_{long}	stiffness sheet in longitudinal direction	N/m
L	length of sheet	m
L	length weir	m
L_s	length of ship	m
m_s	mass of the ship	kg
m_w	mass of the water moving with the ship	kg
M_{down}	downward momentum	Nm
M_{up}	upward momentum	Nm
n	general scale factor	–
n_p	scale factor pressure	–
n_V	scale factor volume	–
$n_{\Delta p}$	scale factor differential pressure	–
n_{EA}	scale factor strain stiffness	–
p	Resulting pressure on sheet (difference inside and outside pressure)	N/m^2
p_0	pressure of gas	N/m^2
p_w	water pressure	N/m^2
p_{model}	pressure model (atmospheric pressure + overpressure model)	N/m^2
p_{proto}	pressure prototype (atmospheric pressure + overpressure prototype)	N/m^2
Q	discharge	m^3/s
q	resulting dynamic pressure on sheet	m
R	hydraulic radius	m
R_m	maximum fender reaction force	N
R_n	radius membrane	m
R_t	strength sheet	N
R_w	radius of circular shape	m
s	distance side ship to bank	m
SCF	stress concentration factor	–

SCF_{test}	stress concentration factor likely to have occurred during	–
T	Tensile force in sheet without own weight	N
t	time	m
T_D	tensile force by dynamic load	m
t_p	clamping plate thickness	mm
T_w	tensile force with own weight	N
u	stretch of the sheet	m
v	water velocity over weir	m/s
V_0^γ	volume of gas	m^3
v_m	scaled velocity	m/s
v_s	velocity component of the ship perpendicular to the structure	m/s
v_1	minimum velocity of ship	m/s
v_2	intermediate velocity of ship	m/s
v_3	intermediate velocity of ship	m/s
v_4	maximum velocity of ship	m/s
$v_{95\%}$	velcotiy 95% confidence interval	m/s
V_{in}	volume inside inflatable weir	m^3
V_{over}	over topping volume water	m^3
w	self weight sheet	N/m
x_s	displacement ship over weir without correction	m
x_w	displacement weir x-direction	m
x_{cor}	correction for ship over weir	m
$x_{s,cor}$	displacement ship over weir with correction	m
y_n	width of layer area	m
z	effective water depth	m
$z\overline{z}$	center of gravity of leakage area for circular shape	m
z_n	vertical coordinate of layer area	m
z_w	water level depression	m
z_{deck}	relative displacement deck sip on weir	m

List of Figures

List of Tables

A

Weirs Meuse and shipping

This appendix includes two tables of the weirs and a fault three based on the ship collision at Grave. The tables describe the bed protection and dimensions with type of the weirs.

A.1. Bed protection weirs

In the table below the bed protection is given for the seven weirs in the Meuse in the Dutch reaches. Reading the table from top to bottom is further downstream from the weir.

	Length* [m]	Class [kg]	Bed protection
Lith	40	40-200	quarry stones poured with asphalt
	25	40-200	quarry stones
	15	10-60	quarry stones
Grave	55**	40-200	quarry stones with colloidal concrete
	55	40-200	quarry stones
Sambeek	-		Stoney part: concrete block 1.5x1x0.95 m Poirée part: concrete blocks 1.5x1x0.8 m
	6	40-200	quarry stones with colloidal concrete
	49	40-200	quarry stones
	15	10-60	quarry stones
Belfeld	8.5		concrete blocks
	2		cofferdam (in Dutch: kistdam)
	25	300-1000	quarry stones
	30	40-200	quarry stones
	2		caisson
Roermond	8.5		concrete blocks
	2		cofferdam
	45	40-200	quarry stones
Linne	20	60-300	Stoney part: quarry stones with colloidal concrete
		300-100	Poirée part: quarry stones with colloidal concrete
	60	60-300	Stoney part: quarry stones
		300-1000	Poirée part: quarry stones
Borgharen***	40	60-300	quarry stones with colloidal concrete

Table A.1: bed protection weirs

* cumulative distance away from the weir from first mentioned to last
** after ship collision extended from 20 m to 55 m colloidal total 85 m
***300-1000 kg and most western opening 40-200 kg

A.2. Dimensions weirs

The table below describes the dimensions of each part of each weir. The parts are also described by their type.

	Total width [m]	Regulation system	Beams	Width [m]	Height [m]	Sill depth [m NAP]
Lith	114	3 x slide		38	7.5	-2.5
Grave	110	1x rotating flap	9	50	5.3	2.7
		1x rotating flap	11	60	5.3	2.7
Sambeek	97	2 x Stoney		17	5.4	5.45
		1 x Poirée	13	63	6.3	8.05
Belfeld	97	2 x Stoney		17	5.65	8.35
		1 x Poirée	13	63	6.66	8.05
Roermond	102	2 x Stoney		17	4.1[1]	11.8
		1 x Poirée	17	68	5.95	11.6
Linne	110	3 x Stoney		17	3.95	16.95
		1 x Poirée	15	60	4.95	15.95
Borgharen	99	3 x valve		23	5.5[2]	39.6
		1 x slide		30	-	38.5

Table A.2: dimensions weirs [8] [16, p. 76-82]

A.3. Shipping fleet

In the next figure the shipping fleet of the Netherlands is shown. In the meantime the ship fleet could have change to different ratios.

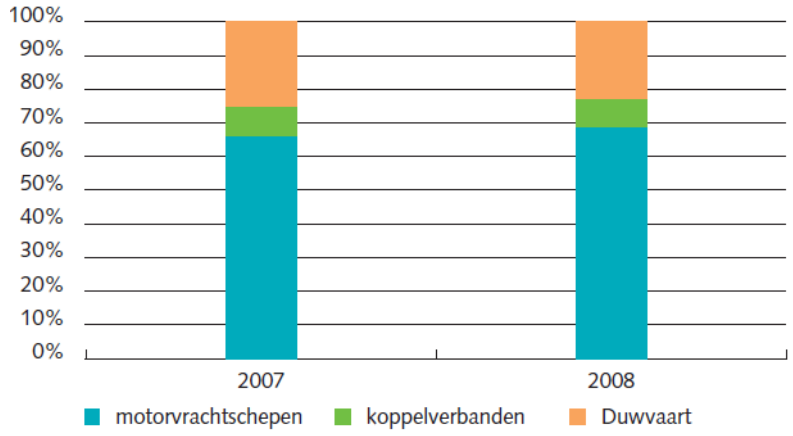

Figure A.1: shipping fleet Netherlands [48]

A.4. Ship collisions

Multiple ship collisions happened in the past in the Netherlands. All ship collision registered are given in the figure below, this also includes recreational inland navigation.

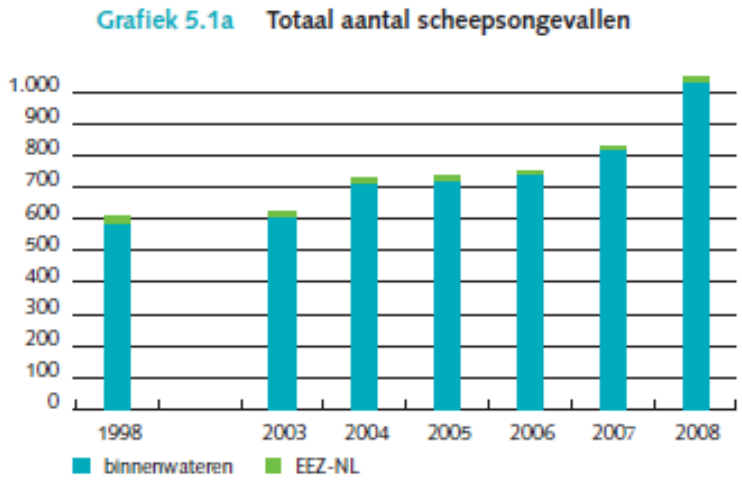

Figure A.2: ship accidents Netherlands [48]

The Dutch Safety Board created a fault tree to determine what factors were playing a role during the ship collision. There was at the time a thick fog with low sight. The fault tree is shown in figure A.3.

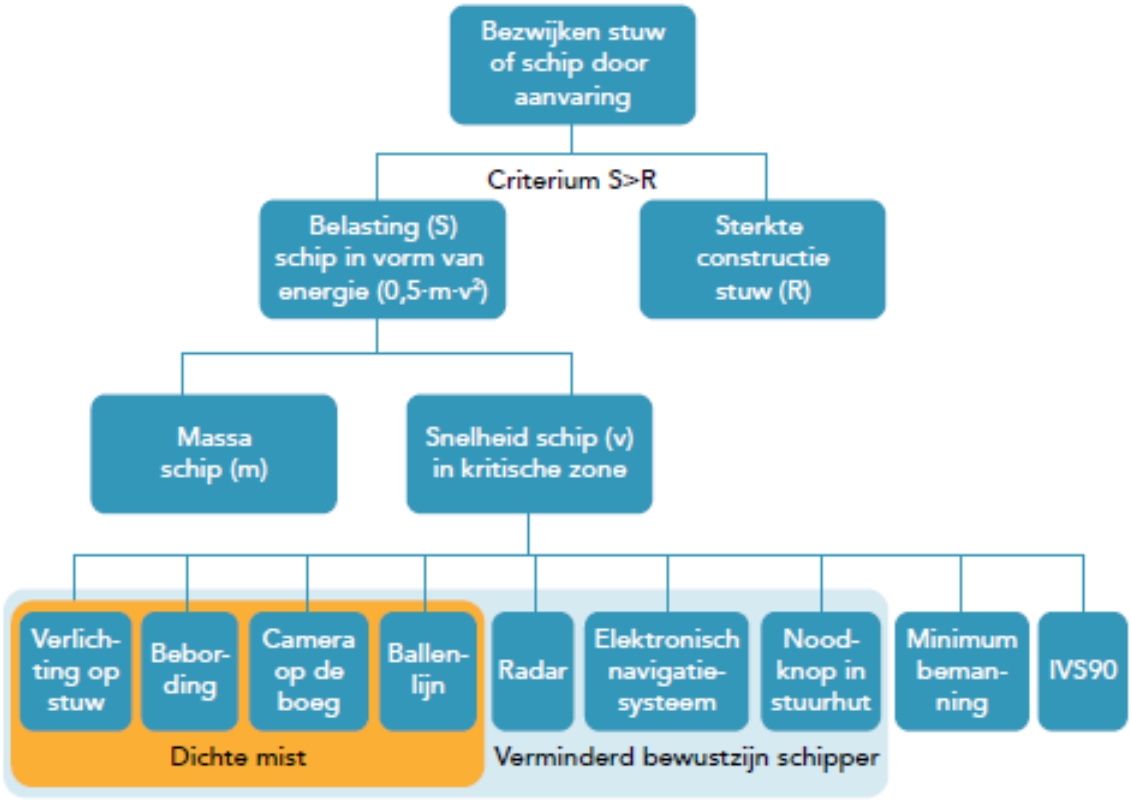

Figure A.3: fault tree ship collision weir Grave [64]

B

Inflatable rubber dams

The inflatable rubber dam is in general used for three different situations:

- individual use for protecting houses
- acting as a dam/weir to produce hydroelectricity or regulate the water level
- acting as a storm surge barrier to prevent areas from flooding

The first option comes to hand where the public water defences fail during a flooding. Individual households can anticipate on this by having an inflatable dam that they can lay around their house. An example is made from Texas. A man protected his house by laying an inflatable dam around its house, see figure B.1. This happened in 2016, when the Brazos river flooded.

Figure B.1: inflatable barrier during flooding homes [15]

The second option is extensively used in Japan and the Hydropower industry. The dams can span up to 100 m and with special membranes even 200 meter can be achieved. The dams for the Hydropower industry and water level regulation are much investigated. Inflatable gates at hydro power structures have generally worked well at passing ice and debris. The membrane also need to be designed so they can be in sunlight for many years. Ultraviolet light accelerates the aging of rubber. This has dramatically been experienced at the Tempe Town Lake Dam gates in Arizona that began to deteriorate after about 10 years under searing sun, until one of them failed and caused the emptying of the lake. They were provided with a sprinkling system for additional protection by extreme sun conditions. But for such frequent desert conditions at location in Arizona it would not suffice. Figure B.2 presents the situation shortly after the dam gate burst (a) and a detail of the sprinkling system (b). The temporary gates installed afterwards were partly put in shadow by a new constructed footbridge. The France uses protective layers and anti-abrasion jackets to extend lifetime.

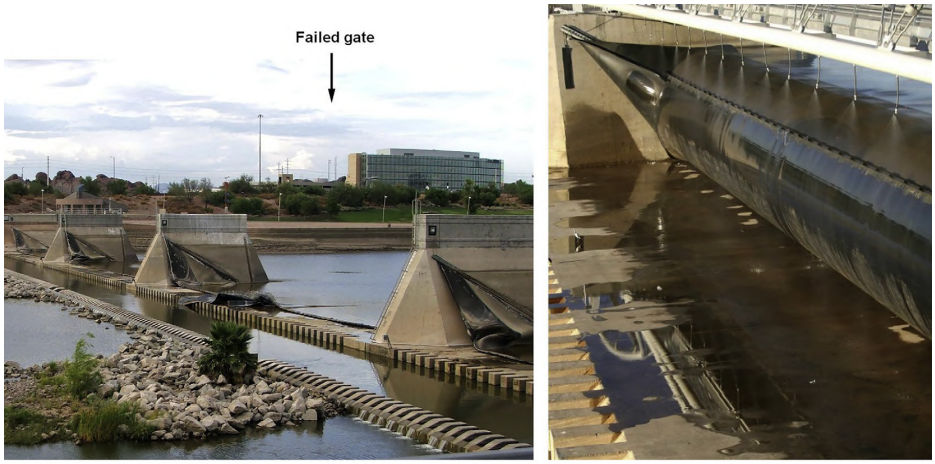

Figure B.2: Arizona inflatable dam [45]

The third option is the storm surge barrier. The most known one is the Ramspol barrier. It is also the biggest inflatable dam in the world. It protects the hinterland of the Netherlands from high storm conditions at the Ijsselmeer. The Ramspol Barrier project actually opened the market of large storm surge barriers to rubber gates in Europe. Outside Europe, a few smaller flood barriers, including the Japanese Naruse Barrier in Miyagi Prefecture, preceded it. In table B.1 some of the most pronounced inflatable dams are listed.

Dam site	Location	No. of gates × L (m) ×H (m)	Construction year	System—inflating (air/water)
Ramspol Barrier	Kampen, Netherlands	3 x 60.0 x 8.20	2002	water and air
Alés Dam	Gard, France	1 x 23.0 x 1.50	2002	air
Lechbruch Dam	Bavaria, Germany	3 x 45.83 x 1.10 1 x 24.75 x 3.15	2002	water
Kiebingen	Tubingen, Germany	2 x 23.0 x 3.40	1998	air
Wertach Dam	Tŕkheim, Germamy	2 x 16.0 x 3.70	1998	air
Marklendorf Weir	L. Saxony, Germany	2 x 23.6 x 2.20	2006	water
Bahnitz Dam	Brandenburg, Germany	2 x 30.3 x 2.40	2007	water
Bannetze Weir	L. Saxony, Germany	2 x 21.0 x 2.35	2009	water
Pocaply Dam	Czech Republic	1 x 21.0 x 1.60	1998	water
Naruse Barrier	Miyagi, Japan	3 x 42.1 x 2.30	1984	air
Kurotani Dam	Okayama, Japan	1 x 35.0 x 6.00	1990s	air
Huaihua Dam	Qingdao City, China	4 x ?	2012?	air
Coon Rapids	Minnesota, USA	2 x 96.0 x 2.4 $1\frac{1}{2}$ x 45.8 x 2.40	1990s	air
Tempe Town Lake	Arizona, USA	4 x 67.0 x 4.80	1999	air
Adam T. Bower	Pennsylvania, USA	6 x 91.4 x 2.44 1 x 57.0 x 2.44	1966, 1988	water and air, since 1988 only air
Highgate Falls	Vermont, USA	1 x 67.0 x 4.60	1994	air
Palmer Dam	New York, USA	Totally 105.4 x 1.83	2001	air, in two parts
Curtis Dam	New York, USA	3 x 63.6 x 1.20 1 x 20.4 X 2.10	2001	air
Rainbow Falls	Montana, USA	2 x 76.2 x 3.60	1992, 2013	air

Table B.1: inflatable rubber dam around the world [45]

The issue of heating up the bladder does not apply to the gates in high spillways, like the Highgate Falls dam shown in figure B.3 (a). This dam makes part of a 9.8 MW hydroelectric plant. Its rubber gate, manufactured by Bridgestone, regulates pool elevation. and is 4.6 m high and 67 m long (15 ft by 220 ft). The plant is owned by the village of Swanton, Vermont, on the Missisquoi River. The rubber gate at this facility is one of the tallest in

the United States and is accessible for inspection and maintenance at one side [45]. The Marklendorf Dam gates, one of which is shown in B.3, can be seen as examples of the recent revival of water-filled rubber gates. This dam act as weir that together with a similar weir at Bannetze controls the navigation conditions on the Aller River. Shortly after putting the rubber dams in operation, they vibration problems under high flows. The installation of flow breaking corbels in 2008 entirely removed this problem. These gates also form evidence that water filling can be applied in the areas of relatively cold winters, as the winter temperatures at this location can drop below -20°C [45].

Figure B.3: (a) Highgate falls dam, USA and (b) flow breaking corbels at Marklendorf Germany [45]

The two applications above represent respectively a hydroelectric plant and a river weir. A disadvantage of those application is that it will block fish migration upstream to river. As regard to this is, it is enough to mention that recent studies proved better performances of steel-rubber gates, which have a rubber bladder to lift the steel gate up and down see figure B.4.

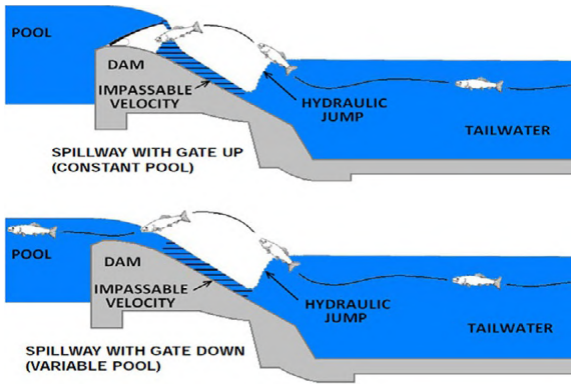

Figure B.4: Old Coon Rapids dam on the right vis passage [45]

Figure B.5: Memorial dam Pennsylvania

The Adam T. Bower Memorial Dam (formerly known as the Sunbury Fabridam) is the world's longest inflatable dam. The dam is located in Pennsylvania just below the confluence of the Western and Main Branches of the Susquehanna, between the towns of Shamokin Dam and Sunbury. The dam is in total 600 meter long and exists of 6 individual dam, see figure B.5. It is raised in the summer to create 12 km^2 Lake Augusta for recreation. The dam and lake are part of Shikellamy State Park.

India dams

The use of a rubber weir is a new concept in India, although more than 2000 inflatable dams already exists and over 10 manufacturers are available. India's first rubber dam was built in 2006 on Janjavati River as a replacement of a gate. Construction of Jhanjavati rubber dam was completed in six months. Erection is simple, less maintenance cost and operation is automatic as well as manual. Later two rubber dams were built in the Musi river in the city of Hyderabad. It was done under the project of Musi River Beautification Project. These two rubber dams presently are not operational because of lack of fresh water in Musi River. To give more flexibility in release and control of water flow across the streams in watershed management, research efforts were made at Directorate of Water Management. Another rubber dam was built for the purpose of irrigation management, which is called Chandeswer-I Kurda Orissa. The reason for using rubber dams is that capital costs is less than concrete dams. The operation of rubber dam is easy and farmers friendly. Details of the rubber dams are given in table B.2 and figure B.6.

Name of site	River	Purpose	H x L	year
21.1 km RD-High Court Hyderabad	Musi River	River management	1.35 x 80.0	2008
22.1 KM RD-Salar Jung Museum Hyderabad	Musi River	River management	1.30 x 73.0	2008
Janjhavathi-Andhra Pradesh	Janjhavati	Irrigation	3.3 x (2x30.0)	2005

Table B.2: India rubber dam

Figure B.6: India rubber dam [58]

C

Design weir Grave

This appendix covers the sub parts for the design process of the inflatable weir at location Grave.

C.1. Steel weirs

Type of steel overflow weirs which can replace the existing weir at Grave are described here. Those weirs are not further included in the design process, but are only described for the reason knowing that they exist. There are five types of steel weirs considered. Flap gates are not considered a feasible design solutions. They require a recess chamber, which is not part of the design of the existing weirs. This will cost extra money to build them. This holds also for the radial gate and sector gate. Drum gates and bear-trap gates are also not applicable, because their maximum height is up to 4.0 m, which is less than the existing weirs in the Meuse.

Flap gates

In open state the flap gate rests on sill. A hoisting mechanism lifts the flap against the water pressure upwards. They can up to 50 m if belly shape is applied like in the figure C.1

Radial gates

The radial or curvature gate is designed such that the resultant force of the water pressure head pass through the rotation axis. This causes the bending moment to be zero and the gate has no tendency to open or close. Flap gates can be mounted on top, which are rotated horizontally in open state. In this ways the sill depth can be reduced.

Sector gates

The sector gates has a skin plate in front of the gate and on top the gate. During closing the skin plate on top closes the recess chamber. The gate operates by subsiding into the recess chamber, due to in- and outflow of water to the recess chamber. With adjusting the inside water pressure, the desired height can be achieved. The height of sector gates is limited to 8 m and the width is theoretically unlimited

Drum gates

Regulation is done by water pressure inside the recess chamber, the same as for the sector gated. The rotation point of the gate is located upstream.

Bear-trap gates

The bear trap gate looks like an inverted V in closed position. The plates are pushed upwards by internal pressure. The mechanism of the bear trap grate makes it possible, to make the recess chamber less deep, than for sector- and drum gates. In open position the flat parts are on top of each other. The disadvantage of the weir is that a larger pressure is needed than the upstream water pressure, therefore a separate pump is needed to initiate the upward motion.

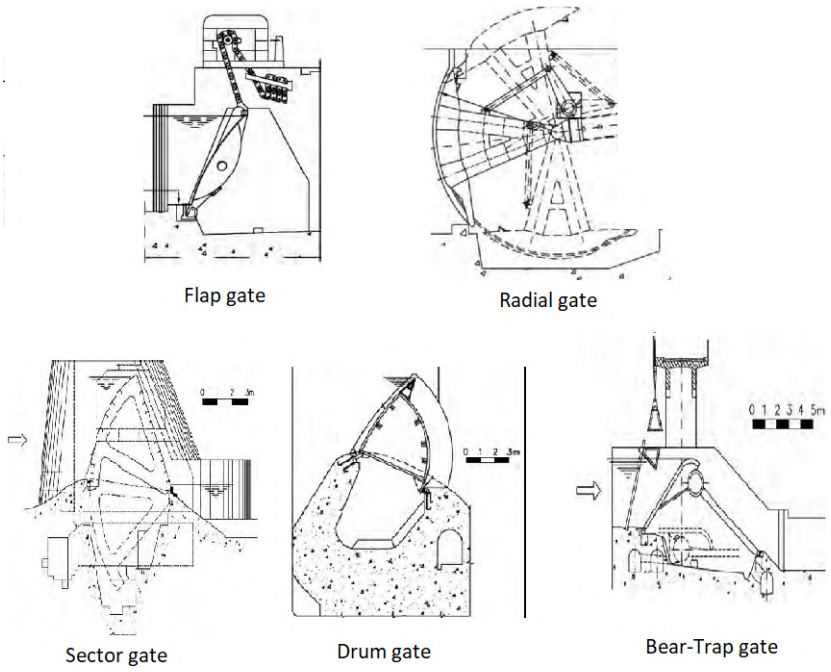

Figure C.1: steel gate types [42]

C.2. Inflatable weir designs

In this section the alternative inflatable weir design are presented and the made multi criteria analysis (MCA) used for the decision of the conceptual design. The designs presented here were the alternatives in the MCA and are not further used in the research.

Design strategies

Further the design possibilities are enhanced, by applying one or more design strategies to the design option. In this case to anticipate on a ship collision. The aim is to reduce the risk of a ship collision accident. This can be done by reducing the probability of ship collision and the consequences of a collision. The risk reducing of the event of ship collision is a high important factor in the design. The designs given below are therefore based to reduce the risk of ship collision. The follow strategies have been set out to pursue appropriate designs for in this case ship collision [4]:

1. Preventing ship collision of occurring or reducing the probability of ship collision or the magnitude of it
2. Protecting the inflatable weir against ship collision
3. Design the inflatable weir that not the whole weir or an important part will fail
4. Design the key elements of the inflatable weir on which it is reliant with extra care
5. Applying design rules which provide a robust weir in normal circumstances

Compartments

This design is based on damage mitigation during accidents and robustness of the inflatable weir. The design is comparably with the standard design of the inflatable weir shown above, only the weir chamber is compartmentalized in multiple chambers. To do this a membrane sheet with the circumferential dimensions is tied up to the membrane. It can be chosen how much length spans one chamber, based on the design needs. A reasonable distance would be around 10 meters in this research of ship collision, since most ships on the Meuse span around 10 meter width. In case of a ship collision one (maximum two chambers) will fail, instead of the whole span. This design is proposed in another research as well [1]. In that case the design was for floating inflatable barriers on sea against ship collision. The conclusion said that the design is good for dissipating the kinetic energy of the ship and deceleration and instability of the ship.

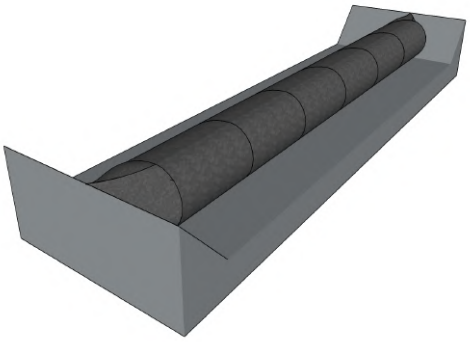

Figure C.2: compartment design

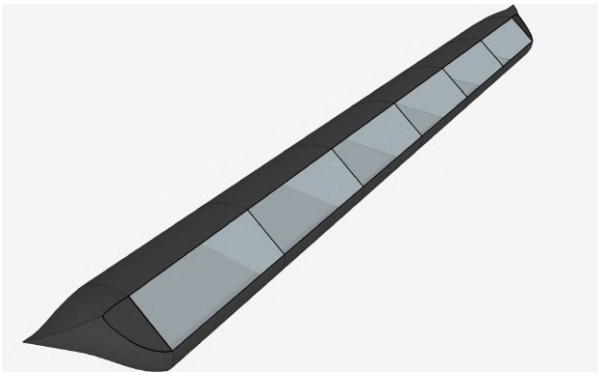

Figure C.3: compartment design section cut

Three dams

The three dam design is upon the assumption a ship collision will be head on guided towards the middle of the weir. Only the balloon in the middle can fail with a larger span still standing. The problem which then arise is a large water flow sucked into the middle of the weir. Extra measures for the bottom protection should be probably needed to prevent erosion. Work on this has been done in another thesis by van Oorschot [16]. Simple calculation if the bottom protection suffices is elaborated in 4.6. There is another advantage on this design based on the assumption of collision on the balloon. There is a decent probability the ship glides over the inflatable balloon and the propeller cuts the sheet. Only the balloon fails in that case. Separation of the inflatable weir is based on the designs in master thesis of Breukelen [38]. Although the reason there was doing it for dealing with the long span. The leakage calculated the that thesis is considerable and can be problematic in this weir design.

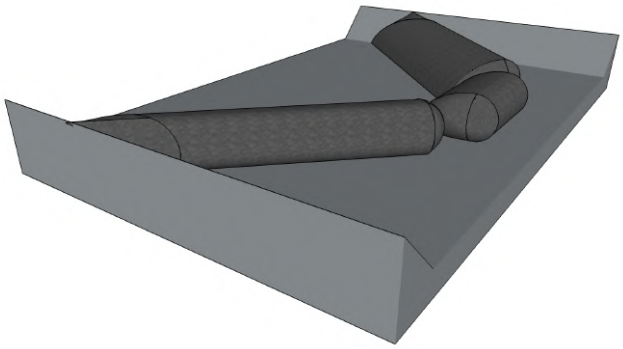

Figure C.4: three dams design

Round design

The round design is based on another weir design that uses a bridge as suspension. The reference design is a concept from Vrijling, who thought of a weir that is made of rubber and has round shapes. The round shape gives a longer length to the weir to span the width. A longer length can also be seen as more stretch the weir can handle. In case of a ship collision in the middle of the weir there is a larger absorption capacity of energy than the standard design, due to the higher stretch. However this longer weir brings higher cost with it and the construction of the clamping is more difficult in a round shape. In case of ship collision this design would be better, but this extra absorption advantage is considered not an overruling factor. A side effect that arises from the round shape is a circular overflow of the weir, a balancing of the overflow forces is enhanced this way. Resonance can have a likely milder effect in this design.

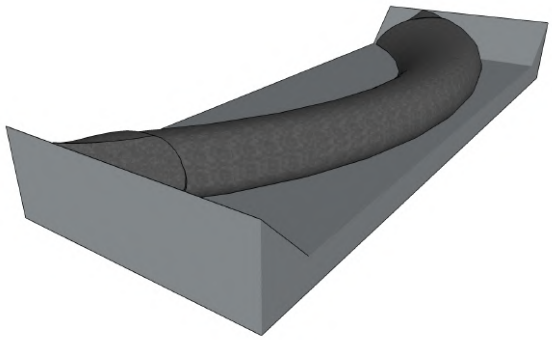

Figure C.5: design based on weir Vrijling [13]

C.2.1. Multi criteria analyses

If the criteria in the list row is more important than the criteria in the column for the corresponding cell a 1 is placed otherwise a 0. In the second last row the total score of the criteria is given. The last row divides the total score of the criteria by the total score of all criteria, this defines the weight factor of each criteria.

	A	B	C	D	E	F	G	Total	Weight factor
Construct ability A		1	0	0	0	1	1	3	3/21=0.14
Inflation ease B	0		1	0	0	1	1	3	3/21=0.14
Robustness C	1	0		0	0	1	0	2	2/21=0.1
Discharge leakage D	1	1	1		0	1	1	5	5/21=0.24
Reliability E	1	1	1	1		1	1	6	6/21=0.29
Maintenance F	0	0	0	0	0		1	1	1/21=0.05
Discharge efficiency G	0	0	1	0	0	0		1	1/21=0.05
Σ								21	1

Table C.1: mutual weight criteria

For each criteria a score is given to the design. How higher the score how better the design complies to the criteria. This is given in the table below. Then the score is multiplied by the weight factor, this gives a weighted score for each criteria per design. The total of the weighted score from each criteria per design is the total score. The highest score is the best out of the analysis

		Standard		Compartments		Three dams		Round	
	WF	Score	WF*score	Score	WF*score	Score	WF*score	Score	WF*score
Construct ability	0.14	9	1.26	7	0.98	5	0.7	6	0.84
Inflation ease	0.14	8	1.12	6	0.84	7	0.98	7	0.98
Robustness	0.1	6	0.6	9	0.9	8	0.8	8	0.8
Discharge leakage	0.24	7	1.68	7	1.68	4	0.96	7	1.68
Reliability	0.29	8	2.32	6	1.74	5	1.45	6	1.74
Maintenance	0.05	7	0.35	7	0.35	7	0.35	7	0.35
Discharge efficiency	0.05	7	0.35	7	0.35	8	0.4	9	0.45
Total			7.68		6.84		5.64		6.84

Table C.2: mutual weight criteria

C.3. Clamping

This section describes the possible clamping lines that can be used. There are multiple options to clamp the sheet to the foundation bottom. The clamping method is also depended if the membrane is two- or one- sided clamped. With the chosen design in chapter 3, the membrane is single line clamped. In the years there have been developed multiple clamping systems. In figure C.6 the different kind of clamping systems can be seen.

The middle type is the most common for new projects. Within this type there can be many differences in angles, width, number of waves and the application of these waves. The type at the left of the figure (typ A) is called the 'dovetail technique' (in Dutch = zwaluwstaarttechniek). The sheet is thickened at the end such that a dovetail arises. Further the bolts connecting the sheet with the foundation do not penetrate the sheet. This system is developed by Obermeyer Hydro Inc (USA). As last there is the type on the right (typ C). This is a variant on typ B and can also be used.

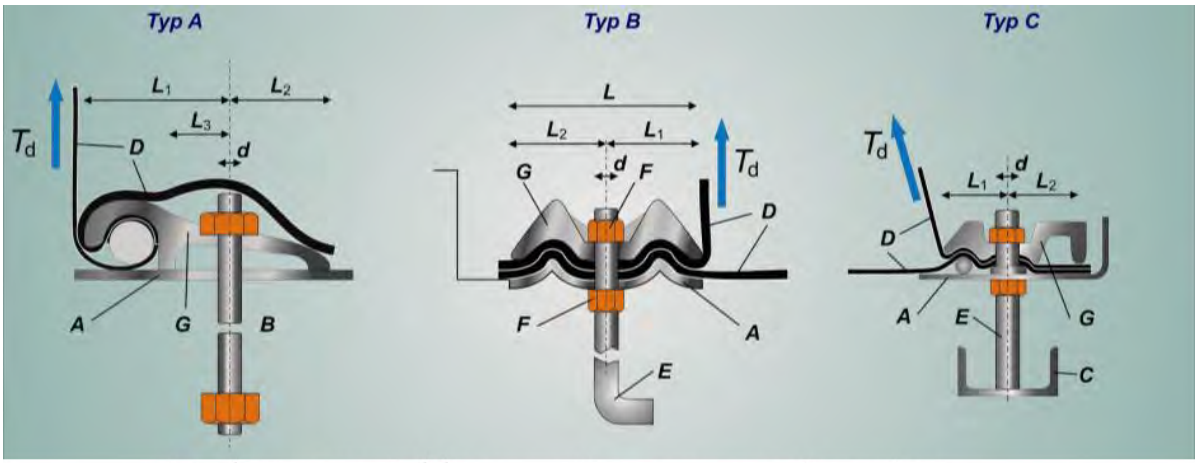

Figure C.6: three different clamping systems [65]

C.3.1. Verify strength clamping

Torquing is applied to the clamping system to pretension the rubber sheet. In this manner it ensures to create enough resistance between the clamping system and the rubber sheet. For the torque, there are differences between manufactures. If the system is only torqued in the beginning, eventually the pretension will be 50% of its starting value.

To test the applicability of the clamping system the behaviour of the rubber fabric is tested with regards to aging, degradation, creep and fatigue. There is no general guideline for this, it is up to the manufacturer to prove the applicability of the clamping system and set requirements. When the testing procedure is full filled, the clamping system can be implemented for mass-production. However when specific project requires changes in the design or extrapolation of the test results, additional testing is recommended. For Ramspol this was the case [37].

C.3.2. Abutment round design calculation

With the case having no abutments and giving the weir a circular shape at the edges will induce a leakage point. The circular shape creates a smaller leakage area then an ellipsoid shape. The amount of leakage by the circular shape is calculated in this section. First the area and centre of leakage point are defined as:

$$A_{leak} = \sum_{n=1}^{j} \frac{z_n y_n}{j} \tag{C.1}$$

where: A_{leak} = leakage area [m^2]
k = amount of area layers between H_{up} and H_{down} [-]
z_n = vertical coordinate of corresponding area layer [m]
y_n = width of corresponding area layer [m]

The vertical coordinate for the centre of gravity comes down to:

$$\overline{z} = \frac{\sum_{n=1}^{j} z_n y_n}{\sum_{n=1}^{j} y_n} \tag{C.2}$$

The width y_n can be found by:

$$y_n = z_n \cos\theta = z_n \cos\left(\sin^{-1}\frac{H_{up}}{R_w}\right) \tag{C.3}$$

For an overview see figure C.7.

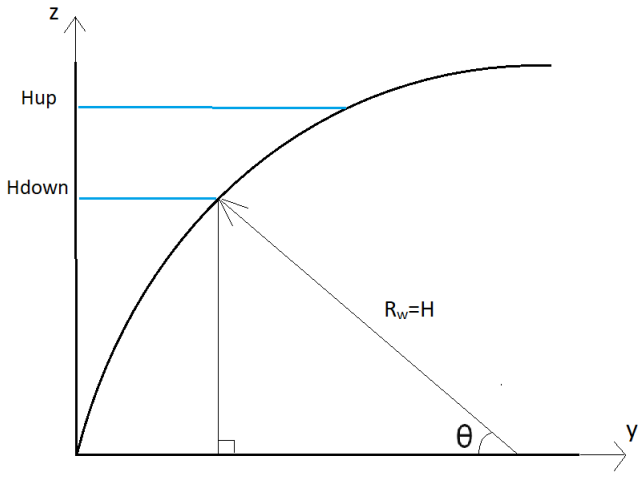

Figure C.7: geometry circular abutment

The discharge can be calculated with Bernoulli's law. It describes the total energy level at a certain cross-section. The assumption is made that there is no energy loss along the longitudinal way. The formula is described as follows:

$$\frac{v^2}{2g} + \overline{z} + \frac{p}{\rho g} = H_{energy} \tag{C.4}$$

As the pressure stays constant the formula reduces to and the velocity follows from:

$$\frac{v^2}{2g} + \overline{z} \longrightarrow v = \sqrt{2g\overline{z}} \tag{C.5}$$

Now the velocity and discharge is known, the discharge can be calculated with 2.3. The discharge per abutment is around 44 m^3/s times four is 176 m^3/s. This is around 16% of the limit discharge, which is a high number. For this reason the leakage is considered too big and not feasible for the design.

C.3.3. Bottom recess

There are (some) times during the year when the weir has to be (completely) deflated. In this case the bottom has to catch the sheet in a whole. The requirement is that the sheet won't fold when it is deflated. There are mainly two options for the bottom floor of an inflatable dam:

- guide rollers
- flat bottom

For a two side clamped inflatable storm surge barrier can be chosen to use guide rollers. These guide rollers are further explained in the appendix E of Ramspol. The guide rollers are not necessary for the inflatable weir at Grave. The inflatable weir at Grave will be one side clamped. When the membrane will be deflated, the flow of the river will do the rest of the work. It pushes the sheet downstream of the river and to the bottom of the foundation as is shown in figure 3.11. So keeping the foundation as bottom recess is efficient for the design of the inflatable weir at Grave.

D

Shape membrane

A theory is derived to get to the shape of the membrane, based on equilibrium of forces. The theory is described by Parbery in his paper, where the work continues on the work of Harrison [47] [17]. Parbery states that the solution of Harrison can be applied for most practical cases [47]. Harrison method is also applied for the barrier at Ramspol. Harrison method has however some constraints. First the equilibrium position may not be unique and second the method needs to be modified in load situation the membrane lays flat at either or both clamping points.

The theory describes the membrane shapes such that there is force equilibrium between internal pressure, outside load, self weight and the axial tensile forces in the sheet. For the theory of the shape of the membrane, the inflated state is used. In the deflated state there is theoretically no force transfer and the sheet lays on the bottom. In the inflated state external forces will be transferred by tensile forces in the membrane to the foundation. The shear forces and moments can be neglected in the equilibrium, since the thickness of the sheet is very thin compared to the size of the membrane. To find the shape of the membrane, the sheet is divided in a finite number of element where the force equilibrium has to be satisfied. An overview of the forces on a small element in figure D.1.

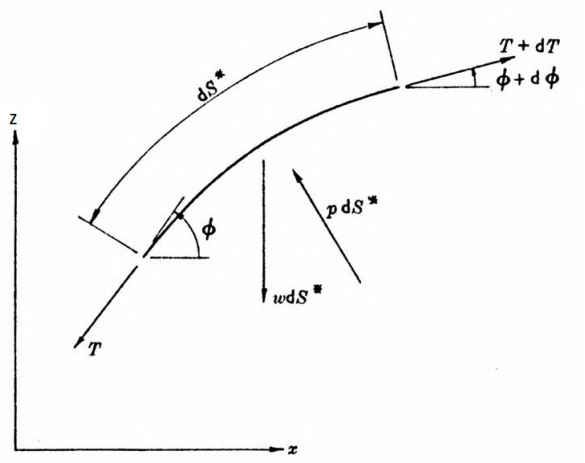

Figure D.1: force equilibrium element [47]

By considering the limit case of an infinitely small sheet element $dS^* \rightarrow 0$, the tensile forces are defined as follow. tangential direction (in direction of the sheet):

$$dT = w dS^* \sin\phi \tag{D.1}$$

where: T = membrane force in axial direction [N]
w = self weight sheet [N/m]
S^* = length of sheet in loaded state [m]
ϕ = angle between horizontal and interface sheet [°]

radial direction (perpendicular to the sheet):

$$-Td\phi = pdS^* - w\cos\phi dS^* \tag{D.2}$$

By assuming the self weight is zero follows that the variation of the tensile force is also zero over the small element. The law of Hooke describes the elongation of the uniform material by the pressure-strain relationship.(By solving for dS*, T and determining E, the elongation dS can be calculated:

$$\frac{dS^*}{dS} = \frac{1}{E}\left(\frac{T}{\delta t}\right) + 1 \tag{D.3}$$

where: S = length of sheet in unloaded state [m]
E = elastic modulus of sheet [N/m^2]
δt = thickness of membrane [m]

The curvature of the membrane is given by:

$$\kappa = \frac{1}{R_n} = -\frac{d\phi}{dS^*} = \frac{p - w\cos\phi}{T} \tag{D.4}$$

where: κ = curvature of sheet [1/m]
R_n = radius of membrane [m]

By taking the weight of the membrane as negligible, the curvature equation ($\frac{d\phi}{dS^*}$) is reduced to and the horizontal 'x' and vertical coordinate 'z' are defined by (curvature is positive by bulging to the outside):

$$\frac{d\phi}{dS^*} = \frac{p}{T} \tag{D.5}$$

$$\frac{dx}{dS^*} = \cos\phi \tag{D.6}$$

$$\frac{dz}{dS^*} = \sin\phi \tag{D.7}$$

The geometrical boundary conditions for the two line clamped system can be defined by, noting that the circumferential length is L and the base width is B_m:

$$\begin{aligned} S = 0: &\quad x = 0,\ z = 0 \\ S = L: &\quad x = B_m,\ z = 0 \end{aligned} \tag{D.8}$$

In the case of the one line clamped weir a certain length lays on the bottom of the floor, because it is pushed down from the upstream side. The boundary conditions for S=L can then be replaced by, where the length (L) is reduced by the unstretched length on the bottom of the foundation.

$$S = L - A_m/(1+\epsilon): \quad x = A_m/(1+\epsilon)\ ,\ z = 0\ ,\ \frac{d\phi}{dS^*} = 0 \tag{D.9}$$

Where 'A_m' is the stretched length that lays unstretched on the bottom. The change in angle has to be zero in order to have also a zero change in z-coordinate, see equations D.5 and D.7.

The origin of the coordinate system has to be defined first to calculate the corresponding coordinates of the elements. The origin of the coordinate system is taken at the clamping point, see figure D.2. It is presumed that the internal pressure and length of the sheet is known. From the origin there are two unknowns 'T' and 'ϕ', which are initially guessed. Then the coordinates of the first element is calculated and so on, until a shape is formed. The shape has to satisfy the boundary conditions D.8, otherwise a new guess is taken for the two

unknowns. Another option is to take the formulas from recent literature to determine the internal pressure 'p' and tensile force 'T' [37], see below.

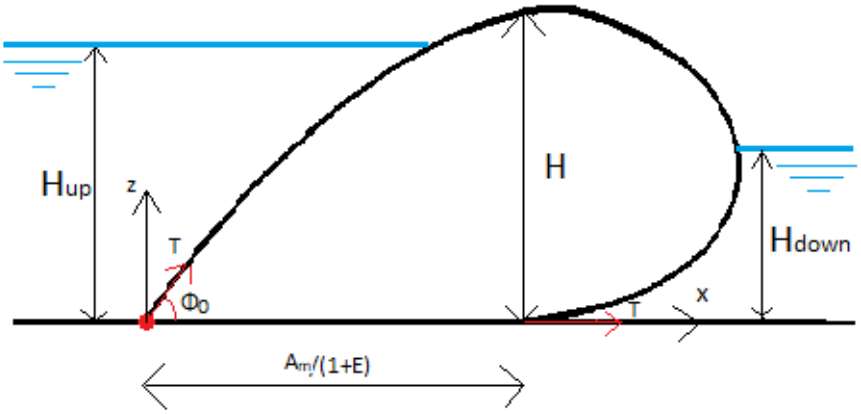

Figure D.2: one and two side clamped with overview parameters

D.1. Length sheet

To determine the length of the sheet in circumferential length some considerations are made. For an one clamped membrane with air filled the smallest circumference length would be πh_d in unloaded state, see figure D.3. Normally the membrane is loaded and the membrane will deform. A high internal pressure compared to the external pressure and high strain stiffness will cause low deformation. However in most cases the internals pressure and external pressure are more in balance. In practice the circumference length will more be like:

$$L = 4H \tag{D.10}$$

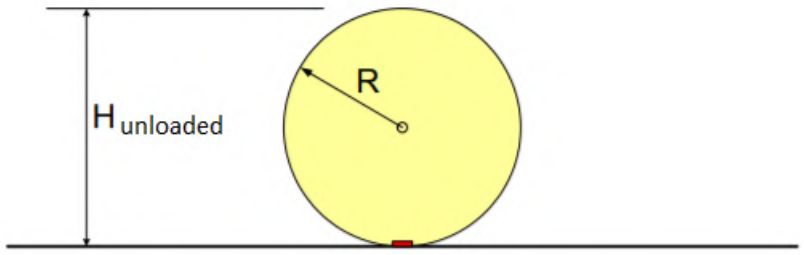

Figure D.3: shape unloaded state no disturbances [62]

D.2. Neglecting self weight

By substituting equation D.7 into equation D.1 and integrating gives the tensile force by:

$$T_w = T + wz \tag{D.11}$$

With this equation it is shown that the self weight is included in the tensile force. The following demonstrates that the self weight can be neglected. Taking the maximum height, self weight and tensile force of the inflatable weir at Grave:
z_{max} = 5.3 [m]
w = 1.09 [kN/m^2] [5]
T = 138 [kN] Gives a relative significance of the self weight:
$5.3 * 1.09/138 = 0,042$ is around 4.2%. That is an acceptable limit to neglect the self weight of the membrane.

D.3. Validation parameters

The shape of the bladder has extensively been investigated in Germany under the conditions presumed here (upper pool pressure over the whole height, no overtop, lower pool dry). The investigations covered FEM analyses (using the ABAQUS software), physical modelling and analytical computing. The bladder geometry was determined for a range of coefficients α varying from slightly above 1.0 to nearly 2.0. Figure D.4 presents global shapes that have been determined for four of these coefficients. The correlation between the results of all the three investigation methods was very good for medium and high values of α and fair for low values of α. These results and the formulas mentioned here offer support in initial design of rubber gates [45].

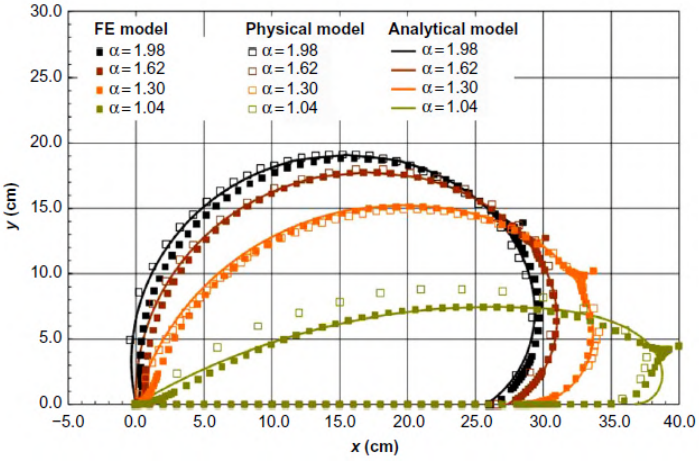

Figure D.4: verification α with models [45]

D.4. Research shape

The shape of a circle is found with the equations D.5, D.6 and D.7. For the circular shape the same height is assumed as the weir at Grave. The initial condition tensile force is determined with D.11 and the initial angle is logically π. The internals pressure is determined from equation 3.3. According to the theory, the length of the sheet should be the circumference of a circle πH.

Parameter	-	value	unit
Design height	H	5.3	m
Internal pressure	p_{in}	53	$\frac{kN}{m}$
Tensile force	T	138	kN
Initial angle	ϕ_0	π	rad
Length sheet	L	16.65	m

Table D.1: parameters

A sheet is taken of 25 meter and divided into 1000 pieces. So 1 piece is 2.5 cm, which is almost a tenth of a percent of the sheet length. Between the piece lengths nodes are situate, wherefore the coordinates are calculated. The circular shape that will be is found looks like figure D.5. It is shown the maximum height is 5.2 m, what is 10 cm lower than the prescribed height. This deviation is not that significant. The length of the sheet can be found by multiplying the number of elements used to get the circular shape times the stretched length of an element dividing by the strain ($n^*dS^*/(1+\epsilon)$). The sheet length that is found for the circular shape is 15.22 m. The height gives a small deviation around 2% from the desired value and the length of around 9%. Although the theory is not completely perfect it comes close to the desired shape.

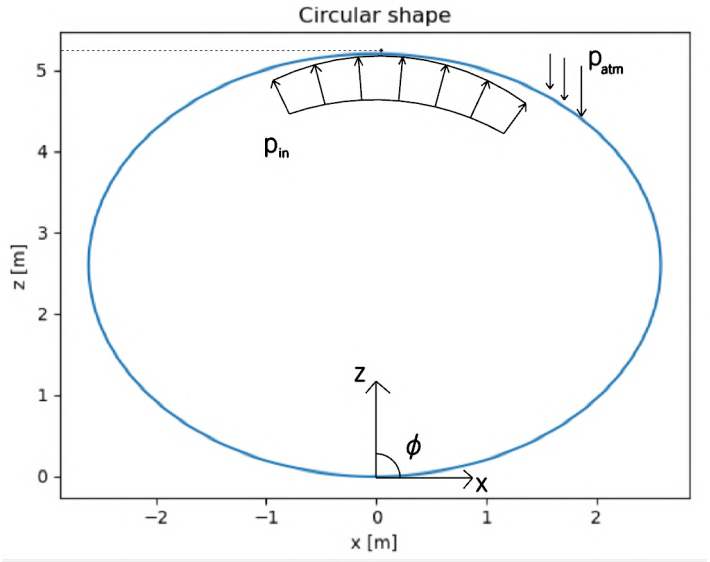

Figure D.5: circular shape membrane

An optimization is tried to make for the inflatable weir shape at Grave. The tensile force is varied between 90 kN and 190 kN and the initial angle between 0 and π. Both are varied with 100 substeps, this creates substeps for the tensile force 1 kN and the initial angle 0.031 rad (1.8°). For every combination a shape is found. The shape that satisfies the following conditions is plotted:

- sheet length is 5% longer or shorter than desired length
- membrane height is 10% higher or lower than desired height
- endpoint x-coordinate is equal or less than desired height

The following shapes are found in figure D.6 and table D.2. It is remarkable that the x-coordinate at the endpoint comes close to the desired membrane height. It can be said that based on this observance a large part of the inflatable weir will lay on the bottom. Besides the shape which comes closest to the desired membrane height also has the tensile force that comes closest to the calculated tensile force.

Tensile force [kN]	Initial angle [rad]	Length sheet [m]	Endpoint [m]	Height [m]
156.0	1.59	19.61	5.14	5.6
156.0	1.63	19.62	4.92	5.69
156.0	1.66	19.63	4.68	5.79
157.0	1.59	19.71	5.18	5.62
157.0	1.63	19.72	4.97	5.71
157.0	1.66	19.73	4.73	5.81
158.0	1.59	19.8	5.23	5.64
158.0	1.63	19.81	5.01	5.73
158.0	1.66	19.82	4.77	5.83
159.0	1.59	19.9	5.28	5.66
159.0	1.63	19.91	5.06	5.75
160.0	1.63	20.01	5.11	5.77
161.0	1.63	20.1	5.15	5.8
162.0	1.63	20.2	5.2	5.82

Table D.2: values optimization shape

The graphs shown in figure D.7, D.8 and D.9 give a representation of the shape membrane study in figure D.6. It calculates a corresponding parameter to that shape of the membrane. It can be seen that there is a transition line from around 2.1 ϕ_0 upward. From this line to the right of the graph the shape becomes instable and for example spiral endlessly.

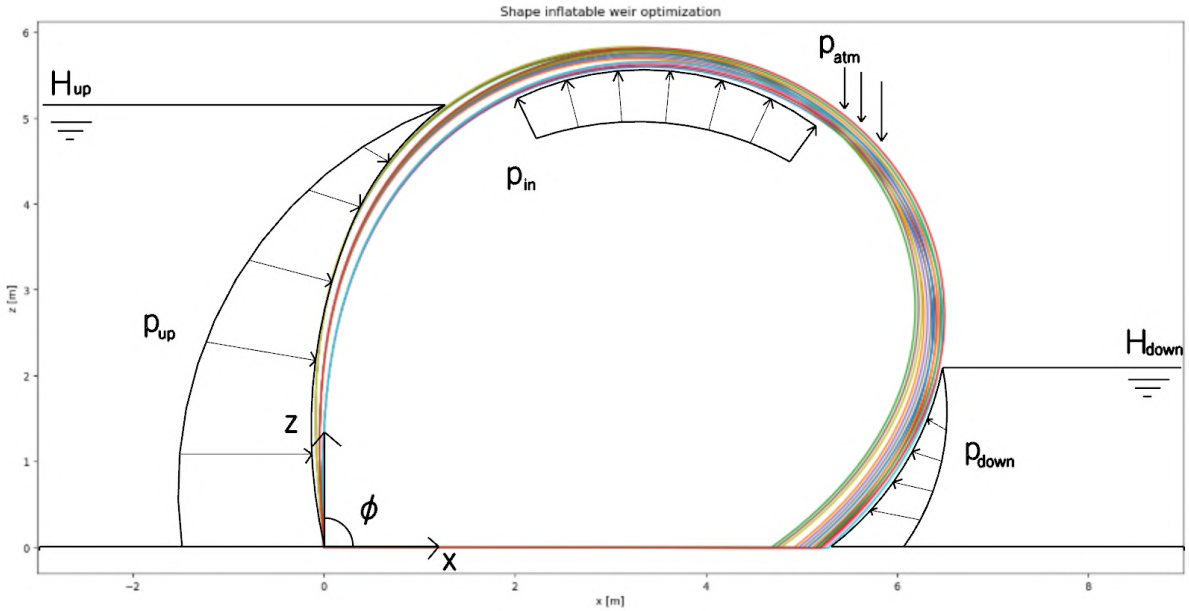

Figure D.6: shape inflatable weir Grave

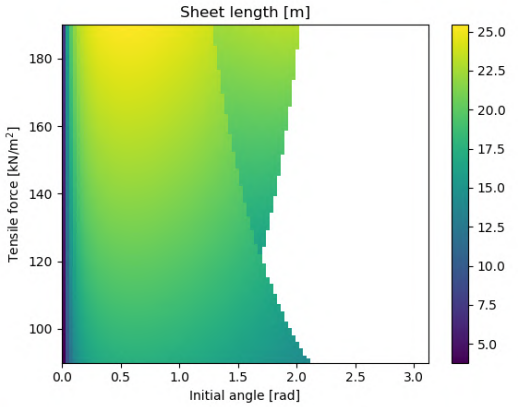

Figure D.7: sheet length

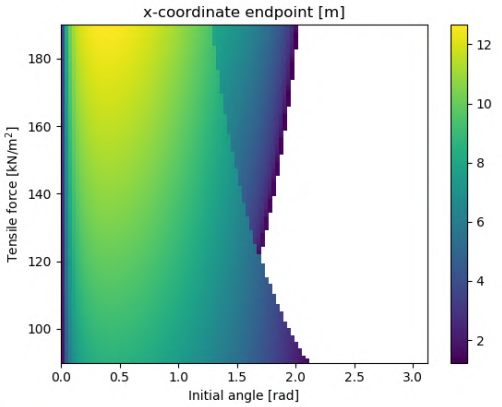

Figure D.8: x-coordinate endpoint

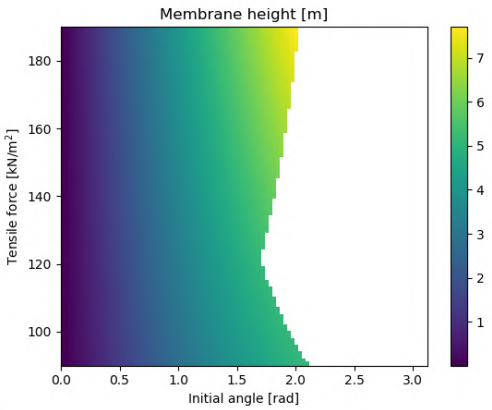

Figure D.9: membrane height

D.5. Dynamic shape

In practice the membrane will not completely act as an static structure. The membrane will vibrate as function of the dynamic forces applied. This can be waves or overflow of the weir for example. For the dynamic shape of the membrane equations of motions need to be derived. The new problem with the dynamic shape is that the system changes from a linear to a non-linear system. The load and the dynamic properties are deformation dependent. Hsieh derived the following equation of motions, where the strain is considered negligible by the dynamic loading. The length dS is thus a comparable to dS^* in equations D.1 and D.2. Also the damping forces are not included in the calculation of Hsieh [24]. In tangential direction:

$$wdS\frac{\partial^2 v_t}{\partial t^2} = \left(T + T_D + \frac{\partial T_D}{\partial S}dS\right)\cos d\phi - (T + T_D) \tag{D.12}$$

In radial direction:

$$wdS\frac{\partial^2 v_w}{\partial t^2} = \left(T + T_D + \frac{\partial T_D}{\partial S}dS\right)\sin\frac{d\phi}{2} + (T + T_D)\sin\frac{d\phi}{2} + (q + p)dS \tag{D.13}$$

where: T = tensile membrane force by static load p [N/m]
T_D = tensile membrane force by dynamic load q [N/m]
q = resulting dynamic pressure on the sheet [N/m]

The tensile force varies as consequence of the dynamic pressure q, and the dynamic pressure q varies also as a function of time and space along the bellow circumference. When taking the limit case. This implies dS→0, the following holds for when taking the Taylor expansion:

- $\cos d\phi \approx 1$
- $\sin d\phi \approx d\phi/2$
- $\sin d\phi \approx d\phi/2$

Also noting that very small times very small can be taken as zero. This is the case for $d\phi dS$. Taking equation D.12 and D.13 and using the limit case, then those equations becomes. In tangential direction:

$$w\frac{\partial^2 v_t}{\partial t^2} = \frac{\partial T_D}{\partial S} \tag{D.14}$$

In radial direction:

$$w\frac{\partial^2 v_w}{\partial t^2} = T\frac{\partial \phi}{\partial S} + T_D\frac{\partial \phi}{\partial S} + (q + p) \tag{D.15}$$

The equilibrium of an element described with the equations above can be seen in figure D.10

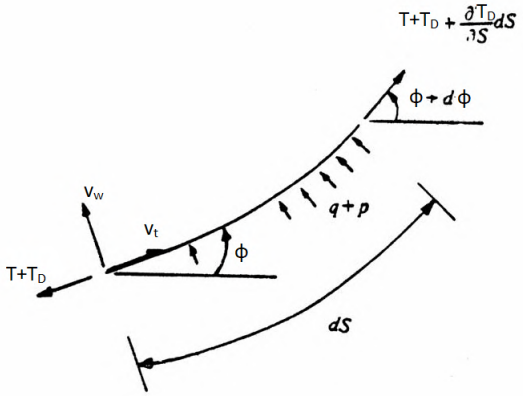

Figure D.10: equilibrium of element by dynamic forcing (adjusted [62])

The boundary conditions are formulated as follow for the dynamic shape:

$$\begin{aligned} S = 0: &\quad x = 0,\ y = 0,\ \frac{dx}{dt} = 0,\ \frac{dz}{dt} = 0 \\ S = L: &\quad x = A_m,\ y = 0,\ \frac{dx}{dt} = 0,\ \frac{dz}{dt} = 0 \end{aligned} \tag{D.16}$$

E

Ramspol

E.1. Collision probability

In figure E.1 the failure probabilities of different events are given for the Ramspol barrier. Ship collision is one of them, which is significantly from the graphs.

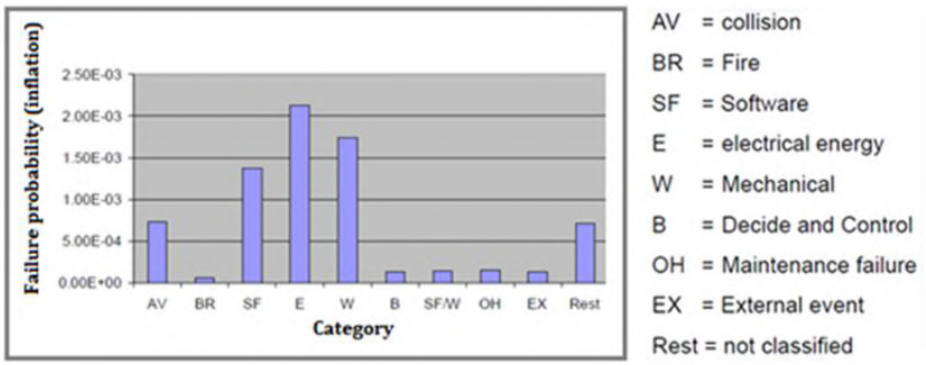

Figure E.1: probability collision Ramspol [38]

E.2. Ship navigation

In Ramspol the data that is available for ship navigation through Ramspol is from 1995. Based on the data from then two prognoses were made for the year 2020. Assuming the prognoses with the most shipment at Ramspol is given by figure E.2 last column [21, p. 42].

		Aantallen schepen			
	1995	2010		2020	
klasse		autonome ontw	TIB	TIB	Geregion. TIB
0	400	<50	<50	<50	<50
I	1.600	200	200	300	300
II	1.800	600	600	700	800
III	900	2.000	2.100	2.300	2.700
IV	300	1.000	1.000	1.200	1.400
Va	100	300	300	300	400
totaal	5.200	4.200	4.200	4.800	5.600
tonnen * mln.	0,9	1,2	1,2	1,4	1,6

Figure E.2: shipment Ramspol estimation [21]

E.3. Sheet material

For Ramspol five fiber materials were tested to apply for the sheet see table E.1 .

Abbreviation	Material	Tensile strength [MPa]	Elongation at break [%]
PP	Polypropeen	600	20
PA6	Polyamide 6 (Nylon)	900	20
PES	Polyester	1100	13
ARA	Aramid	2900	3.6
DYN	Dyneema®	3000	3.6

Table E.1: membrane material properties [38, p. 28]

Also the material POM (polyacetaal) was considered to use as a sheet, but this was not applicable below 5 C°. At Ramspol it is chosen to use Nylon fabrics as reinforcement material, that is layered in a matrix form. The inner layer is made of two thick layers of Nylon which spans the circumferential direction. The layer round it is made of two small layers on both side which spans the longitudinal direction. The cover layer consists of a rubber material, see figure 3.17 for clarification.

E.4. Joints rubber sheet

The manufacturing of the Ramspol barrier sheet is done with joints in between the longitudinal direction. In that time the manufacturer for the sheet was located in Japan. There were two manufacturers: Sumitomo and Bridgestone. Both manufacturers vulcanize the rubber sheet. The difference was that Sumitomo produces the whole sheet in one time and Bridgestone does it in separate strips and later vulcanizes the strips together. See figure E.3

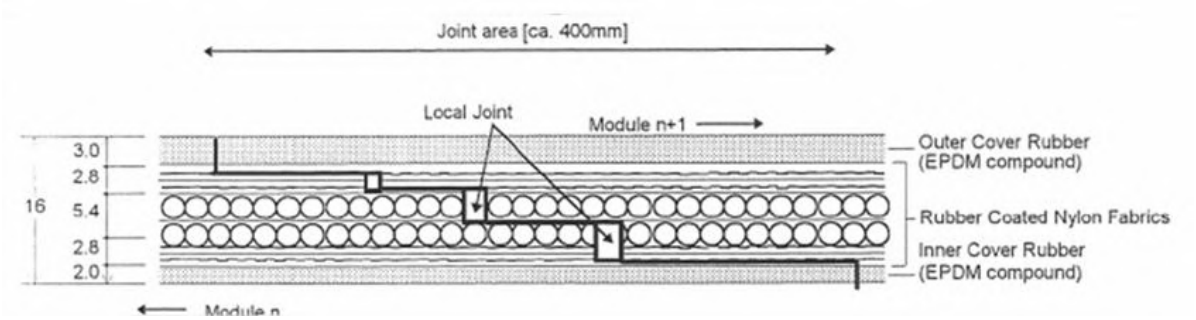

Figure E.3: joints in sheet Ramspol [54]

It was demonstrated that these joints would not significantly influences the strength of the sheet. The combination having low chance of stress concentration and smaller forces are present due to the less fibres in the joint.

E.5. Abutment clamping

The unfavourable effect of the inclined membrane is that high peak stresses develop at the folds, see figure E.9. The folds needs to be small to prevent leakage. In order to do so, the excess length should be distributed over the whole slope. This can be done by making the restraining lines stepped. the restraining lines need also an smooth transitions to the side slopes, see figure E.4.

Several options were developed to clamp the overlength. Finally a stepwise clamping system was used to evenly distribute the sheet. The clamping structure is called the 'Small Wave clamp', see figure E.4. The clamping length for the Ramspol barrier should be 1.27 times longer to clamp the overlength of the sheet. The stepwise clamping at the abutments causes forced strains and stresses [38]. M. van Breukelen proposed a new clamping geometry to reduce the peak stresses. The clamping lines should be straight and with ellipsoid shape [38, p. 68].

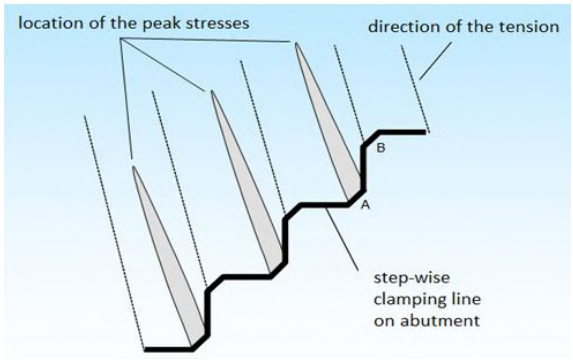

Figure E.4: stepwise clamping with abutments [38]

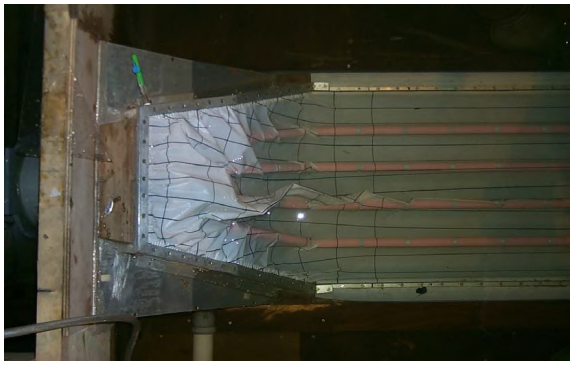

Figure E.5: folds two side clamped [62]

E.6. Foundation

The foundation at Ramspol are made of inclined piles [28], see figure E.6.

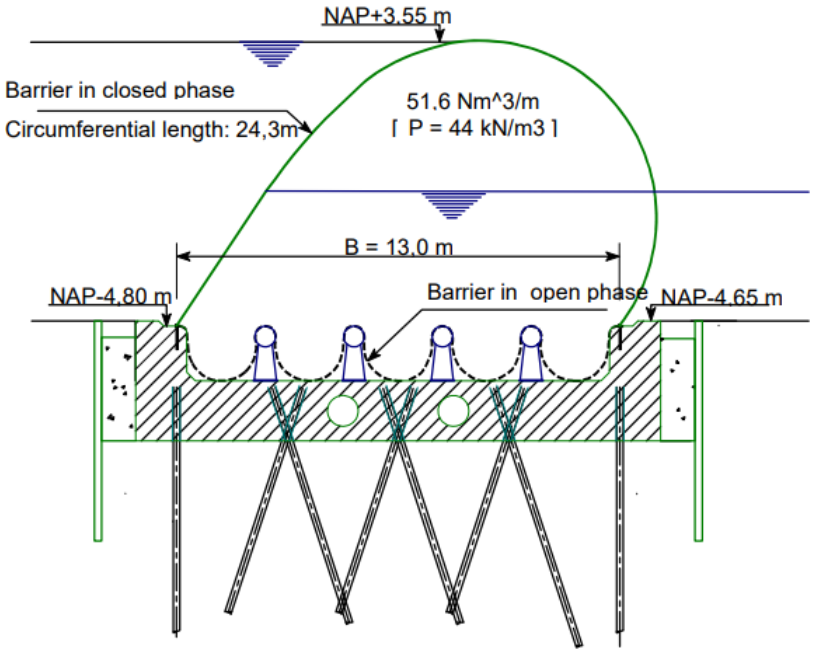

Figure E.6: cross section with foundation Ramspol [28]

In horizontal loading it can take more load than vertical piles. And the piles are already symmetric constructed. However for the weir water has to be retained only from one side. So it is not needed to place the piles in inclined for both sides. It is construction wise more reasonable to make the foundation with vertical piles.

Foundation floor

In tests of Delft hydraulics the guide rollers were tested for different set-ups. From the experiments it was chosen to make 4 rollers in the bottom recess and no rollers on the abutments[38], see figure E.7.

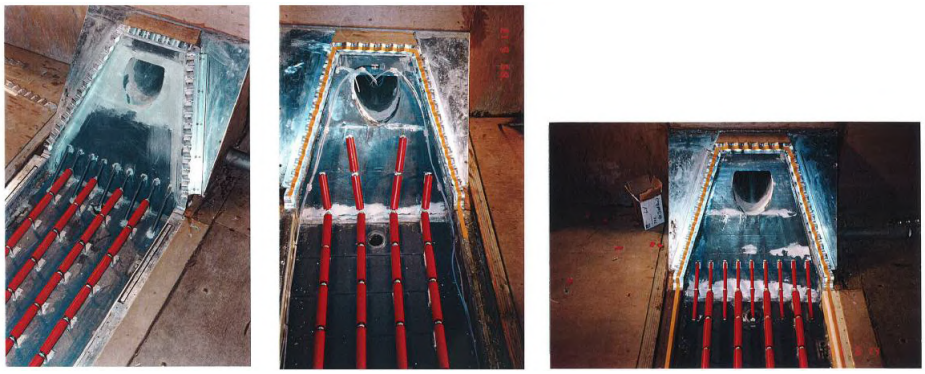

Figure E.7: scale model guide rollers [62]

The advantage of the guide rollers is that the roller can suck on by one the sheet towards itself. By determining the fitting size of the sheet to fit in the bin with guide rollers, almost no bulges form. With an air filled membrane this method failed, this was solved by using rollers in the guidance so that friction forces were reduced significantly [62, p. 7-8]. The second option is to use a sunk bottom. This can be used for a one-sided clamped membrane and the water is flowing from one side, which is the case in the Meuse. However with high flow velocities and waves, the deflated sheet can flap on the bottom. This has to be researched, if it has influence on the sheet quality, see figure E.8

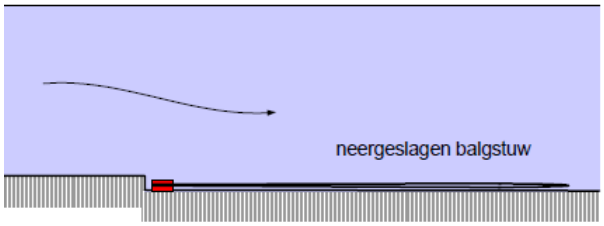

Figure E.8: deflated membrane with sunk bottom [62]

E.7. Folds

The approach in appendix D is most suitable to get an idea of the shape in the middle section of the membrane. Getting closer to the abutments, the shape is more influenced by the inclination of the abutments. The change of the slope will induce folds in the membrane, see figure E.9. In the figure the abutment is shown that is used for the inflatable storm surge barrier at Ramspol on the left. On the right a numerical model is set up to indicate the folds. At those folds high peak stresses develop, which is a critical point of the design. This knowledge should be taken in mind, when only focusing on the cross section. For the design of the weir in the Meuse the cross section model is given in chapter 3 and the numerical model in 5.

Figure E.9: fold with high peak stresses at Ramspol [38]

E.8. Tensile strength

For the Ramspol barrier a different approach was used to determine the strength of the sheet, than in Japan. The tensile strength is determined by the following formula:

$$\frac{R_t SCF_{\text{test}}}{\gamma_{\text{mat}}} > \gamma_{dyn} F_{\text{stat}} SCF \tag{E.1}$$

where: R_t = strength of the rubber sheet [N/m]
T = static membrane force for a two dimensional cross section [N/m]
γ_{mat} = material factor [-]
γ_{dyn} = dynamic coefficient [-]
γ_T = partial factor [-]
SCF = stress concentration factor [-]
SCF_{test} = stress concentration factor likely to have occurred during testing [-]

Since the middle of the sheet is most unlikely for stress concentration (most far away from abutments) the concentration factors SCF and SCF_{test} are said to be 1.0. The factors that are used for the sheet of Ramspol barrier are defined as follow:

	Middle section	Upstream side	Downstream side	Joints
γ_{mat}	1.3	1.3	1.2	1.2
γ_{dyn}	1.3	1.3	1.2	1.3
SCF	1.0	3.65	3.5	3.65
SCF_{test}	1.0	1.35	1.35	1.38
γ_T	1.05	1.0	1.0	1.0

Table E.2: factors design formula Ramspol

As can be seen from table E.2, the upstream side give the normative tensile strength. From the formula of equation E.1 and the upstream side factors a tensile strength of 4.6 times the tensile force inside the membrane is needed. In the strength of the sheet (R_t), the effects of fatigue loading, aging and relaxation is already included. Other factors that can be taken into accounts is creep, water absorption and clamping effect. The factors for the design strength are based on the following:

- The material factor is based on a semi probabilistic approach with: $\gamma_{mat} = e^{\alpha_R \beta V_R}$ and α_R=0.8, β=4.26 and V_R=0.05
- The dynamic component is based on the in- and deflation of the membrane and the wave force.
- The SCF is determined by the stress concentration at the folds, see figure E.9.
- The SCF_{test} is the ratio between external load and maximum sheet strength at tests.
- The partial factor is determined by the required probability of failure

The clamping is determined by full scale test. To represent the sheet, the following measures were taken: saturation (immersed) with water, aging by holding sheet in hot water, fatigue by loading sheet with design load, breaking by simulate the design storm [38].

E.9. Ansys macros

The modelling of the Ramspol barrier was also done in Ansys. The physical scale model of Delft Hydraulics fall short of representing all the geometric and material properties simultaneously. To quantify the shortcomings a computer model is developed to study the hydrodynamic aspects of the barrier. The model is a 2-dimensional slice perpendicular to the length axis of the barrier. That is suited to model the middle section of the barrier. The total modal consists of several parts written in ANSYS parametric design language. The parts are grouped according to their functionality. The calculations done are given below:

- Static: to determine geometric shape
- Model coupled fluid-structure: to determine the damped eigen frequencies of the barrier. The geometric shape of the static calculation is the basis for the coupling with fluid elements.
- Dynamic: The modal dynamic calculations are only used to determine at which frequencies barrier resonances can start. Shift of the frequencies due to non-linear behaviour is not taken into account.
- Transient coupled fluid-structure: to determine non-linear response of the barrier subject to a storm situation with irregular waves. The calculation are performed in the time-domain and all physical behaviour of the barrier can be described simultaneously. Every time step all conditions are updated.

The analyses for the last group are as follows: The wave spectrum is translated into a random time series of incident wave height. The repetition pattern of the time series is 4096, so about one hour of storm . To reach valid results the energy content is checked through the translated random time series of wave height and particle in accelerated generated waves. The calculation of the response of scale and prototype model after the particle acceleration is adapted for the correct energy content.

F

Ship collision model

F.1. Probability collision

In ship collision analysis there are a lot of variables to deal with. Some variables are not fully determined beforehand and they can be approached by an probabilistic manner. The ship velocity is of great importance in collision analysis. A first probabilistic calculation for determination of the ship velocity would use the characteristic velocity and multiply with a safety factor to achieve the design velocity [60]. The difference between the characteristic velocity and the design velocity lies in the safety factor, see figure F.1.

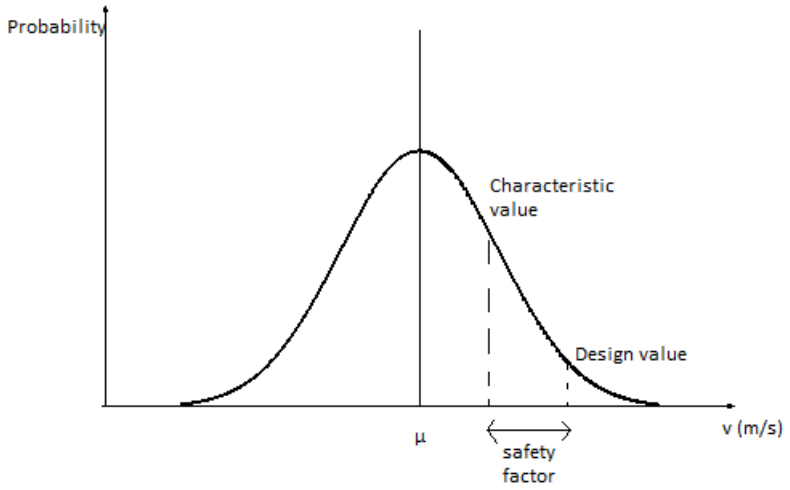

Figure F.1: velocity assumed as normal distribution

In some degree variables load and the material properties stay uncertain. A reliability method categorizes the degree of certainty in the approach. Four different levels are distinguished:

- Level 0: The method uses deterministic values for every parameter. Here no probability is involved.
- Level 1: The method makes use of semi-probabilistic values. This method is described above. It gives a first conservative estimate of a probabilistic manner. The method is widely used in codes.
- Level 2: This method use a probabilistic approach. Approximations are made to come to the stochastic parameters and modelled with a mean an standard deviation. Correlation coefficient give the dependence on mutual parameters
- Level 3: Makes use of full probabilistic approach. Commonly a Monte Carlo simulation is used for this level. The modelling is done by their joint distribution and numerically integrated to find the exact solution

- Level 4: This method also takes the consequences (costs) into account and risk (probability x consequences). Different designs can be considered with this method

For level I analysis partial safety factor are used as mention above. The partial safety factors are categorized into three consequence classes: low , medium and high. For this research a Level 0 approach is used to determine the ship collision impact. Although it can be interesting to investigate

F.1.1. Bayesian network

Studies have investigated the probability of ship collision through Bayesian Networks. These studies were done for waterways near or in a harbour. The Bayesian Network can take all parameters into account and end up with a probability number. To make such a network nodes and edges are defined. The nodes describe the events and the edges define the relations between the events. The events are conditionally dependent within the Bayesian network. The main factors, where events are based on, in ship collision are:

- The waterway system
- Involved ships
- Human factors

One of the recent studies has been done by Jansen [22]. He investigated ship collision in the Scheur at the port of Rotterdam. The study showed a probability of ship collision for one side of the quay as:

$$P_{collision} = 2.73e^{-6} \text{ [1/year/km]}$$

F.1.2. Simplified probability

A pragmatic way is to use a simplified model to identify the probability of ship collision in a waterway [7]. The Cumulative normal distribution for the deviation angle is used. In the normal circumstances the ship will navigate under the bridge. There is a possibility the shipper deviates from the straight line under the bridge, this is shown in figure F.2. For a range of deviation angles the shipper will hit the bridge pier, marked in black. For the case at Grave this argumentation can also be followed. The shipper is heading to the sluice, but has a low chance of choosing the wrong direction this is the deviation angle. An calculation can be made how great the probability is of collision, based on data.

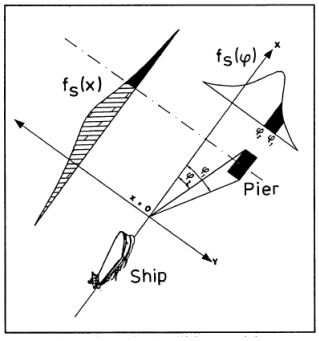

Figure F.2: probability collision [7]

F.2. Collision energy

The collision on a structure indicates an energy transfer from the moving object to the structure. Several guidelines are made to determine the energy that has to be transferred. The first form of this energy is defined as the kinetic energy. The approach was mentioned first by G. Leibniz and J. Bernoulli in formula form:

$$E_{kin} = \frac{1}{2} m_s v_s^2 \tag{F.1}$$

where: E_{kin} = kinetic energy of ship [Nm]
m_s = mass of the ship [kg]
v_s = velocity of the ship [m/s]

Later the coefficients effects where added by F. Vasco Costa (1973) and CETMEF. CETMEF is the French institute

for Inland and Maritime waterways, which contributes to the sustainability of the country. It provides services to the government of France and local authorities. One of the services is to give guidelines on protection of lock gates against ship collision. The approach described below is accepted universally, because the coefficients are customizable to the situation at hand. Also the approach is mentioned in the BS6349 (British Standard) and PIANC report 151 and is noted in the lecture notes of the course Hydraulic Structures [44], [39]. The new formula for the kinetic energy of ship collision is defined as:

$$E_{kin} = \frac{1}{2} m_s v_s^2 C_H C_E C_S C_C \tag{F.2}$$

where: E_{kin} = kinetic energy of ship [J]
m_s = mass of the ship [kg]
v_s = velocity of the ship [m/s]
C_H = hydrodynamic added mass [-]
C_E = yawing of the ship [-]
C_S = elasticity of the ship [-]
C_C = confinement factor [-]

The four coefficients describe side effect of the ship collision. The four coefficients are defined below.

Hydrodynamic added mass

The hydrodynamic mass takes the water moving along with the ship into account. In formula for the added mass is defined as, where m_w is the mass of the water:

$$C_H = \frac{m_s + m_w}{m_s} \tag{F.3}$$

To determine the mass of the water understanding is need of the water moving with the ship. The coefficient can be determined by experiment, numerical simulation or developed theories. One of the studies that gave an estimate of the added mass is done by Shigeru Ueda 1981. His studies were based on model tests and field experiments. The mass of the water moving with the ship is defined as:

$$m_w = \rho L_s D_s^2 \frac{\pi}{2} \tag{F.4}$$

combining F.3 and F.4 gives, where C_b is the block coefficient:

$$C_H = 1 + \frac{\pi D_s}{2 C_b B_s} \tag{F.5}$$

Another representation of the added mass coefficient is given by F. Vasco Costa 1964. This method is most common international standard.

$$C_H = 1 + \frac{2 D_s}{B_s} \tag{F.6}$$

Above determinations are formula based. Also studies has been done where the added mass is determined directly by giving the value of the coefficient. In practice 20% will be added to the kinetic energy to account for added mass [44]. In reality the added mass varies dependent on the hull of the ship and the impact duration.

In 1971 Motorora did physical model tests and hydrodynamic analysis to define the added mass for sway motion. The hydrodynamic added mass could vary between 0.4 and 1.3. The longer impact duration the high added mass [57]. For yaw motion the added mass Zhang and Pedersen found a value of 0.21 [59].

Softness coefficient

This coefficient takes into account the elasticity of the ship with regards to the structure. The ship hull can deform and absorb energy from the collision. However the inflatable weir is very flexible compared to the ship hull, so no energy will be absorbed. The coefficient is taken as 1.0.

Confinement coefficient

The confinement coefficient takes into account the water that is squeezed in between the ship and the structure and dissipates. For structure, where there is little space for the water to move, this coefficient plays a larger role. For the ship collision on the inflatable weir the contribution water can move freely away and the dissipation of energy is minor. The coefficient will be set to 1.0 in that case for a conservative approach.

Eccentricity factor

The eccentricity factor includes the effect of rotation of the ship, if the impact is under an angle. The impact under an angle is commonly happening at berthing facilities.

Eurocode

The Eurocode is the standard for European countries inside European Union. In paragraph 4.6 of the code the impact of ship collision is elaborated [12]. The paragraph deals with collision against solid structures in inland waterways. This means the energy is absorbed fully by the ship with elastic or plastic deformation. The Eurocode has a simpler formulation for the energy impact. It only adds hydrodynamic water mass to the equation, whereby two collision scenarios are defined:

- bow (head-on) impact gives added (hydrodynamic) water mass equal to 10% of the ship mass
- side impact gives added (hydrodynamic) water mass equal to 40% of the ship mass

So the basic equation F.1 for head-on collision changes to:

$$E_{kin} = \frac{1}{2} 1.1 m_s v_s^2 \tag{F.7}$$

Furthermore the Eurocode gives indicative values of the force for sea going ships. This values are excluded of dynamic analysis. The code divides the force into normal (F_{dx}) and perpendicular (F_{dy}) direction of travel. For inland going ships these values are determined, see figure F.3. figure F.1.

CEMT[a] Class	Reference type of ship	Length ℓ (m)	Mass m (ton)[b]	Force F_{dx}[c] (kN)	Force F_{dy}[c] (kN)
I		30-50	200-400	2 000	1 000
II		50-60	400-650	3 000	1 500
III	"Gustav König"	60-80	650-1 000	4 000	2 000
IV	Class „Europe"	80-90	1 000-1 500	5 000	2 500
Va	Big ship	90-110	1 500-3 000	8 000	3 500
Vb	Tow + 2 barges	110-180	3 000-6 000	10 000	4 000
VIa	Tow + 2 barges	110-180	3 000-6 000	10 000	4 000
VIb	Tow + 4 barges	110-190	6 000-12 000	14 000	5 000
VIc	Tow + 6 barges	190-280	10 000-18 000	17 000	8 000
VII	Tow + 9 barges	300	14 000-27 000	20 000	10 000

[a] CEMT: European Conference of Ministers of Transport, classification proposed 19 June 1992, approved by the Council of European Union 29 October 1993.

[b] The mass m in tons (1 ton = 1 000 kg) includes the total mass of the vessel, including the ship structure, the cargo and the fuel. It is often referred to as the displacement tonnage.

[c] The forces F_{dx} and F_{dy} include the effect of hydrodynamic mass and are based on background calculations, using expected conditions for every waterway class.

Figure F.3: component Fdx and Fdy for inclined going ships [12]

To include the dynamic component of the ship collision a dynamic amplification factor is multiplied with the indicating values. The dynamic coefficient is given as:

- head-on / perpendicular collision give 1.3
- lateral collision give 1.7
- side and stern gives 0.3

AASHTO

The AASHTO is the American Association of State Highway and Transportation Officials, who also defined their own formulation for ship collision. They developed a formulation in 1991 for ship collisions on bridges. Their aim was to design bridges able to withstand ship collision. The formulation is closely related to the Eurocode, whereby only hydrodynamic added mass is extra included to basic equation F.1. The American code give the kinetic energy as:

$$E_{kin} = \frac{1}{2} C_h m_s v_s^2 \tag{F.8}$$

where the added mass coefficient is:

$$C_h = \begin{cases} 1.05 & \text{for underkeel clearance } > 0.5 \cdot \text{ draught} \\ 1.25 & \text{for underkeel clearance } < 0.1 \cdot \text{ draught} \end{cases}$$

This coefficient is slightly higher/lower than for the Eurocode.

F.3. Absorption efficiency fenders

A PIANC work group described in 2002 a formula to determine the energy absorbed by the fender :

$$E_{kin,f} = f R_m d_m \tag{F.9}$$

where: f = factor representing the energy absorbing efficiency of the fender system (between 0 and 1) [-]
R_m = maximum fender reaction force [kN]
d_m = maximum fender deflection [m]

factor f is determined between the relation of the deflection and reaction force of the fender system, see figure F.4. The $R/E_{kin,f}$-ratio (Fender Factor) gives knowledge of the fender system. the ratio shall be taken at the design deflection of the fender. A low $R/E_{kin,f}$-ratio indicates that low reaction force are generated to absorb the kinetic energy, which is favourable for accidental ship collision. When the ratio is high large force is generated for the absorbed energy, favourable for surface-protecting fenders. Part of the kinetic energy is returned to the ship (pushing back) and partially dissipated in the form of energy.

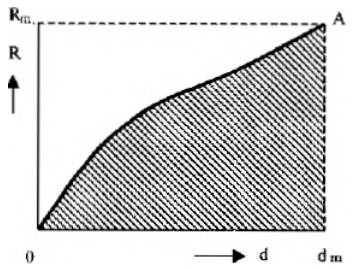

Figure F.4: reaction force versus deflection fender [43]

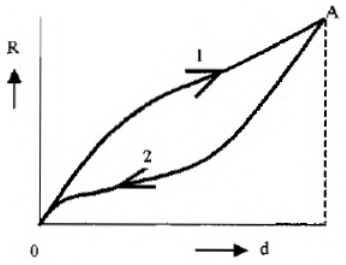

Figure F.5: reaction force versus deflection fender for loading and unloading [43]

An example is made with a tested fender system. The cylindrical fender tested has an outside diameter 1500 mm inner diameter 800 mm and is 1500 mm long. For fender system the ratio is high for small force i.e. small ship and small for high forces i.e. big ships. So the fenders can take lot of energy without large reaction force for big ships, which is favourable. For small ships the fender gives a high reaction force compared to the transferred energy in other words, behaves stiffer. The maximum rated deflection for compression fender is around 50%. An higher compression would result in a larger ratio, which is unfavourable for large ships.

F.4. Ship velocity

The ship velocity is of great importance withing the ship collision calculation. the ship velocity is squared in the kinetic energy equation. the ship velocity can deviate per collision scenario. Therefore Delft Hydraulics has made an inventories of ship collisions in the Netherlands [3]. In they determined the ship velocity at 10 m and 100 m before the lock gates. In this thesis collision is considered for a weir. Therefore the value at 100 m is taken. The velocities are determined for ship class IV, V and VI, see figure F.6.

	aantal	gemidd. vaarsn. (m/s)	stand.afw. vaarsn. (m/s)	max. vaarsn. (m/s)
Alle schepen op 100m	129	1.93	.74	4.4
Alle schepen op 10m	128	1.74	.63	3.6
Ongeladen schepen op 100m	56	2.16	.82	4.4
Ongeladen schepen op 10m	57	1.98	.67	3.6
Geladen schepen op 100m	73	1.76	.61	3.3
Geladen schepen op 10m	71	1.54	.53	2.9

Figure F.6: ship velocity in front of lock gates Netherlands [3, p. 37]

According to the Eurocode the governing ship velocity that should be taken is

$$v_{95\%} = \mu + 1.645\sigma_d \tag{F.10}$$

So the max ship velocity calculated by delft Hydraulics is approximately the same as the one calculated in the Eurocode.

F.5. Bow

The straight bow is taken as reference for the ship collision model. This is KN2. in figure F.7.The top right graph shows a side view of the bow shape. The KN2. line represents a straight bow, where the dimensions of the bow are as follows:

- Length bow is 19.7 m
- Height bow bottom is 4.4 m
- Height bow top is 1.14 m

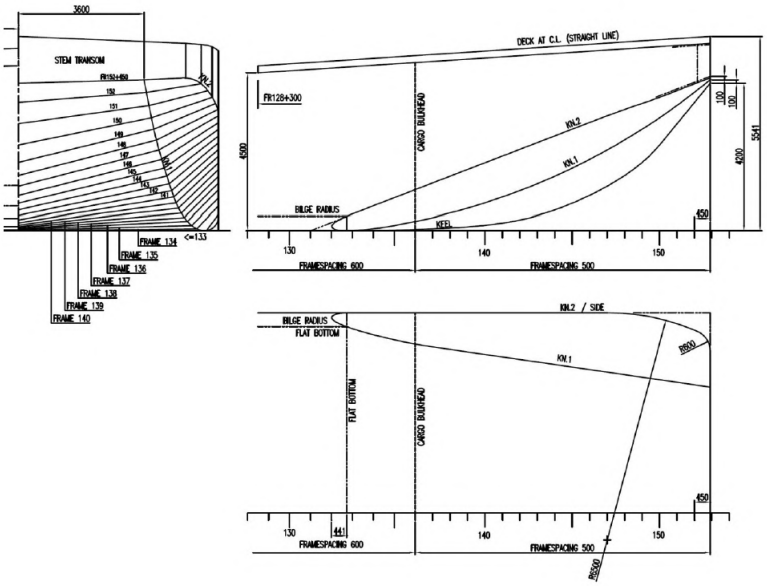

Figure F.7: dimensions bow for push convoys [66]

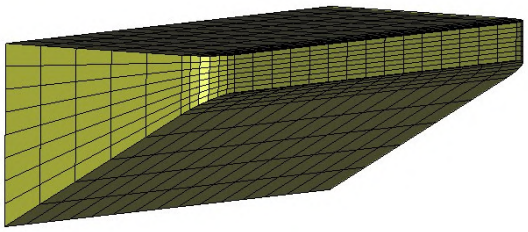

Figure F.8: bow push convoy in finite element program [66]

F.6. Tree

[36] The standard loading of inflatable dams is by top and bottom water thus pressure. However, the surface water can carry trees or other floating objects. The impact of a tree increases the stresses in the inflatable dam near the impact zone and for this reason affects the stress concentration factor. 6 b) M. Gebhardt, A.

Maurer and K. Schweizerhof. In the finite element simulations the tree is modelled by a cylinder of length 5m and weight 4t which swims with a constant velocity and hits the inflated dam under an angle between 0° and 90°. To show the effects of the filling the dams have been filled with different water heights and gas pressures. Considerations show, that – not unexpected - a higher velocity of the tree or a completely gas filled dam with a low gas pressure would cause the longest deformations and highest stresses. In Figure 7 the finite-element setting in an inflated state with the tree at initial position and the impact of the tree is shown. To show a case with a relatively large deformation of the dam the initial pressure has been set to a low pressure of 0,2bar and the velocity of the tree at time of impact 4 m/s. To compare stresses in this extreme example the stresses of the area of impact have been compared with the stresses of the complete dam. The stresses in the area of impact increase during the impact, but reduce shortly after the tree leaves the dam, see Figure 8. After a longer time period which is not included in the figure, the stresses and the geometry return to the state before the impact.

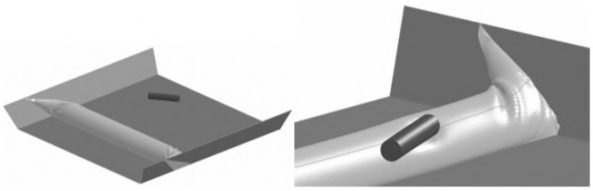

Figure F.9: tree hit with FEM [36]

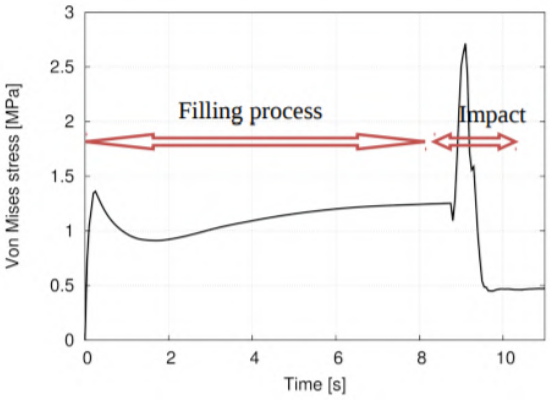

Figure F.10: analysing stress concentration tree hit [36]

Comparing these maximum stresses in the area of impact with the maximum stresses near the flanges shows that these impact stresses do not change the stress concentration factor which is important for design. The maximum von Mises stresses in this particular inflatable dam are about 6 MPa, while the maximum stresses in the impact area do not exceed 2,9 MPa.

F.7. Ship waves

The bow creates diverging waves as it cuts itself through the water. The velocity of the diverging waves are slower than the velocity of the ship which is accounted for by $c = v_s \cos(\phi)$. The waves created at the stern of the ship are created by the discontinuity at the hull. This creates transferal wave, which follow a circular pattern. At the interfering point of these waves cusps are formed, what gives the normative wave height. The direction of these cusps is about 35° of the sailing line. The line of cusps wave is about 20° of the sailing line.

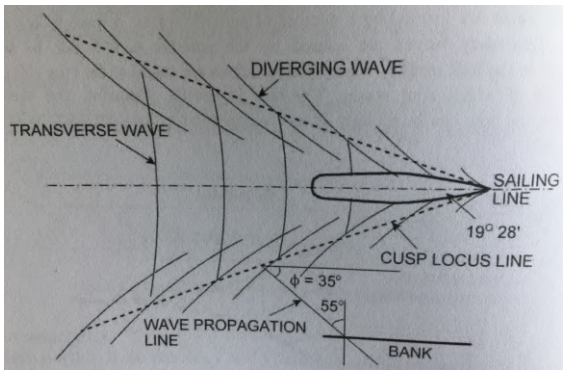

Figure F.11: ship waves [14]

G

Numerical model

Boxes where the values are manually adjusted are found in this appendix. Further to mention the connection type is contact.

Definition	
Type	Frictional
Friction Coefficient	5,e-002
Scope Mode	Manual
Behavior	Asymmetric
Trim Contact	Program Controlled
Suppressed	No

Figure G.1: friction settings

Advanced	
Formulation	Augmented Lagrange
Small Sliding	Program Controlled
Detection Method	Program Controlled
Penetration Tolerance	Program Controlled
Elastic Slip Tolerance	Program Controlled
Normal Stiffness	Program Controlled
Update Stiffness	Each Iteration
Stabilization Damping Factor	0,1
Pinball Region	Radius
Pinball Radius	5,e-002 m
Time Step Controls	None

Figure G.2: advanced settings

Step Controls	
Number Of Steps	1,
Current Step Number	1,
Step End Time	20, s
Auto Time Stepping	On
Define By	Substeps
Initial Substeps	20000
Minimum Substeps	2000,
Maximum Substeps	2,e+005
Time Integration	On

Figure G.3: step control settings

H

Experimental model

This appendix describes the background information belonging to the scale model tests in chapter 6.

H.1. Scale model tests

Before the scale model test was done in this research, others already were performed for other projects. Some are elaborated here to give an idea [62].

- Inflatable weir berkelse zwet: scale 12.5. This model was made to determine the process of raising and lowering the membrane in a controlled way, the desired bending stiffness, the required capacity of filling emptying system, outgoing of a maximal fill time of 20 minutes, is determined.
- Orienting study Inflatable barrier: scale 25 This model was made to determine the process of raising and lowering the membrane in a controlled way, and some attention to the vibrations of the membrane.
- Inflatable barrier Ramspol: design without bottom floor: scale 25. Operation of the membrane is studied in the scale model. Some attention is given to response of waves
- Inflatable barrier Ramspol: design with ribbed floor: scale 25 In this model the process of store the sheet in the bottom floor. Variables were: amount slots, shape of the ribbings, bending stiffness sheet, water- and air filling, flow velocity during storing.
- Inflatable barrier Ramspol: design BAM with bottom floor: scale 25. The following is researched: behaviour in inflated status, under influence of perpendicular and oblique waves. And the transmission of forces to the foundation, water movement inside membrane by influence of waves, operation of the membrane during opening with special attention to store sheet in bottom floor, operation of the membrane during closure and strength top layer of dumping stones bottom protection.
- Inflatable barrier on quay along the IJssel, Kampen: scale = 7.5.

Research: Much research is done in the form of model scale tests for the vibrations of the inflatable dam. The vibrations are developed by overflowing water, or with a lowered membrane due to the passing current. In the cross sectional view the vibrations in water filled membranes appear to develop with greater overflowing water than for air filled membranes. Also the vibration amplitude for water filled membranes appears to be smaller. Nonetheless the vibrations appear to be stronger in water filled membranes then air filled membranes. Stiffer membranes are less vibration sensitive. With completely stiff membrane pressure fluctuations develop in the circumference of the membrane. Conclusion is that the possibility of vibration development increases with increasing upstream water level. The other circumstances are not extensively researched in scale model tests. With numerical models the complicated process of loads, response and interaction can be calculated .

H.2. Model test scaling

The scale model is designed such, that it is capable of simulating the behaviour during ship collision on the Meuse. For a reliable prediction from the scale model an unambiguously correlation has to exist between the behaviour of the model and reality. For designing of the model three conditions need to be satisfied.

- Geometric uniformity: every dimension is scaled with the same factor
- Kinematic uniformity: the movements are scaled in the same extent. In this case the velocity of the ship. When length- and velocity scale are set also timescale is set.
- Dynamic uniformity: The loads on the liquid and structure is scaled also in the same extent.

In practice it is not possible to satisfy all three uniformity requirements are met at the same time. Scale modelling therefore is primarily focused on a right reproduction of the most important physical processes and subordinate phenomena are represented less accurate.

In general it is how bigger the scale (how smaller the model) how more difficult it is to represent the physical processes correctly (scale effects become more important). In practice reasons are given to make the scale models not so big for the manageability of the models. The choice of the length scale is therefore mostly determined by following considerations:

- possibility of correct reproduction of hydraulic and hydrodynamic phenomena
- possibility of accurately simulate the constructive details and material properties
- accuracy of measure devices, and possibly of implementing instruments in scale model without influence the experiment.
- manageability and accessibility of the scale model
- dimensions and possibly of available research facilities.

For response research of the inflatable weir serve in special the stiffness characteristics of the membrane and the mass involved by membrane movements. Because the mass of the membrane sheet is much smaller than the accompanied added mass, the mass of the membrane sheet does not need to be precisely on scale. For the air filled inflatable weir, the air cannot be scaled but is important for the scaling of the compression stiffness of the membrane. Another difficulty is reproducing of the elastic characteristics of the membrane sheet. The scaling of these difficulties is described below

H.2.1. Air

In the scale model, the atmospheric pressure is not scaled. The surrounding pressure is too high for the scale model and therefore also the absolute pressure p_0 in the membrane. The compression modulus of air is dependent on the prevailing pressure. A scale effect is present for the compressibility of air in the membrane and a correction is needed for this. The correction is realised by making the scale model volume bigger than results from the normal volume-scale rule. The volume increase is realised by adding extra volumes boxes beside the membrane, that is open connection with the membrane. How big the extra volume has to is derived here.

When scaling the inflatable weir, the volume of air in the membrane is also scaled. The scaling of air changes its compressibility. The compressibility of air is dependent on the internal pressure and the initial volume. According to the equation of change of state:

$$p_0 V_0^{\gamma} = \gamma \tag{H.1}$$

Differentiating gives:

$$dp = -\gamma p_0 \frac{dV}{V} = -K \frac{dV}{v} \tag{H.2}$$

where: p_0 = internal pressure [N/m^2]
V_0 = initial air volume [m^3]
γ = Poisson constant (= 1.0 for isothermal compression)
K = compression stiffness (γ p_0/V) [N/m^2]
dp = internal pressure change [N/m^2]

The compression modulus is dependent on the internal pressure p_0 in the membrane. Without scale of the atmospheric pressure the compression stiffness in the membrane is too high. The compression stiffness is of importance by movements of the membrane, where the air is compressed.

For static equilibrium the over pressure Δp in the membrane is the defining factor. This over pressure influences the axial strain and membrane stiffness and is also influence the curvature, which follows from element equilibrium defined in paragraph [xx]. The curvature again is dependent on the overflow on the membrane and the flow load that develop (because how stronger the curvature how bigger the suction).

The over pressure must therefore be well reproduced in the scale model. The over pressure is scaled by the normal pressure scale rule, in this case:

$$n_{\Delta p} = n_L = 25 \tag{H.3}$$

where: $n_{\Delta p}$ = scale factor over pressure [-]
n = general scale factor [-]

At the same time the compression stiffness K has to be on scale. It is assumed the Poisson constant γ is the same in the scale model as in reality, then as scale rule for the compression stiffness holds:

$$n_{\gamma p_0/V} = \frac{n_p}{n_V} = \frac{n}{n^3} = \frac{1}{n^2} \tag{H.4}$$

Both conditions can be satisfied by an deviating scale rule for the air volume. The scale factor of the air pressure n_p is defined as:

$$n_p = \frac{p_{proto}}{p_{model}} = \frac{1\,atm + \Delta p}{1\,atm + \frac{\Delta p}{n_{\Delta p}}} = \frac{1+5.3}{1+5.3/25} = 5.20 \tag{H.5}$$

Now the scale factor of air volume can be found with for the deviating scale rule:

$$n_V = n_p * n^2 = 5.20 * 25^2 = 3249 \tag{H.6}$$

According to the normal geometric scale rule the volume is scaled with n^3, which the inflatable weir is scaled with. To also scale the compression stiffness, the volume that has to be added is

$$\frac{n^3}{n_V} - 1 = \frac{n}{n_p} - 1 = \frac{25}{5.2} - 1 = 3.81 \tag{H.7}$$

times the inflatable weir volume.

Air boxes

The two wooden boxes on both sides provide the extra air volume that is needed. For the first experiment set two boxes are made of 0.6m^3. It was not decided yet if the length of the sheet from the literature or the calculated would be used. The one from the literature gave a larger volume needed. It was decided to use the sheet length from the calculation. Therefore a 0.15 m layer styrofoam is added in the boxes to reduce the volume. Now the boxes have the desired volume $2 * 0.6^2 * 0.45 = 0.325 m^3$, see figure H.1 left side. It showed the boxes were not completely are tight, therefore new boxes are made for the second experiment set. These boxes are taped from the inside and have more seamless sides.

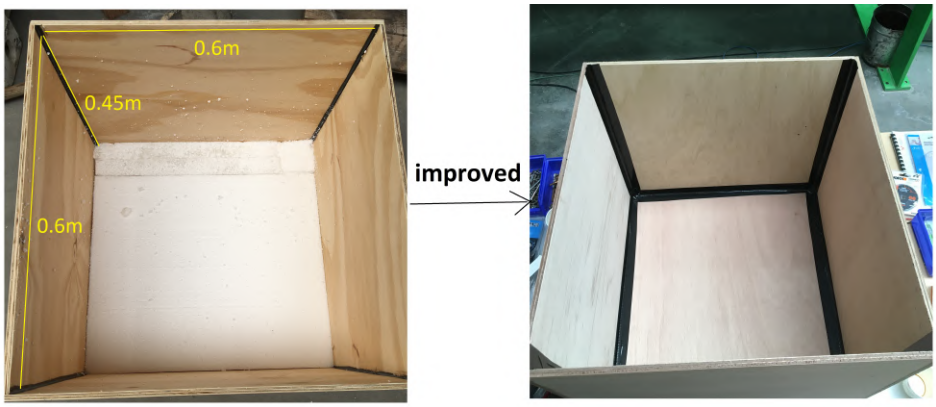

Figure H.1: inside of boxes

Air pressure

The pressure of the inflating equipment (see figure H.2) is tested with a piezometer. As can be seen in the figure the inflating equipment is (airtight) connected with a bicycle tube. The piezometer is connected (airtight) with the valve. In figure H.3 the piezometer is shown in unpressurized state. Every distance between the red bars indicate 2.5 cm. Now the inflating equipment is put on and the height in the piezometer is measured 12 cm. Measuring the waterdrop height gives 21 cm. This is equal to $rho_w * d = 1000 * 0.21 = 210 kg/m^2 = 2.1 kN/m^2$. This is ideally the pressure that is need for the model scale tests.

The piezometer is also connected to the inflatable weir during the model scale tests. When inflating the inflatable weir with the same inflating equipment the resulting pressure in the piezometer is shown in figure H.5. From the figure a water height is read off 8.5 cm. This gives a water drop height of 17cm. Converted to the pressure in the inflatable weir this is 1.7 kN/m^2. The pressure loss is significant when connecting the inflating equipment to the inflatable weir. With the help of soap lubricating to the seams of the air boxes, it was shown that they were leaking. Also the tubes connected with the side opening of the scaled inflatable weir showed some leakage. The first air boxes showed exact the same problem as the new air boxes. It is very likely that it is very difficult to get the structure air tight.

Figure H.2: inflating equipment

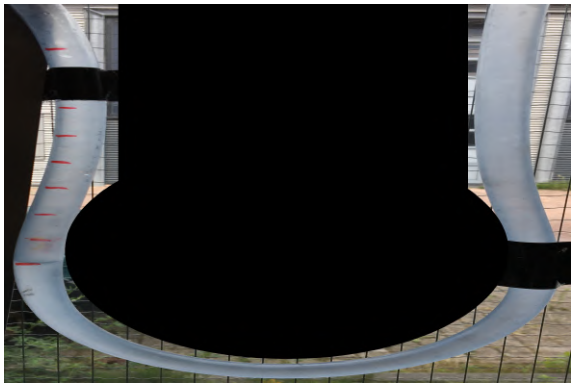

Figure H.3: unpressurized piezometer

Figure H.4: ideal pressure piezometer

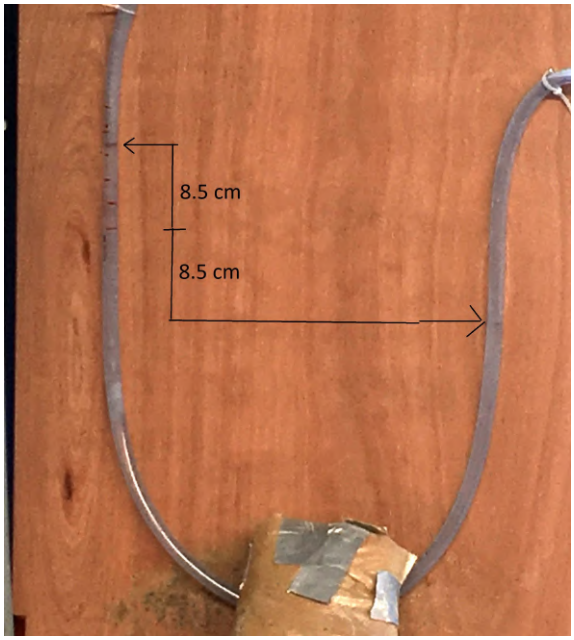

Figure H.5: pressure piezometer

H.2.2. Strain rigidity

Here is described how the strain rigidity of the sheet is scaled. The strain rigidity is superior to scale. The thickness and self weight of the sheet normally does not influence the model. The self weight is much lower than the mass of the water. The thickness of the sheet will influence the bending stiffness. The bending stiffness plays a role in in- and deflating of the membrane, but this is not scope of the research. The strain rigidity is found with Hookes law:

$$\begin{aligned} \sigma &= E\epsilon \\ \frac{F}{A} &= E\epsilon \\ EA &= \frac{F}{\epsilon} \end{aligned} \tag{H.8}$$

The strain stiffness holds for per unit width of the sheet, which is 1 m. The strain stiffness scale factor can the be found by squaring the scale factor:

$$n_{EA} = n^2 = 25^2 = 625 \tag{H.9}$$

Ramspol scale sheet

For Ramspol these tensile tests are already done and are an example how to scale the strain rigidity. The tensile test is done with FDA-Buna, 0.55 mm thick. The 5 cm wide test strip was step wise loaded to 40 N (800 N per m width in prototype) in a small tensile testing machine. Both ends were clamped in the tensile testing machine. After 1 loading step 10 minutes is waited. In the graph of figure H.6 is shown that the stress in the test strip thereby declined (relaxation). The strain stiffness for the sheet is 4600 N per meter width for the area until 400 N per meter width see the graph (for prototype it is 2.9e3 kN per meter in the area until 250 kN per meter width; this is the membrane force at Ramspol in design condition of 4.4 m decay)

For the ship collision case, the sheet is tested for stretched until its ultimate limit state (=ULS), which is a strain of 20%. In that case the strain stiffness become 700/0.2=3500 N per meter width. The strain stiffness needed for the scale model is ULS for prototype Ramspol divided by the scale factor gives $7500e3/25^2$ = 12000 N per meter width, this means a thickness of the sheet of 12000/3500 * 0.55 = 1.89 mm. While the desired thickness is 1.6*10 / 25 = 0.64 mm. The needed thickness is around 3 times larger.

The time dependent phenomena creep is researched by means of a long-duration experiment. The test piece is for 3 days loaded with a constant load of 19.6 N and subsequently the weight got removed and the strain was measured until 3 days thereafter. The load compares to the prototype with a membrane force of 245 kN per meter width. From the graph H.6 of the tests it shows that the sheet strains for a while after applying the load. After removing the load a certain strain remains which disappear after a longer time. With other sheet material namely coated nylon sheet, the creep was much higher a factor 3, which means a larger permanent deformation after removing the load.

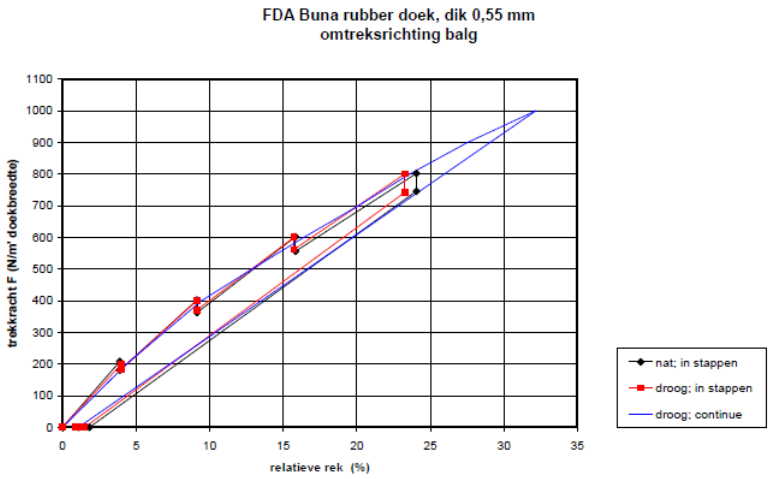

Figure H.6: strain stress graph scale model sheet Ramspol [62]

H.2.3. Bending stiffness

Since the bending stiffness is of subordinate importance, it is not scaled.

H.2.4. Ship velocity

Forces involved in a collision are hydro static, dynamic, gravitational, inertial and the contact force. Ratio of these forces in the scale model with prototype have to apply. Dynamic similarity must be maintained. Two things are required for this:

- geometric similarity
- kinematic similarity (similarity of motion)

The kinematic similarity implies both geometric similarity and similarity of time intervals. Two dimensionless parameters are of importance to achieve kinematic similarity, which are based upon the following forces:

- Inertia force: $F_{I,s}\ \rho_w L_s^2 v_s$
- Gravitational force: $F_G\ \rho_w g L_s^3$
- Viscous shear force: $F_{\mu_v}\ \mu_v v_s L_s$

The Froude number defines resistance of making waves and is defined by the square root of inertia and gravity force:

$$Fe = \sqrt{\frac{F_I}{F_G}} = \sqrt{\frac{\rho_w L_s^2 v_S^2}{\rho_w g L_s^3}} = \frac{v_s}{\sqrt{g L_s}} \tag{H.10}$$

The Reynolds number defines if a flow is turbulent or laminar and is defined by the inertia force and viscous force:

$$Re = \frac{F_I}{F_{\mu_v}} = \frac{\rho L_s^2 v_s^2}{\mu_v v L_s} = \frac{\rho L_s v_s}{\mu_v} \tag{H.11}$$

These non-dimensional values do not depend on the scale, hence for both scale model and prototype they have to be the same. However to keep the Froude number the same it follows that the velocity becomes:

$$v_m = \frac{v_s}{\sqrt{n}} \tag{H.12}$$

and so the scaling factor:

$$n_v = \frac{1}{\sqrt{n}} = \frac{1}{\sqrt{25}} = 5 \tag{H.13}$$

and to keep the Reynolds number the same it follows:

$$v_m = v_s n \tag{H.14}$$

Above two equations cannot be satisfied simultaneously. However, the viscous forces do play a lesser role than the high acceleration forces. The velocities of pitch are considered low and thus the viscous forces are. The viscous forces are small compared to the inertial forces. Therefore the Froude scaling law eq. H.12 is used for the velocity. As a result the Reynolds number is too small and thus frictional forces induced are too high [30].

H.2.5. Sheet thickness

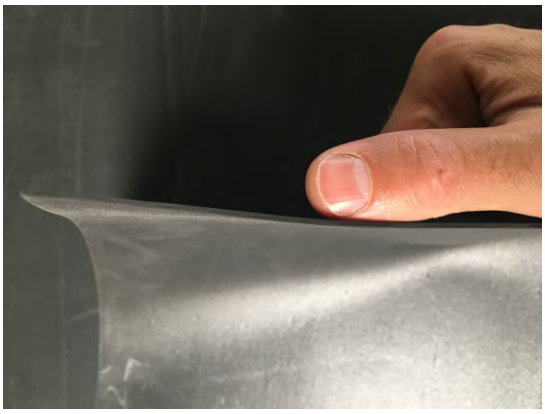

Figure H.7: thickness model sheet

H.2.6. Ship mass/draught

The ship is just like the foundation made of 18 mm plywood (in Dutch multiplex). The ship itself weights 37 kg. By adding bags of sand the weight of the ship can be adjusted. In figure H.9 the small sacks represent 5 kg of sand and the large ones 25 kg of sand. To achieve the desired draught the following weight is added:

- D=0.08m : 37 + 3 * 25 = 112 kg
- D=0.10m : 37 + 4 * 25 + 5 = 142 kg
- D=0.12m : 37 + 5 * 25 + 2 * 5 = 172 kg
- D=0.14m : 37 + 6 * 25 + 3 * 5 = 202 kg

In figure H.8 it can be seen that both stern and bow of the ship are marked with draught stripes, when looking closely. Those stripes are used to measure the draught and distributing the mass equally over the ship's length. Both draught stripes need to be in line with the water level, to have a balanced ship. The centre of mass is then laying around the middle of the ship.

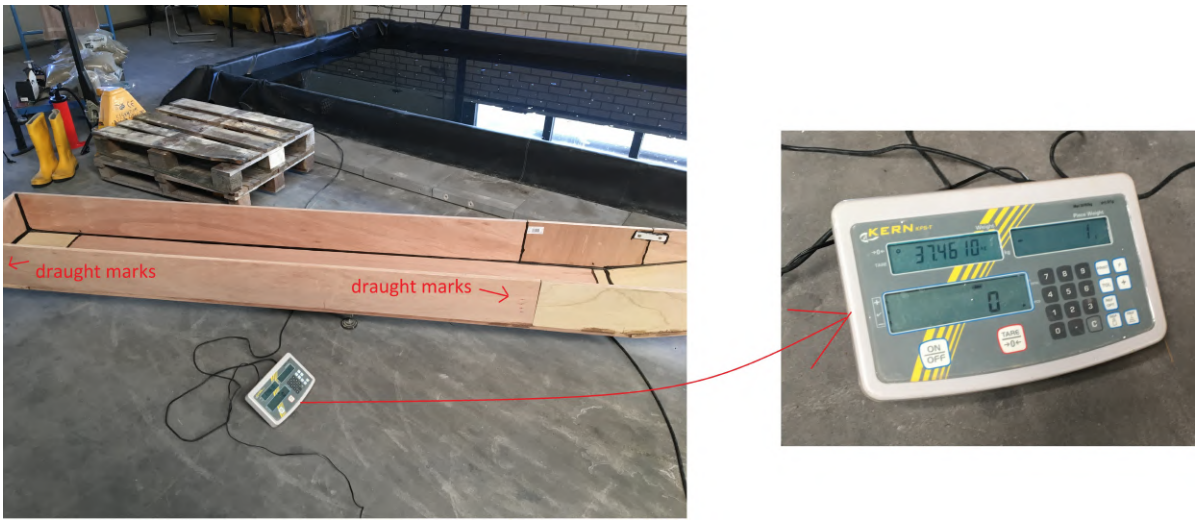

Figure H.8: ship on the balance

Figure H.9: sandbags

H.3. Testing procedure

The following steps are done in chronologically order for one set of experiments, where the one set consists of one draught/mass tested with four different velocities:

1. *The blower is put on to inflate the inflatable weir. At the same time the submersible pump is put on to pump water from the downstream side to the upstream side.
2. ** The first sandbags are loaded on the ship to achieve the least draught (0.08m).
3. The ship is pulled to the far upstream side of the basin and is tighten up.
4. If the overflow from the previous test caused a water level rise of the downstream basin of more than 0.5 cm, then the submersible pump is but on again to adjust the water level.
5. The bucket is filled with the desired amount of sand.
6. **The top view camera is put on and is put in place attached to a crane. Also the side view camera is put on.
7. A note is put in front of the camera which test is started.
8. The submersible pump is put off, when the desired water levels are achieved.
9. The ship is let loose from the upstream end and collides into the weir.
10. The bucket is emptied from the sand.
11. *The blower is put off and new sandbags are loaded on the ship.

*This is only done once between every four tests or at a new draught.
**This is only once at the start.

H.4. First experiment set results

This paragraph shows the results in graphs from the first experiment set. Below a table is given for the first experiment set, how many frames are counted 0.5 m before the weir until the ship hits the weir. This is converted into a velocity.

	D = 0.08 m FPS 60	D = 0.10 m FPS 60	D = 0.12 m FPS 50	D = 0.14 m FPS 50
Mass (kg)	Frames	Frames	Frames	Frames
2	48	55	49	55
5	33	38	34	38
10	25	28	26	26.5
15	23.5	23	21	23.5

Table H.1: velocity calibration with frames

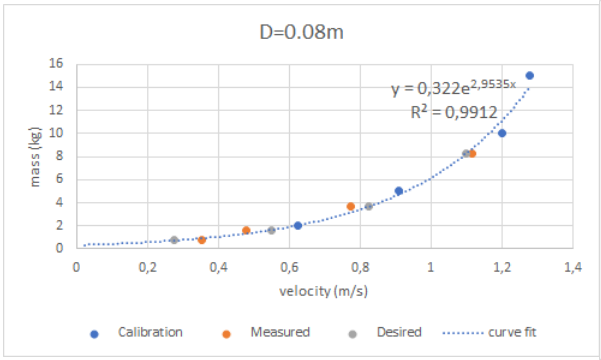

Figure H.10: calibration 0.08 m

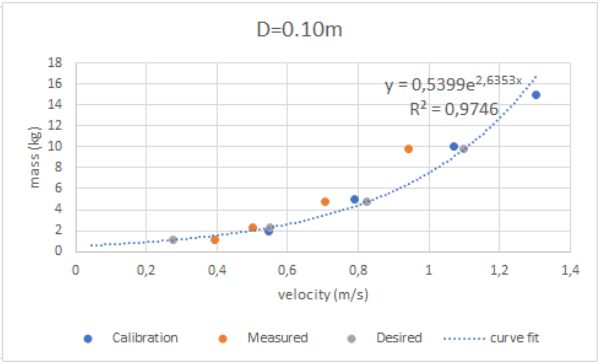

Figure H.11: calibration 0.10 m

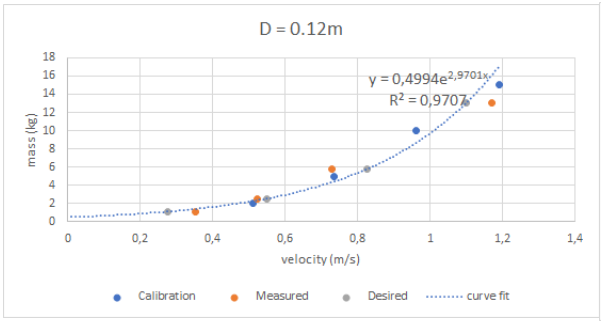

Figure H.12: calibration 0.12 m

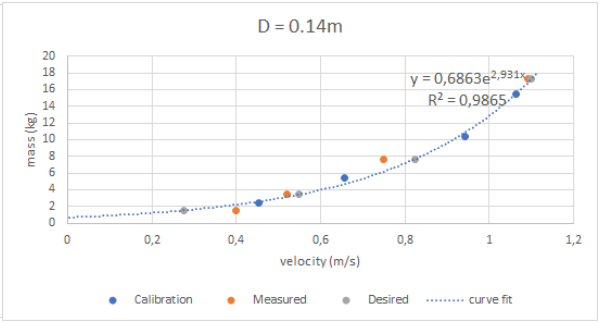

Figure H.13: calibration 0.14 m

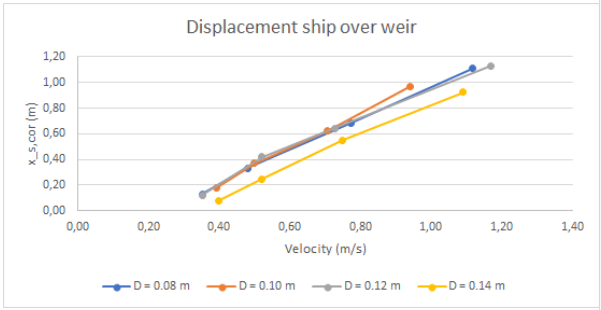

Figure H.14: displacement over weir

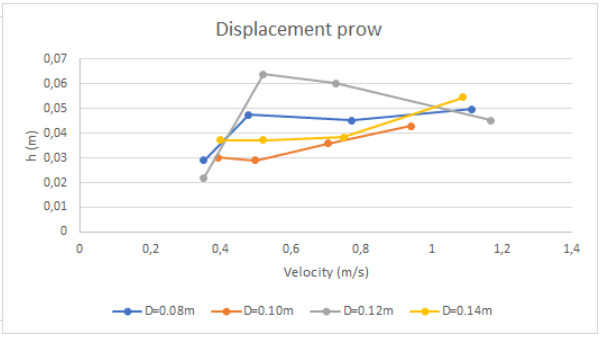

Figure H.15: displacement front bow

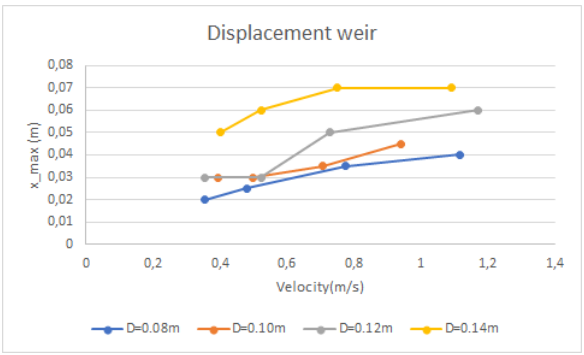

Figure H.16: displacement weir

H.5. Folds change

Below two snapshots are taken for the experiment the the largest draught an velocity. Looking carefully in both snapshots the folds do not move with respect to the initial state (above two snapshots). A side note to folds is given, as this is an interesting feature of the membrane. In inflated stat the folds are shown at the abutments. In the scale model the folds were touched to see what happens. It showed that folds moved position, meaning there are multiple equilibrium states.

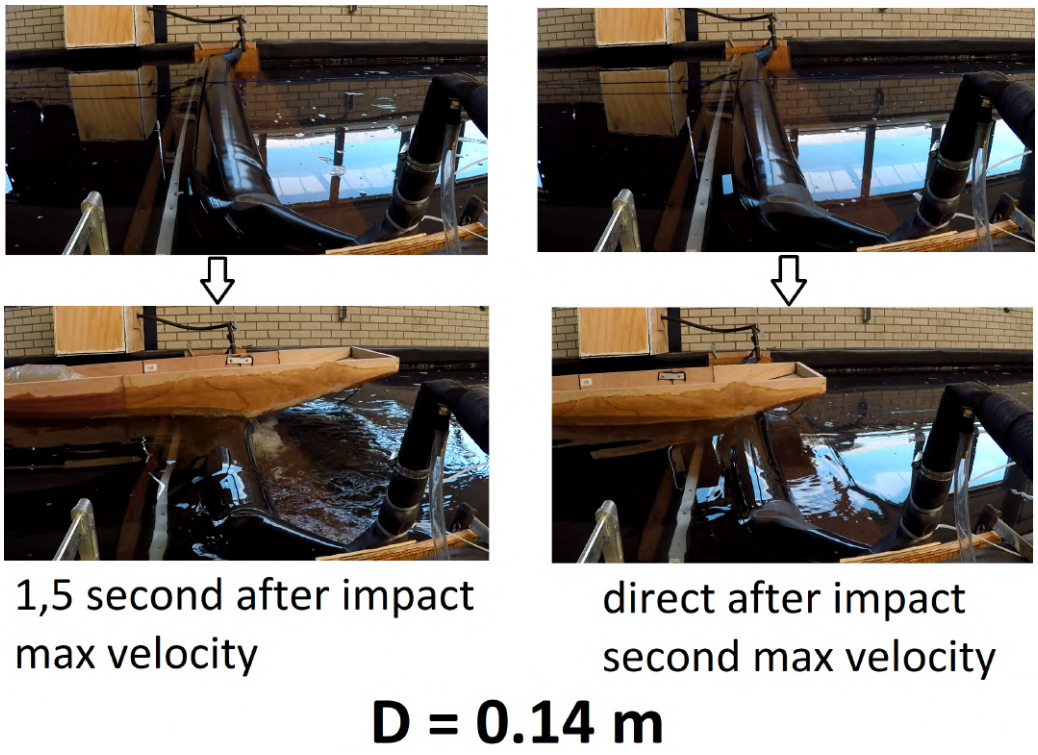

Figure H.17: folds show no change

References

[1] Aboshio A. and Green S. Dynamic response of inflatable offshore barrier structures under impact loading. 09 2013.

[2] van Winden A. Jaarverslag rijn en maas in 2015, 2015.

[3] Vrijburcht A. Aanvaarrisico's voor sluisdeuren. Technical report, Delft Hydraulics, 1992.

[4] Vrouwenvelder A.C.W.M. Design for ship impact according to eurocode 1, part 2. 7. In *Ship collision analysis*, 1998.

[5] Hollandsche beton-en waterbouw bv and Bouwdienst Rijkswaterstaat. Detailontwerp nylon balgdoek. Technical report, -, February 2000.

[6] Suribabu C.R., R.M. Sabarish, R. Narasimhan, and Chandhru A.R. Backwater rise and drag characteristics of bridge piers under subcritical flow conditions. 2011.

[7] Kunz C.U. Ship bridge collision in rive traffic, analysis and design practice. In *Ship collision analysis*, 1998.

[8] de Jong D. Vervangingsopgave natte kunstwerken (vonk), stuwen maas, investeringsraming preverkenningsfase. Technical report, Antea group, 2014.

[9] Tagwi D. Inflatable weir hydraulics. Master's thesis, Stellenbosch University, 2015.

[10] de Vries and van de Wiel. Welkom op de projectwebstie verrruimen julianakanaal, 2014.

[11] Dyrhoff. Sungei tampines, singapore, 2014.

[12] EN1991-1-7. Eurocode 1 - actions on structures - part 1-7: General actions - accidental actions. Technical report, CEN, 2006.

[13] van der Ziel F. Movable water barrier for the 21st century. Master's thesis, TU Delft, 2009.

[14] Schiereck G.J. and Verhagen H.J. *Introduction to Bed, bank and shore protection.* Delft Academic press, 2nd edition edition, 2016.

[15] Skaggs H. Texas man uses massive inflatable dam to save house, June 2016.

[16] van Oorschot H. Stability of rock-based emergency measure, based on the grave weir. Master's thesis, TU Delft, 2018.

[17] Harrison H.B. and Anwar H.O. The analysis and behaviour of inflatable membrane dams under static loading. In *Proceedings of the Institution of Civil Engineers*, volume 45, pages 661–676, 1970.

[18] Verheij H.J. and Laboyrie J.H. Aantasting van dwarsprofielen in vaarwegen: Technische aanbevelingen voor oeververdediging van losgestorte en gezette steen: samenvattend verslag. Technical report, Delft Hydraulics, 1988.

[19] Verheij H.J., Stolker C., and Groenveld R. *Inland Waterways: Ports, waterways and inland navigation.* VSSD, 2008. Lecture notes CT4330.

[20] Berger H.J.E. and Mugie A.L. Hydrologische systeembeschrijving maas. Technical report, Rijkswaterstaat, June 1994.

[21] Driebergen J. Verkenning vaarweg meppel-ramspol. Technical report, Rijkswaterstaat, 1999.

[22] Jansen J. Ship collision on temporary structures: Combi-walls under collision loading. Master's thesis, TU Delft, 2019.

[23] van Schrojenstein Lantman J. Hoogwatervoorspellingen op de maas in crisissituaties. Master's thesis, University Twente, 2004.

[24] Hsieh J. C. *Free vibrations of inflatable dams*. PhD thesis, Virginia Polytechnic Institute and State University, Blacksburg, 1988.

[25] JICE. Technical standard for rubber gates. 2000b.

[26] Schillings J.J.M. Balgstuw ramspol finite element analysis fluid-structure dynamics users' manual ansys macros. Technical report, COMPUTATIONAL SOFTWARE TECHNOLOGIES, April 2001.

[27] Beguin J.L.P.M.G. Richtlijnen ontwerp kunstwerken rok 1.4. Technical report, Rijkswaterstaat, 2017.

[28] Reedijk J.S. Case study inflatable storm surge barrier ramspol. In *Post Academic Course Delft University*, 1999.

[29] Schot J.W., Lintsen H.W., Rip A., and A.A.A. de la Bruhèze. *Techniek in Nederland in de twintigste eeuw*, volume Deel 1. Techniek in ontwikkeling, waterstaat, kantoor en informatietechnologie, 1998.

[30] Tabri K., Määttänen J., and Ranta J. Model-scale experiments of symmetric ship collisions. *Journal of Marine Science and Technology*, 13:71–84, 02 2008.

[31] van der Valk K. Life cycle costs: a comparison between inflatable and traditional barriers. Master's thesis, TU Delft, 2014.

[32] Buldgen L., Andreea B., and Philippe R. Simplified analytical methods to analyze lock gates submitted to ship collisions and earthquakes. *Mathematical Modelling in Civil Engineering*, 11, 09 2015.

[33] Visser L.J. Levensduur stuwen in de maas. Technical report, IV-Infra, 2014.

[34] de Rooij M. Assessing the functional performance of the meuse river: The impact of bed developments and an altering discharge regime on future river functioning. Master's thesis, TU Delft, 2020.

[35] Gebhardt M. Inflatable structures in hydraulic engineering. In *SMART RIVERS 2013*, September 2013.

[36] Gebhardt M., Maurer A., and Schweizerhof K. On the hydraulic and structural design of fluid and gas filled inflatable dams to control water flows in rivers. October 2011.

[37] Gebhardt M., Aubonnet J, J. Berterottière, de Heyder B., Jansen P., Lechtenberg J.W., Maruyama I., Mason D., Rigo P., Wachholz T., and Paulus T. Inflatable structures in hydraulic engineering. Technical report, PIANC, 2018.

[38] van Breukelen M. Improvement and scale enlargement of the inflatable rubber barrier concept. Master's thesis, TU Delft, December 2013.

[39] Voorendt M.Z. and Molenaar W.F. *Manual Hydraulic Structures 2019*, February 2019.

[40] United Nations. Review of marine transport. In *United nations on trade and development*, 2019.

[41] Koedijk O.C., van der Sluijs A., and Steijn M.L.W. Richtlijnen vaarwegen 2017. Technical report, Rijkswaterstaat, 2017.

[42] Erbisti P.C.F. *Design of Hydraulic Gates*. CRC Press, 2nd edition, 2014.

[43] PIANC. Guidelines for the design of fender systems: 2002. Technical Report Report 33, PIANC, 2002.

[44] PIANC. Design of lock gates for ship collision. Technical Report Report 151, PIANC, 2014.

[45] Daniel R. and Paulus T. *Lock Gates and Other Closures in Hydraulic Projects*. Butterworth-Heinemann, 1st edition edition, 2018.

[46] de Roos R. and Kortlever W. Aanvaring stuw bij grave, November 2017.

[47] Parbery R.D. and Harrison H.B. A continuous method of analysis for the inflatable dam. In *Proceedings of the Institution of Civil Engineers*, volume 61, pages 725–736, 1976.

[48] Rijkswaterstaat. Scheepvaartinformatie hoofdvaarwegen. Technical report, 2009.

[49] Rijkswaterstaat. Betekkingslijnen 2016 2017. Technical report, RWS, 2017a.

[50] Rijkswaterstaat. Maas, 2019.

[51] Rijkswaterstaat. Stormvloedkering ramspol, Sep 2019.

[52] Rijkswaterstaat. Maas: reparatie stuw linne, 2020.

[53] Rijkswaterstaat. Vervangingsopgave grip op de maas, june 2020.

[54] Bouwdienst Rijkswaterstaat. Kennis- en ervaringsdocument balgkering ramspol. Technical report, Rijkswaterstaat, December 2007.

[55] Frijns R.S.J. Design of an adaptive weir. Master's thesis, TU Delft, 2019.

[56] Caelen S. Tegen stuw vastgelopen duwbakken terug naar maasbracht, february 2020.

[57] Motora S., Fujino M., SUGIURA M., and Sugita M. Equivalent added mass of ships in collisions. *J of Soc of Naval Arch of Japan*, 7, 1971.

[58] ul Islam S. and Arun K. Inflatable dams for shp projects. Technical report, Renewable and Sustainable Energy Reviews, 2016.

[59] Zhang S. and Pedersen P.T. *The mechanics of ship collisions.* PhD thesis, Technical University of Denmark, 1999.

[60] Jonkman S.N., Steenbergen R.D.J.M., Morales-Nápoles O., Vrouwenvelder A.C.W.M., and Vrijling J.K. Probabilistic design: Risk and reliability analysis in civil engineering. Technical report, TU Delft, 2107.

[61] Jongeling T.H.G. Balgkering ramspol : modified design of abutments. Technical report, Delft Hydraulics, 1998.

[62] Jongeling T.H.G. and Vrijburcht A. Hydraulische aspecten van balgstuwen en waterkeringen. Technical report, Delft hydraulics, 2005.

[63] Jongeling T.H.G. and Rövekamp N.H. Wave-induced response of inflatable barrier. Technical report, 1999.

[64] Joustra T.H.J., Muller E.R., and van Asselt M.B.A. Stuwaanvaring door benzeentanker bij grave, 2018.

[65] Gabrys U. Bemessung und konstruktion der verankerungen von schlauchwehren. Technical report, Mitteilungsblatt der Bundesanstalt für Wasserbau, 2007.

[66] Ministerie van Infrastructuur en Milieu. Europese overeenkomst voor het internationale vervoer van gevaarlijke goederen over de binnenwateren (adn). 2013.

[67] Molenaar W.F. *Hydraulic Structures Locks*, March 2011.

[68] Molenaar W.F. Rijkswaterstaat. Interview, November 2020.

[69] van Dommelen W.J.G. Moving load on guide works during a brush collision with a vessel. Master's thesis, TU Delft, 2020.